Experimental and Numerical Characterization of Mycelium-based Bio-Composites as Building Insulation Materials

by

Seyedsina MOTAMEDI

DISSERTATION PRESENTED TO ÉCOLE DE TECHNOLOGIE SUPÉRIEURE IN FULFILLMENT OF THE REQUIREMENTS FOR THE DEGREE OF DOCTOR OF PHILOSOPHY
Ph.D.

MONTREAL, FEBRUARY 13TH, 2026

ÉCOLE DE TECHNOLOGIE SUPÉRIEURE
UNIVERSITÉ DU QUÉBEC

BOARD OF EXAMINERS

THIS THESIS HAS BEEN EVALUATED

BY THE FOLLOWING BOARD OF EXAMINERS

Mr. Daniel R. Rousse, Thesis Supervisor
Mechanical Engineering Department at École de technologie supérieure

Mr. Geoffrey Promis, Thesis Co-supervisor
IUT Amiens – Department of Civil Engineering and Sustainable Construction, Laboratoire des Technologies Innovantes (LTI), Université de Picardie Jules Verne

Mr. Ricardo Izquierdo, President of the Board of Examiners
Electrical Engineering Department at École de technologie supérieure

Mr. Wahid Maref, Member of the jury
Construction Engineering Department at École de technologie supérieure

Mr. Laurent Zalewski, Member of the jury
Laboratoire de Génie Civil et géo-Environnement (LGCgE), Faculty of Applied Sciences, University of Artois

THIS THESIS WAS PRESENTED AND DEFENDED

IN THE PRESENCE OF A BOARD OF EXAMINERS AND PUBLIC

ON DECEMBER 4TH, 2025

AT ÉCOLE DE TECHNOLOGIE SUPÉRIEURE

ACKNOWLEDGEMENTS

I would like to express my profound gratitude to my supervisors, Prof. Daniel Rousse and Prof. Geoffrey Promis, whose unwavering support, insightful guidance, and tireless commitment have shaped every stage of this research. I am deeply thankful for their patience, generosity, and willingness to share their knowledge, which not only enriched this dissertation but also inspired me to pursue excellence in my academic and professional journey. This work would not have been possible without their mentorship, encouragement, and trust.

My appreciation extends to my home institution, École de technologie supérieure (ÉTS), University of Quebec, and to the Laboratoire des Technologies Innovantes (LTI), Université de Picardie Jules Verne (UPJV) in Amiens, for their continued support of international academic activities. I am also grateful to Mitacs for their scholarship, which facilitated my visiting research in Amiens and enabled this fruitful international collaboration. Special thanks go to Arash Jamali from the Plateforme de Microscopie Électronique at UPJV and Rose Marie Dheilly from the LTI, UPJV, for their valuable assistance and expertise in acquiring and analyzing the SEM images used in this study.

I would also like to acknowledge the memory of Simon Knight, whose passion and inspiration for this project remain unforgettable, and to give special thanks to Bob Mitchell, who first introduced me to the wonderful world of mycelium and its potential role in the decarbonization of industries.

Last but not least, the journey of this PhD unfolded during a period marked by the challenges of early immigration, family issues, and the complicated situation in my home country. I am sincerely grateful to my loved ones for their unwavering support and companionship during the most difficult stages of this journey, which helped me persevere through personal hardships while remaining committed to my research.

CARACTÉRISATION EXPÉRIMENTALE ET NUMÉRIQUE DES BIOCOMPOSITES À BASE DE MYCÉLIUM EN TANT QUE MATÉRIAUX D'ISOLATION POUR LA CONSTRUCTION

Seyedsina MOTAMEDI

RÉSUMÉ

Cette thèse introduit et caractérise des composites à base de mycélium (MBC) au moyen d'analyses expérimentales et numériques multi-échelles. Ces composites associent des agrégats végétaux à une matrice fongique, créant un matériau isolant naturel au potentiel de neutralité carbone. Pour une application dans les enveloppes de bâtiments, une compréhension détaillée de leurs propriétés hygrothermiques est essentielle, car les comportements thermiques et hydriques sont fortement interdépendants. Une analyse intégrée des transferts de chaleur et d'humidité, incluant la mesure des propriétés, l'analyse de corrélation et la simulation, a donc été réalisée.

Des lacunes de recherche subsistent dans la connaissance de l'ensemble du spectre du comportement hygrique, de leur pertinence vis-à-vis des propriétés thermiques et microstructurales, ainsi que dans le développement de modèles numériques intégrant les phénomènes d'adsorption–désorption, l'hystérésis et le couplage des transferts de chaleur et de masse. Pour répondre à ces enjeux, une méthodologie en trois étapes a été appliquée. Premièrement, des essais de fabrication ont exploré divers substrats, champignons, additifs et procédés afin d'optimiser l'homogénéité et la croissance fongique, en tenant compte de la compatibilité des constituants tels que la composition cellulose-lignine du substrat, leur interaction avec le mycélium et les types de mycélium et d'additifs incorporés. Deuxièmement, des campagnes expérimentales ont évalué la performance isolante, la capacité de régulation hygrique, la conductivité thermique et certaines propriétés microstructurales. Troisièmement, un modèle couplé de transfert de chaleur et de masse a été implémenté dans COMSOL, avec des modèles de sorption calibrés à partir des résultats expérimentaux et validés par rapport à la valeur mesurée du tampon hygrique (MBV), un indice qui quantifie la capacité d'un matériau à modérer les fluctuations d'humidité intérieure. Des simulations isothermes et non isothermes, incluant les effets d'hystérésis, ont été réalisées.

Les résultats confirment l'aptitude des MBC à remplacer de manière durable les matériaux isolants à forte intensité carbone tels que le polystyrène expansé. Les pratiques de fabrication développées, la gamme de résultats expérimentaux obtenus et le modèle numérique précis et fiable constituent également une base solide pour de futures recherches sur des formulations alternatives et des prédictions de performance dans divers climats et configurations d'enveloppe du bâtiment.

Mots-clés: Matériaux biosourcés, isolation, caractérisation hygrothermique expérimentale, simulations numériques, neutralité carbone, carbone incorporé, efficacité énergétique, tampon d'humidité

EXPERIMENTAL AND NUMERICAL CHARACTERIZATION OF MYCELIUM-BASED BIO COMPOSITES AS BUILDING INSULATION MATERIALS

Seyedsina MOTAMEDI

ABSTRACT

This thesis introduces and characterizes mycelium-based composites (MBCs) through multi-scale experimental and numerical analyses. These composites combine plant aggregates with a fungal matrix, creating a natural insulation material with net-zero carbon potential. For practical applications in building envelopes, a detailed understanding of their hygrothermal properties is crucial, as thermal and moisture behaviors are strongly interdependent. An integrated analysis of heat and moisture transfer, including property measurement, correlation analysis, and simulation, was therefore undertaken.

Research gaps remain in the measurement covering the spectrum of hygric behavior, in their relevance to thermal and microstructural properties, and in the development of numerical models that incorporate sorption–desorption patterns, hysteresis, and coupled heat–mass transfer. To address this, a three-stage methodology was applied. First, fabrication trials explored substrates, fungi, additives, and processing methods to optimize homogeneity and fungal growth, considering the compatibility of constituents such as the cellulose-lignin composition of the substrate, their interaction with mycelium, and the types of incorporated mycelium and additives. Second, experimental campaigns evaluated insulation performance, moisture buffering, thermal conductivity, and selected microstructural properties. Third, a coupled heat and mass transfer model was implemented in COMSOL, with sorption models calibrated using the experimental results and validated against the measured moisture buffer value (MBV), an index that quantifies a material's capacity to moderate indoor humidity fluctuations. Both isothermal and non-isothermal simulations, including hysteresis effects, were performed.

The results confirm the suitability of MBCs as sustainable replacements for carbon-intensive insulation materials such as Styrofoam. The developed fabrication practices, the obtained range of experimental results, and the highly accurate and reliable numerical model provide a foundation for future research on alternative formulations and performance predictions under diverse climatic and envelope conditions.

Keywords: Bio-based materials, insulation, experimental hygrothermal characterization, numerical simulations, carbon neutrality, embodied carbon, energy efficiency, moisture buffer

TABLE OF CONTENTS

Page

LIST OF TABLES

Page

LIST OF FIGURES

Page

LIST OF ABBREVIATIONS

AKD	Alkyl Ketene Dimer
ANOVA	Analysis of Variance
CAD	Computer-Aided Design
CNF	Cellulose Nanofibrils / Cellulose Nano Fibers
CO_2-eq	Carbon Dioxide Equivalent
DIW	Direct Ink Writing
DVS	Dynamic Vapor Sorption
EPS	Expanded Polystyrene / Extruded Polystyrene
EU	European Union
FLC	Flax Lime Concrete
GAB	Guggenheim, Anderson and de Boer
GHG	Greenhouse Gas / Greenhouse Gas Emission
GHOP	*Ganoderma lucidum*, Hemp, Without Additive, Pasteurized
GHOPC	*Ganoderma lucidum*, Hemp, Without Additive, Pasteurized, Cylindrical
GHOPC-MBV	*Ganoderma lucidum*, Hemp, Without Additive, Pasteurized, Cylindrical, fabricated for the MBV test

GHOPR	*Ganoderma lucidum*, Hemp, Without Additive, Pasteurized, Rectangular
GHOPR-L	*Ganoderma lucidum*, Hemp, Without Additive, Pasteurized, Rectangular, Large size
GHWP	*Ganoderma lucidum*, Hemp, With Additive, Pasteurized
GHOS	*Ganoderma lucidum*, Hemp, Without Additive, Sterilized
GHOSC	*Ganoderma lucidum*, Hemp, Without Additive, Sterilized, Cylindrical
GHOU	*Ganoderma lucidum*, Hemp, Without Additive, Unpasteurized
GHOUC	*Ganoderma lucidum*, Hemp, Without Additive, Unpasteurized, Cylindrical
GHOUR-L	*Ganoderma lucidum*, Hemp, Without Additive, Unpasteurized, Rectangular
GHWPR	*Ganoderma lucidum*, Hemp, With Additive, Pasteurized, Rectangular
GHWU	*Ganoderma lucidum*, Hemp, With Additive, Unpasteurized
GHWUC	*Ganoderma lucidum*, Hemp, With Additive, Unpasteurized, Cylindrical
GHWUR	*Ganoderma lucidum*, Hemp, With Additive, Unpasteurized, Rectangular
GHWS	*Ganoderma lucidum*, Hemp, With Additive, Sterilized
GHWSC	*Ganoderma lucidum*, Hemp, With Additive, Sterilized, Cylindrical
GMOS	*Ganoderma lucidum*, Miscanthus, Without Additive, Sterilized
GMWS	*Ganoderma lucidum*, Miscanthus, With Additive, Sterilized
GSOS	*Ganoderma lucidum*, Straw, Without Additive, Sterilized

GSOSC	*Ganoderma lucidum*, Straw, Without Additive, Sterilized, Cylindrical
GSWP	*Ganoderma lucidum*, Straw, With Additive, Pasteurized
GSWPC	*Ganoderma lucidum*, Straw, With Additive, Pasteurized, Cylindrical
GSWPR	*Ganoderma lucidum*, Straw, With Additive, Pasteurized, Rectangular
GSWS	*Ganoderma lucidum*, Straw, With Additive, Sterilized
HAM	Heat, Air, Moisture
ILUC	Indirect Land Use Change
IUPAC	International Union of Pure and Applied Chemistry
LCA	Life Cycle Assessment
LCZEB	Life Cycle Zero Energy Building(s)
LHC	Lime Hemp Concrete
MAPE	Mean Average Percentage Error
MBV	Moisture Buffer Value
MBC	Mycelium Bio-Composite / Mycelium-Based Composites
MDF	Medium Density Fiber / Medium Density Fiberboard
PDE	Partial Differential Equation
PHBH	Poly(3-hydroxybutyrate-co-3-hydroxyhexanoate)

PIR	Polyisocyanurate
PLA	Polylactic Acid
PVA	Polyvinyl Alcohol
PVC	Polyvinyl Chloride
R&D	Research and Development
RH	Relative Humidity
SEM	Scanning Electron Microscopy
SSE	Sum of Squares Error
TPS	Transient Plane Source
UTS	Ultimate Tensile Strength
UV	Ultraviolet
VHOP	*Trametes versicolor*, Hemp, Without Additive, Pasteurized
VHOPC	*Trametes versicolor*, Hemp, Without Additive, Pasteurized, Cylindrical
VHOS	*Trametes versicolor*, Hemp, Without Additive, Sterilized
VHWS	*Trametes versicolor*, Hemp, With Additive, Sterilized
VSOP	*Trametes versicolor*, Straw, Without Additive, Pasteurized
VSOPC	*Trametes versicolor*, Straw, Without Additive, Pasteurized, Cylindrical

VSOS	*Trametes versicolor*, Straw, Without Additive, Sterilized
XPS	Extruded Polystyrene
ZEB	Zero Energy Building(s)

LIST OF SYMBOLS

A	Surface Area, m^2
A_c	Absorption coefficient of water, $kg \cdot m^{-2} \cdot s^{-1/2}$
b_m	Mositure effusivity, $kg \cdot m^{-2} \cdot s^{-1/2} \cdot Pa^{-1}$
C_p	Specific heat capacity, $J \cdot kg^{-1} \cdot K^{-1}$
C_{p_m}	Average specific heat capacity, $J \cdot kg^{-1} \cdot K^{-1}$
d_p	Penetration depth of the moisture in MBV test, m
$D_{l,w}$	Liquid diffusion coefficient as a function of moisture content, $m^2 \cdot s^{-1}$
D_{vT}	Vapor transport coefficient under a temperature gradient, $kg \cdot m^{-2} \cdot s^{-1} \cdot K^{-1}$
$D_{v,w}$	Vapor diffusion coefficient as a function of moisture content, $m^2 \cdot s^{-1}$
$D_{v,\varphi}$	Vapor diffusion coefficient as a function of relative humidity, $kg \cdot m^{-1} \cdot s^{-1}$
D_w	Moisture diffusion (in MBV equation), $m^2 \cdot s^{-1}$
D_{ws}	Capillary suction transport coefficient, $kg \cdot m^2 \cdot s^{-1/2}$
D_{wT}	Liquid transport coefficient under a temperature gradient, $kg \cdot m^{-2} \cdot s^{-1} \cdot K^{-1}$
D_T	Mass transport coefficient associated with a temperature gradient, $m^2 \cdot s^{-1} \cdot K^{-1}$
$D_{T,v}$	Vapor transport coefficient associated with a temperature gradient, $m^2 \cdot s^{-1} \cdot K^{-1}$
$D_{T,l}$	Liquid transport coefficient associated with a temperature gradient, $m^2 \cdot s^{-1} \cdot K^{-1}$
D_φ	Moisture transport coefficient associated with relative humidity, $kg \cdot m^{-2} \cdot s^{-1}$

e	Thickness, m
g	Total vapor and liquid flux, $kg \cdot m^{-2} \cdot s^{-1}$
g_v	Vapor flux, $kg \cdot m^{-2} \cdot s^{-1}$
g_l	Liquid flux, $kg \cdot m^{-2} \cdot s^{-1}$
$H(P_c)$	Cumulative function associated with adsorption, [-]
h_c	Thermal convection coefficient, $W \cdot m^{-2}$
h_c	Thermal convection coefficient, $W \cdot m^{-2}$
$h_{M,e}$	Exterior mass transfer coefficients, $kg \cdot m^{-2} \cdot s^{-1} \cdot Pa^{-1}$
$h_{M,i}$	Interior mass transfer coefficients, $kg \cdot m^{-2} \cdot s^{-1} \cdot Pa^{-1}$
$h_{T,e}$	Exterior convective heat transfer coefficients, $W \cdot m^{-2} \cdot K^{-1}$
$h_{T,i}$	Interior convective heat transfer coefficients, $W \cdot m^{-2} \cdot K^{-1}$
L_v	Latent heat of evaporation, $J \cdot kg^{-1}$
$L(P_c)$	Cumulative function associated with desorption, [-]
M_l	Molar mass of water, 0.018, $kg \cdot mol^{-1}$
M_v	Molar mass of water vapor, $kg \cdot mol^{-1}$
n	Open porosity of the material, [-]
P_c	Capillary pressure, Pa
$P_{c,1}$	First reversal points in hysteresis scanning curves, Pa

$P_{c,N}$	Nth reversal points in hysteresis scanning curves, Pa
P_v	Water vapor pressure, Pa
$P_{v,sat}$	Saturation vapor pressure, Pa
$P_{ve,a,e}$	Exterior ambient vapor pressures, Pa
$P_{ve,a,i}$	Interior ambient vapor pressures, Pa
$P_{ve,s,e}$	Exterior surface vapor pressures, Pa
$P_{ve,s,i}$	Interior surface vapor pressures, Pa
q	Heat flux density, $W \cdot m^{-2}$
Q	Average heat flux (between two plates in heat flux meter test), J
$Q_{st}(u)$	Molar isosteric heat of sorption, $J \cdot mol^{-1}$
$q_{st}(u)$	Specific isosteric heat of sorption, $J \cdot kg^{-1}$
R	Gas constant, 8.314, $J \cdot mol^{-1} \cdot K^{-1}$
R_{SI}	Thermal resistance (SI Unit), $m^2 \cdot K \cdot W^{-1}$
R_{US}	Thermal resistance (Imperial unit), $ft^2 \cdot °F \cdot h \cdot BTU^{-1}$
RH_{max}	Maximum relative humidity level, %
RH_{min}	Minimum relative humidity level, %
S	Exposed surface area of the sample, m^2
$S_{ads}(P_c)$	Primary adsorption curves, [-]

$S_{des}(P_c)$	Primary desorption curves, [-]
S_t	Moisture state at step t in hysteresis scanning formulation, [-]
t_p	Duration of MBV test, s
T	Temperature, K
$T_{a,e}$	Ambient air temperatures at the exterior sides, K
$T_{a,i}$	Ambient air temperatures at the interior sides, K
$T_{s,e}$	Surface temperatures at the exterior sides, K
$T_{s,i}$	Surface temperatures at the interior sides, K
u	Moisture content, %
w	Moisture content, $kg \cdot m^{-3}$
w	Width, m
w_f	Free water saturation, $kg \cdot m^{-3}$
α	Thermal diffusivity, $m^2 \cdot s^{-1}$
β	Compressibility, %
δ	Water vapor permeability in air, $kg \cdot m^{-1} \cdot s^{-1} \cdot Pa^{-1}$
δ_p	Water vapor permeability, $kg \cdot m^{-1} \cdot s^{-1} \cdot Pa^{-1}$
θ	Volumic moisture content, $m^3 \cdot m^{-3}$
$\lambda(T, \theta)$	Thermal conductivity as a function of temperature and moisture content, $W \cdot m^{-1} \cdot K^{-1}$

μ	Water vapor diffusion resistance factor in dry condition (3-50% RH), [-]
μ^*	Water vapor diffusion resistance factor in dry condition (50-93% RH), [-]
ξ_ϕ	Slope of the sorption isotherm, kg·m^{-3}
ρ_w	Density of water, kg·m^{-3}
ρ_0	Dry density of the material, kg·m^{-3}
ϕ	Relative humidity, %
$\phi_{rad,e}$	Exterior radiative heat fluxes, W·m^{-2}
$\phi_{rad,i}$	Interior radiative heat fluxes, W·m^{-2}

INTRODUCTION

Problem Statement

The construction industry is a major contributor to global energy consumption and greenhouse gas (GHG) emissions, making it a critical sector for implementing sustainability measures. Traditional approaches have primarily focused on improving the operational energy efficiency of buildings, often neglecting the significant embodied energy within building materials themselves. This embodied energy, along with associated GHG emissions, can constitute a significant portion of a building's total environmental impact, exceeding 30 % in certain instances. Therefore, addressing both operational and embodied energy is essential for achieving comprehensive energy efficiency and sustainability in the construction sector.

In recent years, there has been a growing interest in bio-based building materials that offer lower embodied energy and environmental impacts compared to conventional materials like concrete and steel. These bio-based materials, including mycelium bio-composites (MBCs), present a promising solution due to their low toxicity, durability, and minimal processing requirements. MBCs are innovative materials created by combining fungal mycelium with organic substrates such as agricultural and forestry residues. The mycelium acts as a natural binder, growing through and around the substrate particles to form a cohesive, lightweight, and insulating composite material.

Effective insulation is critical for reducing the operational energy demands of buildings, and MBCs have shown significant potential as high-performance insulation materials. However, the full potential of MBCs, particularly in terms of their hygrothermal properties and scalability, remains underexplored. To promote their application and deployment as net-zero building insulation materials, a thorough understanding of their hygrothermal properties is necessary. This includes how these materials interact in different combinations of hygric and thermal conditions, which could directly impact their insulation performance and durability.

Furthermore, numerical models that simulate the interaction of heat and moisture under real-scale conditions, including the wetting and drying cycles and moisture sorption hysteresis of MBCs, have not yet been developed in the literature. Such models are essential for accurately predicting the performance of MBCs in building applications and must be calibrated and validated through experimental data.

Research objectives

In the above-mentioned context, the primary goal of this thesis is to investigate the hygrothermal properties of mycelium bio-composites (MBCs) and develop a numerical model for their application in building insulation. To achieve this overarching goal, the specific objectives are as follows:

1. **Provide a comprehensive literature review:**
   This section involves a thorough review of current research on the fabrication practices and hygrothermal characterization of MBCs. It encompasses an analysis of prior studies focusing on their hygric and mechanical properties, thermal insulation capabilities, and interactions with moisture. The review also addresses scalability and durability as significant challenges in industrial production. It concludes with a detailed table summarizing sample compositions from the reviewed studies and their applications across various industries.

2. **Propose a fabrication methodology:**
   To refine the fabrication methodology of mycelium bio-composites, experimental trials focus on selecting suitable organic substrates and fungal species. This process involves optimizing growth conditions and testing various processing techniques to enhance material properties.

3. **Measure hygrothermal characteristics:**
   Experimental characterization of the hygrothermal behavior of the fabricated mycelium bio-composites is conducted at this step. This includes measuring properties such as thermal conductivity, moisture absorption and desorption rates, and thermal diffusivity under various environmental conditions. The experimental setup will simulate real-world building conditions to ensure the relevance and applicability of the data.

4. **Formulate, implement, and validate a numerical model:**
   Development and validation of a numerical model that simulates the hygrothermal performance of mycelium bio-composites. The model incorporated experimental data to accurately predict how MBCs interact with heat and moisture over time. This involves modeling the material's response to temperature and humidity changes, including wetting and drying cycles. The model was calibrated and validated against the experimental results to ensure its accuracy and reliability.

Thesis structure

The first chapter provides a literature review of the fabrication practices and the subsequent hygrothermal characterization of these composites. Studies on MBCs' scalability and durability have been cited and discussed. Characteristics of mycelium that enable new forms of reconciliation between art and engineering have been reviewed in the last part of this chapter.

The second chapter is dedicated to outlining the fabrication methodology for mycelium-based bio composites MBCs. By refining the composition and customizing that based on their weight, moisture content, and shrinkage, and through trial-and-error it is attempted to achieve optimal characteristics. This meticulous examination provides a comprehensive overview of the fabrication practices which were employed for developing different mixtures of mycelium-based bio composites.

The third chapter focuses on the experimental analysis and characterization of the hygrothermal behavior of the fabricated composites. It first presents the experimental setup, along with their testing protocols. In this chapter, mechanical and hygrothermal properties of the materials have been characterized and correlated with the physical properties of fabricated mixtures. This part facilitates the interpretation of the hygrothermal phenomena and contributes to feeding the numerical simulation models, by providing both calibration inputs and validation results.

Completing the dissertation, the fourth chapter details the numerical model developed using COMSOL. It provides a comprehensive overview of the governing equations incorporated into the numerical simulation to model the interdependence of heat, air, and moisture (HAM) under various boundary conditions. The chapter presents validated numerical results based on their experimental counterparts. Discrepancies in the results and potential sources of errors are discussed, and the reliability of the numerical model is evaluated.

The thesis ends with classical concluding remarks reminding the context, objectives, and methodology. Then, it reminds the principal results and synthesis. The conclusion ends with several recommendations.

CHAPTER 1

A REVIEW OF MYCELIUM BIO-COMPOSITES AS ENERGY-EFFICIENT SUSTAINABLE BUILDING MATERIALS

Abstract

The increasing demand for sustainable building solutions has directed attention toward bio-based materials, among which mycelium bio-composites (MBCs) have emerged as promising alternatives to traditional insulation materials. Grown from fungal mycelium and lignocellulosic waste, MBCs offer low embodied energy, biodegradability, and effective hygrothermal performance. This review assesses the current state of the art in MBC fabrication and hygrothermal properties, encompassing both laboratory-scale and industrial methods. MBCs demonstrate thermal conductivity values in the range of 0.036–0.06 $W \cdot m^{-1} \cdot K^{-1}$, moisture buffering capacity comparable to plant-fiber composites, and up to 70% lower embodied carbon than conventional materials. Key challenges are identified, including process standardization, scalability, and durability under real-world conditions. These composites also offer moisture buffering, compostability, and design flexibility. Moreover, recent advancements in additive manufacturing and microstructural optimization suggest a path toward broader adoption of MBCs in construction. By highlighting critical technical and scientific developments, this review identifies targeted research priorities, including the development of standardized fabrication protocols, quantitative lifecycle assessment of MBCs across varying climates, and strategies to scale up production while maintaining mechanical and hygrothermal consistency.

1.1 Introduction

Improving energy efficiency, lowering embodied energy, and reducing greenhouse gas emissions is nowadays becoming the key issue in all sectors. In particular, the construction sector is one of the most energy-consuming industries (Moussa et al., 2018) and therefore, one of the biggest contributors to GHG emissions (Khasreen et al., 2009). Today, there is a strong

effort to meet increasingly stringent energy efficiency criteria, which is essential for the environment and global sustainability (Jansson et al., 2013; Pan et al., 2015). The building sector contributes significantly to mankind's environmental footprint (Takano et al., 2014). Buildings are responsible for 40 % of energy consumption and 36 % of carbon emissions in the EU (Jones & Brischke, 2017). In 2020, residential buildings accounted for 14 % of Canada's total energy consumption, while commercial and institutional buildings accounted for 13 % (Canada Energy Regulator, 2023).

A key feature of sustainable buildings is energy efficiency, both during operation and throughout the lifecycle of each component. Historically, sustainability measures have focused on operational energy, but a full life cycle analysis provides a more comprehensive view of a building's total energy use and GHG emissions. Embodied energy, often overlooked, can account for 10–30 % of a building's total carbon emissions (Beccali et al., 2013; Cuéllar-Franca & Azapagic, 2012; Lawrence, 2015). Thus, it requires an exhaustive approach when it comes to the study of the life cycle of materials and their embodied energy, as well as their corresponding associated GHG emissions.

There is a growing shift in the construction sector toward bio-based, low-embodied-energy, and locally sourced materials. Compared to conventional materials like concrete, steel, and plastics, these alternatives offer lower toxicity, high durability, low emissions, strong recyclability, and minimal processing requirements (Joseph & Tretsiakova-McNally, 2010). In other words, moving from zero energy buildings (ZEB) to life-cycle ZEBs (LCZEB) is seen as a key strategy to address sustainability issues (Dutil et al., 2011). Therefore, selecting building materials should involve evaluating their entire lifecycle and prioritizing those with minimal environmental impact (Joseph & Tretsiakova-McNally, 2010).

Materials such as hempcrete and flax-lime composites have already entered niche markets; however, challenges remain regarding scalability, mechanical strength, and moisture durability. A major barrier to adoption is balancing environmental benefits with performance metrics, including thermal resistance and structural viability at scale. Additionally, many rely

on energy-intensive binders like lime, which undermine their sustainability. A recent review of crop-based materials reported favorable thermal conductivity (0.04–0.12 $W \cdot m^{-1} \cdot K^{-1}$) and moisture buffering capacity for options like hempcrete and straw, while identifying mycelium-based composites as promising but underdeveloped. This highlights the need for further research on fabrication consistency, long-term performance, and structural applicability (Motamedi et al., 2023).

Mycelium bio-composites (MBCs) are an emerging class of crop-based materials that use fungal mycelium as a natural binder. Cultivated from lignocellulosic waste and fungal strains, these composites exhibit low environmental impact and favorable thermal properties. Beyond their environmental benefits, mycelium bio-composites also contribute to energy performance goals in the building sector. Due to their inherently low embodied energy and strong thermal insulation capabilities, MBCs can support both passive heating and cooling strategies. This dual benefit—lowering both operational and material production energy— positions MBCs as strong candidates for energy-efficient and net-zero buildings. Recent studies have further demonstrated the effectiveness of bio-based insulation materials—such as MBCs—in climate-responsive net-zero building design, particularly when combined with shading and roof vegetation strategies (Es-sakali et al., 2025).

The specific interest in these materials is rooted in their three-dimensional structure, which grows on a base substrate typically composed of residues of other agricultural and forestry materials (Cerimi et al., 2019; Stelzer et al., 2021). Despite growing interest, MBCs face significant technical challenges. These include variability in mechanical and hygrothermal properties, absence of standardized fabrication protocols, and sensitivity to moisture, which can compromise durability. Additionally, most experimental studies are conducted at lab scale, and methods for reliable industrial-scale production are still under development. In the literature, research on bio-based materials typically falls into four categories: environmental impacts, thermo-hygro-mechanical characteristics, social aspects and economic feasibility, and affordability (Gorse et al., 2016).

While recent studies have explored various aspects of MBC fabrication and performance, there is limited synthesis connecting fabrication methods and microstructural development to hygrothermal and mechanical behavior, particularly in the context of real-world building applications aimed at evaluating their suitability as net-zero carbon insulation materials. Furthermore, existing literature often treats lab-scale and industrial practices separately, without bridging them to material performance outcomes or assessing their potential for real-world implementation. This review fills that gap by articulating a clear framework that links fabrication parameters to thermal and moisture performance and evaluating key barriers to scalability and long-term durability.

This paper presents a two-fold review: first, it surveys recent advances in MBC fabrication—including traditional molding and emerging 3D printing techniques, highlighting the influence of fungal species, substrates, and processing conditions. Second, it examines hygrothermal performance data, such as thermal conductivity, water absorption, and vapor permeability, in relation to microstructural characteristics. By linking fabrication parameters with material properties, the review aims to identify key enablers and barriers to the effective deployment of MBCs as building insulation.

The paper is organized as follows: Section 2 details the review methodology. Section 3 reviews lab-scale and industrial-scale fabrication techniques. Section 4 addresses issues related to scalability and durability. Section 5 focuses on the mechanical and hygrothermal characterization of MBCs, including recent insights into microstructural effects. The review concludes with a synthesis of findings and recommendations for future research.

1.2 Review methodology

This review focuses on two primary aspects: the fabrication techniques reported in the existing literature and the comprehensive thermo-hygro-mechanical characterization. Its main objective is to assess the technical feasibility of mycelium-based building materials for use in modern construction. This evaluation focuses on their physical properties and potential to

replace energy-intensive conventional materials. The study spans a wide range of MBCs, from basic formulations to advanced agglomerates and fabrication methods, demonstrating their suitability for use in construction.

The search strategy incorporated thematic keywords across three categories:
(i) Material and fabrication technologies: mycelium-based building materials, extrusion, 3D printing, robotic manufacturing, modular growth;
(ii) Performance and characterization: thermal conductivity, thermal resistance, thermal effusivity, moisture buffering, vapor permeability, mechanical strength, fire resistance, durability;
(iii) Sustainability and application context: embodied energy, low-carbon materials, energy efficiency, regenerative design, life cycle assessment (LCA), scalability, and standardization.
Geographical limitations are not imposed, although the primary focus pertains to Europe and North America, both for technical advancements and industry standards. Within the category of physical characteristics, studies with similar properties are filtered based on material proximity and specific experimental methods.

The review was carried out in a three-step process:

- Titles and abstracts of the retrieved studies are screened, focusing on embedded concepts, keywords, and specific terms. The 80 reviewed references were retrieved primarily from peer-reviewed databases, with the majority published by MDPI (25 %) and Elsevier (16.25 %). Additional sources include ACS, Springer, Nature Publishing Group, IEEE, Wiley, and Taylor & Francis, with 37.5 % of sources categorized as grey literature or unclassified.
- Then, the full texts of the selected studies from Step 1 were reviewed to extract detailed data, considering parameters including physical characteristics, replacement of traditional energy-intensive building materials, and their contribution to regenerative design and waste valorization. A short and relevant description and a reference for each contribution were written at that stage. Numerous mycological and biological

references pertain to mycelium, yet they fall outside the purview of this review, and, as such, are omitted from the study's scope.

- At the final step, a qualitative assessment of the data extracted from stage 2 was conducted to identify common themes, trends, and knowledge gaps. The reviewed literature was synthesized under two main topics: Fabrication of Mycelium Bio-Composites, which includes lab-scale processes, industrial production methods, additive manufacturing, and scalability; and Performance Characterization of MBCs, covering mechanical properties, hygrothermal behavior, durability, fire resistance, and environmental impact.

1.3 Fabrication of mycelium bio-composites: from lab to industry

1.3.1 Laboratory methods

MBC development is based on a controlled laboratory process that allows researchers to tailor material performance through substrate selection, fungal growth, and process optimization. In laboratory settings, MBCs are generally produced by cultivating filamentous fungi that grow dense mycelial networks over lignocellulosic substrates (Stelzer et al., 2021). The core fabrication stages, sterilization, inoculation, and incubation, are broadly standardized across studies, although variations are employed to fine-tune material properties. As shown in Figure 1.1, these stages are often supplemented by molding, pre-compression, and post-incubation drying, each step contributing to specific mechanical or hygrothermal characteristics (Elsacker et al., 2019). The images in section (c) of the figure are from the authors' own fabrication campaign for MBCs, which were subsequently characterized and presented in (Motamedi et al., 2025).

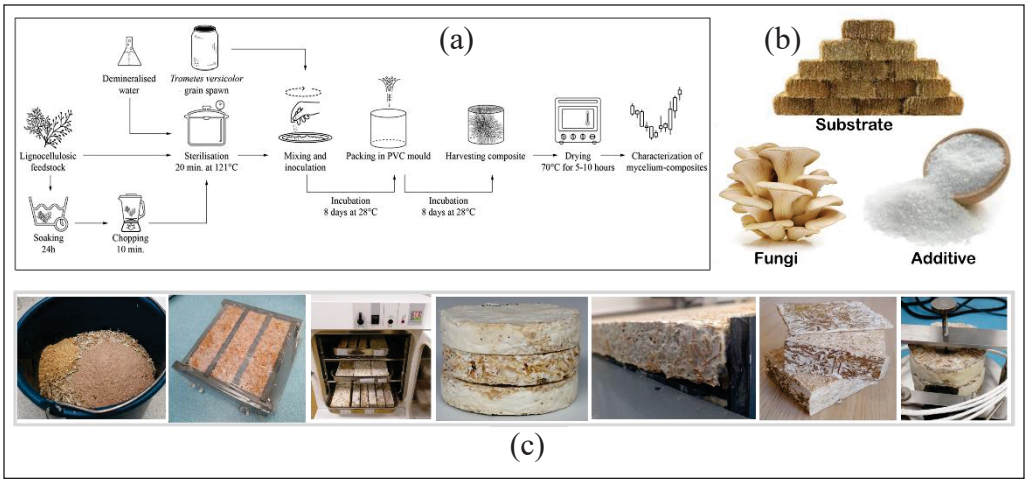

Figure 1.1 (a) Step-by-step fabrication process of mycelium bio-composites (reproduced from Elsacker et al. (2019) ;(b) primary constituents; (c) representative images showing the process from raw materials to fully grown samples
Part (a) taken from Elsacker et al. (2019, p. 5)

Figure 1.1a illustrates the fabrication process of MBCs, which begins with soaking, chopping, and sterilizing lignocellulosic feedstock prior to inoculation with grain spawn. The inoculated substrate is packed into PVC molds and incubated at 28°C for two 8-day cycles to ensure full colonization. After harvesting, the samples are dried at 70 °C for 5–10 hours. The accompanying photos depict: (b) the constituent materials; and (c) the progression from raw materials to finished samples.

A detailed three-stage cultivation strategy was described by Stelzer et al. (2021) and Meyer et al. (2020). The process begins with agar-based fungal inoculation in a pre-culture medium, followed by a secondary inoculation on a sterilized intermediate substrate (e.g., rye), and culminates in the colonization of a final substrate, such as hemp shiv. This multistage approach enhances fungal distribution and composite uniformity. Escobar and Laibach (2021) emphasized that substrate selection, fungal species, and processing technique play a critical role in determining the mechanical and hygric behavior of the final material.

Barta et al. (2024) demonstrated that cellulose-rich feedstocks like straw promote rapid mycelial colonization and denser composite structures. The selection of fungal strain has also

been shown to significantly influence growth consistency and final properties. Nussbaumer et al. (2023) compared *Trametes versicolor* and *T. pubescens*, revealing that strain-specific growth patterns affect mechanical properties and that post-growth pressing improves uniformity only in some strains. Their findings underscore the importance of aligning strain morphology with fabrication and post-processing protocols.

Camilleri et al. (2025) further emphasized the lack of standardization in lab-scale methods and its contribution to inconsistencies in structure and performance across studies. They advocate for tighter control of process parameters and the development of reproducible protocols during sterilization, inoculation, and incubation phases. Mohseni et al. (2023) proposed a comparative framework outlining key fabrication steps, from autoclave sterilization to incubation in humid, sterile containers, highlighting the critical importance of contamination control during colonization.

1.3.2 Additive manufacturing

Beyond traditional mold-based fabrication, additive manufacturing is reshaping how MBCs are scaled and formed. Scott et al. (2022) proposed a hybrid method that combines knitted wool scaffolds with mycelium and bacterial cellulose, enabling precise growth through parametric modeling. This approach enhances structural strength and imparts water resistance, although substrate uniformity remains a challenge. To address such limitations, paste-like agglomerates have been suggested as alternatives to fibrous substrates, offering better consistency (Attias et al., 2020; Elsacker, Søndergaard, et al., 2021; Jones et al., 2017).

Meanwhile, extrusion-based 3D printing has emerged as a mold-free fabrication route for MBCs. Structure optimization through Direct Ink Writing (DIW) and material extrusion enables control over composition and porosity, allowing the creation of functionally graded, multi-material mycelium structures. Teoh et al. (2024) demonstrated that nutrient-modified inks can guide fungal growth spatially, resulting in tailored mycelial density and microstructures, which support localized property tuning and multi-scale reinforcement. Soh

et al. (2023) developed a waste-based agar ink suitable for non-sterile environments, using coffee grounds to increase compressive strength and reduce contamination risk. Luo et al. (2025) developed a “Mycofluid” ink using coffee grounds and rice flour, enabling 3D-printed composites that fully colonize in non-sterile environments and exhibit strong mechanical performance and compostability after drying. Figure 1.2 depicts this 3D printing process and the composition of the fungal paste. Rahman et al. (2022) optimized extrusion timing for improved print quality, while Soh et al. (2020) enhanced mechanical properties by incorporating bamboo microfibers. Bhardwaj et al. (2020) added psyllium husk to stabilize the ink and prevent nozzle clogging.

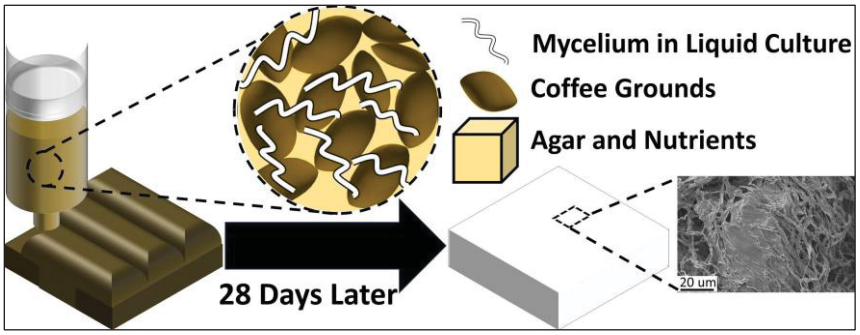

Figure 1.2 Schematic of 3D printing process
Taken from Soh et al. (2019, Graphical Abstract)

This figure illustrates the 3D printing process using the waste-based ink. The formulation composed of liquid-cultured mycelium, coffee grounds, agar, and nutrients. After 28 days, the printed structure becomes fully colonized, resulting in a cohesive composite. The Scanning Electron Microscopy (SEM) image confirms the formation of a dense mycelial network within the material.

To address the limitations of mold-based growth and enhance structural control, Soh et al. (2023) optimized printing parameters for their mycelium-based ink to improve resolution, consistency, and mycelial colonization across complex geometries. Figure 1.3 depicts the impact of these optimizations on print quality and fungal development.

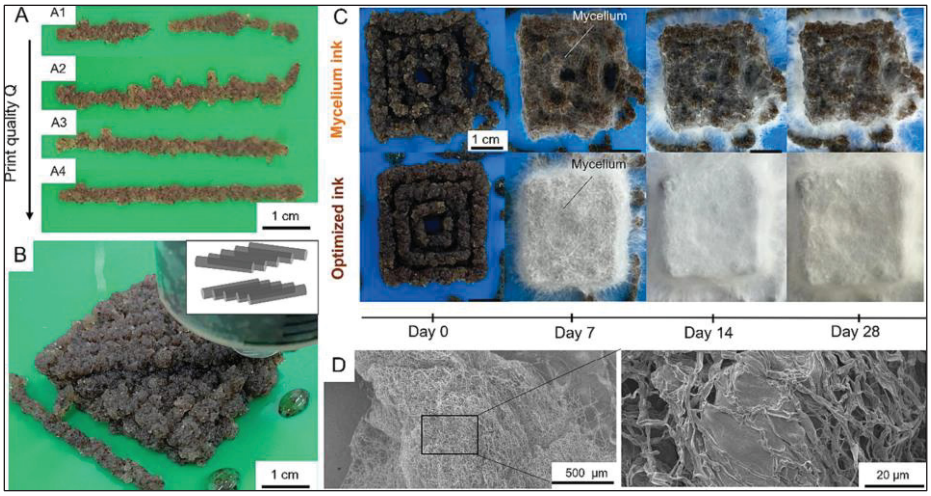

Figure 1.3 3D printing and mycelium growth; (A) Pictures of 3D printed filaments using the mycelium ink with varying printing parameters (A1 – A4) showing improvement in the print quality; (B) Picture and schematics of a 3D printed multi-layered lay-up structure; (C) Optical images of square patterned block prints using mycelium and optimized inks over 28 days; (D) Electron micrographs of mycelium growth on printed optimized ink for 28 days
Taken from Soh et al. (2019, p. 8)

Optimized printing parameters and ink formulations improve the definition, structural integrity, and mycelial colonization of 3D-printed composites. The improved ink enabled uniform fungal growth and denser mycelial networks, as confirmed by SEM imaging. Together, knitting-based and 3D-printed methods offer distinct advantages: the former offers design flexibility suited to architectural components, while the latter improves scalability and production efficiency. Both contribute to expanding the role of mycelium composites as practical, eco-friendly materials for diverse design and construction applications.

Regarding the effect of additive manufacturing on the properties of the material, Chen et al. (2024) reinforced planar mycelium mats by 3D-printing thin layers of biopolymers (PHBH or PLA) onto them, resulting in significant improvements of tensile performance. The pure mycelium mat had an ultimate tensile strength (UTS) of approximately ~0.65 MPa and Young's modulus ~4.5 MPa, but printing a PLA lattice raised the UTS nearly fivefold (to ~3.1 MPa) and stiffness ~30-fold (to ~136 MPa). Even a biodegradable PHBH pattern produced a ~70 % UTS increase (to ~1.1 MPa). The authors further highlight that altering line spacing or

using auxetic infill patterns can redistribute stress and further improve both strength and toughness. Wang et al. (2024) developed a lightweight entangled network composite where mycelial hyphae interweave with a PVA polymer phase, achieving a high specific strength of 8.15 $MPa \cdot cm^3 \cdot g^{-1}$. Notably, the material exhibits 90 % strength recovery after self-healing through mycelial regrowth across cracks.

3D-printed mycelium structures demonstrate improved hygric and thermal performance due to their tunable porosity and the intrinsic chemistry of fungal biomass. Their porous architecture enables effective thermal insulation, achieving densities as low as 0.12 $g \cdot cm^{-3}$, comparable to conventional foams (Chen et al., 2024). Moisture resistance is also enhanced; surface hydrophobins and post-print treatments contribute to water repellency (Chen et al., 2024). For example, coffee-ground-based mycelium prints exhibit hydrophobic properties (Luo et al., 2025), and entangled mycelium–PVA composites absorb only ~33 % of their weight in water after 15 days—a relatively low value for a bio-based material (Wang et al., 2024). Post-processing methods such as calcium crosslinking further improve dimensional stability in wet conditions, enabling MBCs to buffer moisture effectively without structural degradation (Chen et al., 2024).

Collectively, the cross-study comparison reveals both consistencies and discrepancies in lab-scale experimental approaches. Most lab-scale protocols follow a three-stage inoculation–molding–drying sequence, yet reported uniformity of final samples vary widely. Barta et al. (2024) and Nussbaumer et al. (2023) both confirm that high-cellulose substrates (e.g., straw) accelerate colonization. However, Camilleri et al. (2025) show that without strict sterilization and humidity control, substrate choice alone cannot guarantee uniform growth. Scott et al. (2022) and Bhardwaj et al. (2020) demonstrate that hybrid scaffolds (e.g., knitted textile or 3D-printed paste) can improve form factor and speed, but Mohseni et al. (2023) caution that these novel methods can introduce new sources of contamination or heterogeneity. Overall, these findings suggest a trade-off: purely mold-based growth yields reproducible but geometrically-limited samples, while additive manufacturing routes boost design freedom at the cost of process control.

1.3.3 Industrial-scale production

Over the past decade, industrial-scale MBC production has progressed through scalable fabrication methods, structural enhancements, and commercial initiatives. While the majority of research is still conducted at laboratory scale, several manufacturing techniques demonstrated the potential for integrating MBCs into engineered materials for insulation, furniture, and structural applications.

Sun et al. (2019) introduced two distinct methods for producing hybrid composites, composed of wood particles, mycelium, and cellulose nanofibrils (CNFs). In the first method (Group 1), wood particles are bound exclusively by mycelium growth, leading to high water permeability and dimensional instability. In the second method (Group 2), the addition of CNFs serves as a secondary binder, significantly improving moisture resistance and mechanical performance. As illustrated in Figure 1.4 and Figure 1.5, Group 2 composites demonstrate markedly reduced water adsorption and thickness swelling, offering better long-term dimensional stability. While reduced water uptake may limit performance in applications requiring high moisture buffering, the enhanced structural integrity presents clear advantages for insulation and paneling applications.

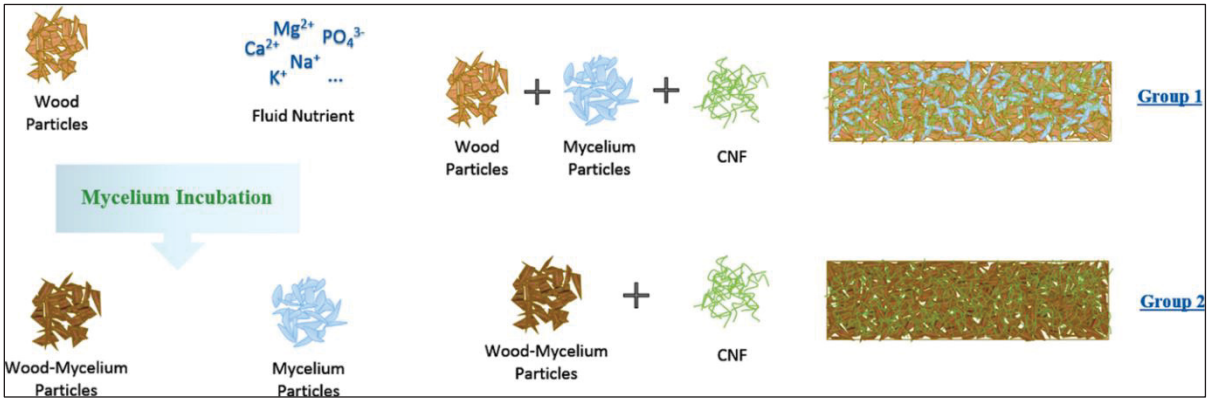

Figure 1.4 Two production methods of mycelium bio-composites; Group 1 involves the direct integration of mycelium with woody particles; Group 2 incorporates cellulose nanofibrils (CNFs) as a binder to improve structural stability and moisture resistance
Taken from Sun et al. (2019, p. 2)

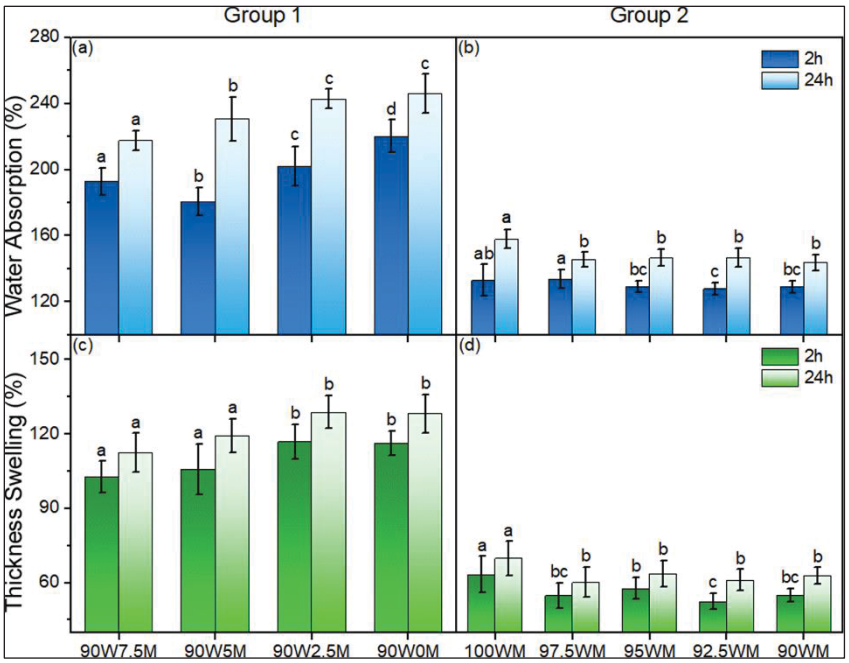

Figure 1.5 (a) Water absorption (%) after 2 h and 24 h for Group 1 composites fabricated with wood particles bound solely by mycelium; (b) Water absorption (%) after 2 h and 24 h for Group 2 composites incorporating cellulose nanofibrils (CNFs) as an additional binder; (c) Thickness swelling (%) after 2 h and 24 h for Group 1 composites; (d) Thickness swelling (%) after 2 h and 24 h for Group 2 composites. W and M on the horizontal axis represent the percentage of wood and mycelium in different fabricated samples. The letters "a", "b", "c", "ab" and "bc" indicate statistically significant groupings based on ANOVA and Tukey's HSD test ($p < 0.05$)
Taken from Sun et al. (2019, p. 6)

Jiang et al. (2017) developed sandwich-structured composites consisting of a mycelium core, textile skins (e.g., jute or hemp), and a bio-resin matrix. They observed that the stiffness of the resulting panels was primarily influenced by the colonization density of the mycelium, while the tensile strength was determined by the textile skin. Their manufacturing workflow (Figure 1.6) integrates conventional composite fabrication techniques with the biological growth phase characteristic of MBCs. The process includes gluing, mold filling with pre-colonized substrate, incubation for growth, drying, and resin infusion, as illustrated in Figure 1.6.

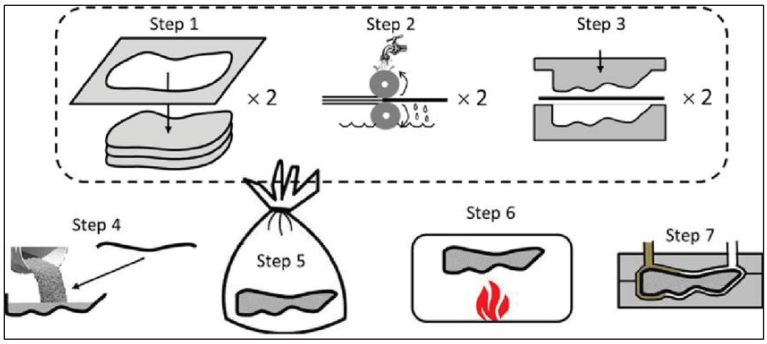

Figure 1.6 The manufacturing process of mycelium fiber composites
Taken from Jiang et al. (2017, p. 52)

1.3.4 Scalability of production

The scalability of MBCs depends on their ability to be adapted for both digital design and modular fabrication. Attias et al. (2020) illustrated this potential of MBCs through two design-driven case studies, an insulating container shell and a modular architectural unit, fabricated using CAD-based mold design and local agricultural waste. Their study not only showcases the feasibility of reproducible, large-scale geometries but also underscores the role of MBCs in integrating sustainable materials into contemporary industrial design workflows (Figure 1.7). These examples highlight how mycelium composites can be designed and fabricated at multiple scales with reproducible geometry and minimal environmental impact.

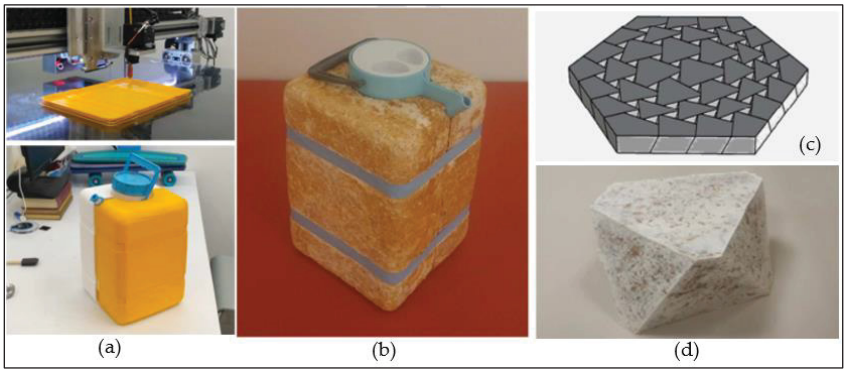

Figure 1.7 (a) Scalable production practice of mycelium; (b) CAD-aided industrial design; (c) CAD-aided architectural design; (d) unit element
Adapted from Attias et al. (2020, p. 14)

Scalability remains a significant barrier to widespread MBC commercialization. As emphasized by Alaneme et al. (2023), the biological nature of MBC production, where materials are "grown" rather than assembled, makes the process inherently time- consuming and sensitive to environmental fluctuations. Their review identifies key limitations to scaling, including contamination risks, variability in fungal growth, and the lack of standardized protocols across fabrication methods such as molding, additive manufacturing, and hybrid composites. These factors lead to inconsistency in material performance, thereby undermining reproducibility at industrial scales. Additionally, restricted access to proprietary fabrication techniques, held by companies such as Ecovative, Green Island, New York, USA and MycoMaterials, Green Island, New York, USA, limits innovation and impedes the development of scalable, open-source solutions.

Bitting et al. (2022) reviewed the limitations to MBC upscaling and noted that inconsistencies in density, strength, and surface quality often prevent these materials from meeting industry certification standards. They identified variability in environmental conditions such as temperature, humidity, airflow, as key contributors to structural inconsistency in the structure of the material. Wattanavichean et al. (2025) similarly noted that without standardized growth conditions, ensuring the mechanical reliability of MBCs at scale becomes difficult.

Efforts to address these challenges are being led by companies such as Ecovative and Biohm, which apply genetic engineering, strain refinement, and the incorporation of supplementary microorganisms into the production process. Moreover, Shin et al. (2025) reported efforts to genetically optimize fungal strains to improve growth rate, colonization uniformity, and bonding strength. These advancements, combined with supplementary microbial consortia, have improved batch-to-batch consistency and predictability.

Elsacker, Søndergaard, et al. (2021) proposed a modular and robotic hybrid approach to scalability, combining layered fabrication, robotic wire cutting, and the self-healing ability of fungal hyphae to produce larger components (Figure 1.8). Modular growth allows each unit to be optimized and later fused into a larger structure, while robotic cutting ensures design

precision. The biological bonding ability of mycelium at seams enables structural continuity without adhesives, offering a scalable method without compromising material integrity.

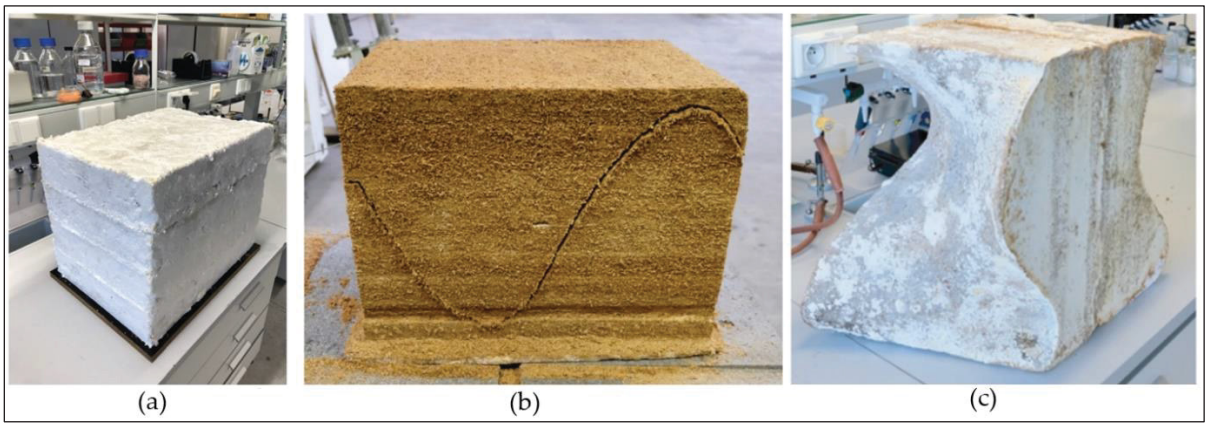

Figure 1.8 Bio-hybrid practice; (a) modular layered fabrication; (b) wire-cutting; (c) self-healed composites
Adapted from Elsacker et al. (2021, p. 12)

As shown above, this figure illustrates the practical outcomes of this bio-hybrid fabrication strategy. Image (a) shows stacked modules grown separately. In (b), precision wire-cutting is used to shape complex geometries directly into the material. Image (c) demonstrates successful biological fusion across segments, highlighting the potential for seamless large-scale components without mechanical fasteners.

1.3.5 Durability

Long-term durability is critical for the integration of MBCs into building applications. A primary concern is their hygroscopic nature, which can lead to moisture absorption, swelling, fungal decay, or degradation of mechanical performance. Post-treatment strategies such as heat drying, surface coatings, and material densification are commonly employed to enhance durability, although these methods often introduce added cost and complexity (Camilleri et al., 2025).

Schultz et al. (2024) further evaluated the performance of mycelium-based composites under accelerated weathering conditions. When subjected to wet-dry and freeze-thaw cycles, the materials maintained mechanical integrity, with only minor surface softening observed in surface layers. Crucially, thermal stability and impact strength remained largely unaffected, which confirms the resilience of MBCs under environmental stress. However, prolonged exposure to uncontrolled humidity can eventually degrade the material. Outdoor trials of mycelium structures showed they remained intact for several weeks, but after four months they developed cracks, decay, pest infestation, and microbial contamination (Gan et al., 2022). These findings indicate that long-term durability without protection is limited, as MBCs will gradually biodegrade under environmental conditions.

Biological degradation is a double-edged sword for MBCs: their compostability aligns with sustainability goals, but it means they are susceptible to breakdown when exposed to prolonged moisture. Soil burial experiments have quantified this susceptibility. For example, mycelium–hemp composite samples lost up to 43 % of their mass after 16 weeks in moist soil, with the mycelial binder decomposing first (Van Wylick et al., 2022). These findings confirm that in a high-humidity or soil-contact environment, mycelium composites will biodegrade within months. Even in less extreme conditions, high relative humidity can encourage mold growth on the material's surface. MBCs' natural fungal origins are prone to "biological corrosion" (mold/mildew) when damp (Camilleri et al., 2025). Ensuring long-term durability thus requires mitigating moisture ingress and biological attack.

Notably, coatings and treatments have proven effective in extending MBC lifespan. Gan et al. (2022) found that applying sustainable protective coatings can slow down degradation. In one case, an *uncoated* mycelium panel had a useful life before biodegrading within 5 months, whereas a coated panel lasted significantly longer. The coated samples resisted moisture uptake and retained mechanical strength for a longer period. Gauvin and Vette (2020) highlighted the low vapor permeability of MBC as a durability concern in insulation. Resin coatings have been widely adopted to mitigate moisture uptake; however, their weak adhesion to the mycelial surface often results in poor long-term performance. The study proposes an alternative

strategy: cultivating engineered dense mycelium structures, either through extended growth cycles or genetic optimization, to inherently reduce porosity and improve hydrophobicity. In simulated climatic aging tests, involving extreme temperature and humidity cycling, the materials exhibited no notable decline in performance, confirming the feasibility of this approach. Applying water-repellent coatings is an effective way to protect MBCs from humidity. Recent studies favor bio-based coatings (to preserve sustainability) such as plant waxes and oils. Farrahnoor et al. (2024) coated mycelium composites with a beeswax–coconut oil blend, drastically reducing water absorption and preventing mold growth. The best-performing coating (80 % beeswax) cut water uptake to 26 % and prevented fungal/mold growth for 36 days, whereas uncoated samples readily grew mold.

Another approach is to combine mycelium with other materials that impart strength or water resistance. Natural polymer additives have shown promise. For instance, researchers have reinforced mycelium composites with bacterial cellulose, a strong biopolymer produced by certain bacteria. Elsacker, Vandelook, et al. (2021), incorporating bacterial cellulose into a mycelium-hemp composite (followed by hot pressing) significantly strengthened the internal bonding of the material. The resulting hybrid had tunable mechanical properties and improved structural integrity. Complementary findings by Alemu et al. (2022) demonstrate that mechanically pressed MBCs, primarily used in furniture applications, demonstrate enhanced durability due to reduced porosity. Nussbaumer et al. (2023) quantified this effect, showing that hot-pressed MBCs derived from *Trametes* species had lower water absorption and higher structural integrity compared to unpressed samples. Additionally, pressing helps collapse pore structures, thus reducing moisture ingress and dimensional instability.

Recent studies have explored how fungal strain selection can improve MBC durability. Certain strains produce thicker, more hydrophobic hyphae, contributing to the development of naturally water-resistant surfaces (Nussbaumer et al., 2023). For example, *Trametes hirsuta* fungus grows a dense, continuous mycelial network that creates a firm outer shell on the composite. This shell was shown to confer remarkable shape stability even when the composite is soaked — remaining flexible and intact in the wet state, unlike a composite made with a

looser mycelium network (*Pleurotus ostreatus*) (Kuribayashi et al., 2022). While promising, this strategy requires further optimization of growth conditions and strain-specific protocols.

Patent analysis by Cerimi et al. (2019) confirms that industry stakeholders are actively pursuing scalable solutions to durability, as evidenced by a growing number of patents focused on densification methods, hybrid matrices, and surface treatments. Collectively, studies in the literature identify key fabrication parameters (Figure 1.9), such as fungal strain, substrate type, growth time, and pressing pressure, that directly influence durability.

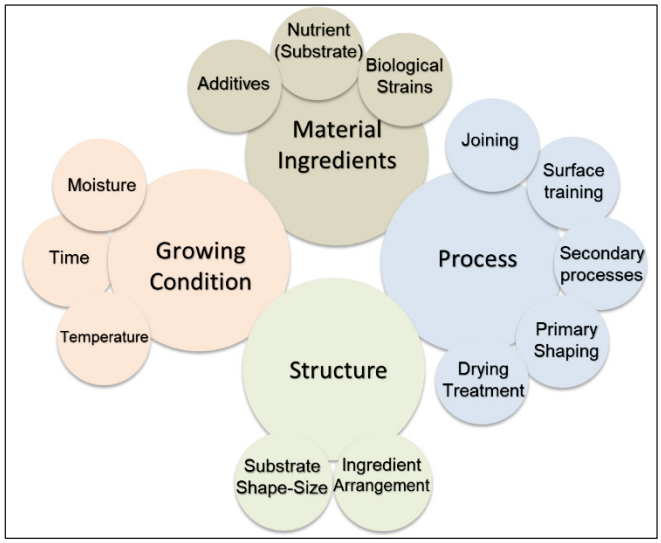

Figure 1.9 Fabrication parameters of mycelium bio-composite
Adapted from Karana (2018, p. 125)

1.3.6 Real-world demonstrations

Several artistic and architectural projects have demonstrated the transition of MBCs from lab research to real-world applications. Recently, mycelium has been employed in full-scale installations by artists. This interdisciplinary convergence is an emerging trend in studies and related projects.

“Grown” architecture enables organic structures with complex geometries that are difficult to build using conventional materials. This approach supports interdisciplinary collaboration, where science informs growth protocols, engineering enables material functionality, and design drives cultural and aesthetic expression.

One of the most notable architectural applications of mycelium is the growing pavilion project (Figure 1.10). It was constructed in Floriade Expo 2022 for the Dutch Design Week. The 10-ton CO_2-equivalent-negative and 95 % circular structure, composed of five bio-based materials: wood, mycelium, agricultural residuals, bulrush, and cotton, presents a visually distinctive form with organic textures and colors. Other full-scale demonstrations, such as MycoTree, developed for the 2017 Seoul Biennale, have explored the structural capabilities of MBCs in load-bearing applications. In that project, a network of bamboo struts and mycelium nodes formed a self-supporting spatial structure. While many current implementations focus on non-load-bearing elements, these examples show the expanding architectural potential of mycelium.

Despite their promise, most MBC-based installations remain temporary and experimental. While the moisture buffering capacity and durability of MBCs are recognized, further investigation is needed on their long-term performance under UV radiation, biological decay, and fluctuating weather conditions. Drawing parallels from other bio-based materials, Es-sakali et al. (2023) reported that hemp-clay bricks maintained significant moisture buffering value (2.25 $g \cdot m^{-2} \cdot \%RH$) and thermal insulation (0.31 $W \cdot m^{-1} \cdot K^{-1}$) even after four years of outdoor exposure without protective treatment. This suggests that with proper formulation and application strategies, bio-based composites like MBCs may also sustain hygrothermal functionality and structural performance over time.

Moreover, building regulations and certification requirements must adapt to accommodate this new class of materials. Nonetheless, these proof-of-concept projects are vital. They validate material behavior at scale, stimulate innovation, and shift public perception around regenerative architecture. As fabrication techniques mature and material consistency improves,

MBCs are likely to move from conceptual showcases to integral components of mainstream sustainable construction.

Figure 1.10 Growing pavilion in Dutch design week

To summarize, the reviewed fabrication techniques—from lab-scale protocols to industrial-scale methods—demonstrate the versatility of MBC production but also highlight significant variation in control, consistency, and scalability. The selection of substrates, fungal strains,

and fabrication routes directly affects both structural and hygrothermal outcomes. The following key points synthesize the main insights from Section 3:

- MBCs can be fabricated through mold-based, additive manufacturing, and industrial hybrid methods, each with trade-offs between reproducibility and geometric complexity.
- Substrate type, fungal strain, and incubation protocols significantly affect mycelial growth and material performance.
- Additive manufacturing offers design flexibility but presents challenges in contamination control and material consistency.
- Industrial-scale production methods increasingly use composite layering, textile reinforcement, and CNFs to enhance structure and moisture resistance.
- Scalability remains constrained by biological variability, IP protection, and lack of standardized growth protocols.

These observations are further summarized in Table 1.1 below, which contrasts lab-scale and industrial-scale MBC fabrication methods across key technical metrics.

Table 1.1 Comparison of lab-scale and industrial-scale MBC fabrication methods, thermal properties, and scalability limitations

Category	Lab-Scale Methods	Industrial-Scale Methods
Typical Techniques	Mold growth, hot pressing, 3D printing	Panel pressing, sandwich composites, modular units
Control & Consistency	High variability; limited standardization	Moderate consistency; early-stage standardization
Microstructural Tuning	High potential (custom molds, SEM studies)	SEM studies) Limited but improving (pressing, additives)
Thermal Conductivity	0.036–0.048 $W \cdot m^{-1} \cdot K^{-1}$ (depending on substrate)	~0.040–0.060 $W \cdot m^{-1} \cdot K^{-1}$ (less optimized)
Scalability	Low (manual processes, contamination risks)	Moderate (batch production, robotic cutting)
Limitations	Inconsistency, contamination, shape limits	Cost, IP protection, production speed

1.4 Performance characterization of MBCs

Mechanical and hygrothermal performance are critical to the suitability of MBCs in building, yet they are rarely evaluated in conjunction. Variations in fungal species, substrate composition, and processing methods allow for the development of composites tailored to a wide range of architectural functions. This section reviews recent studies examining how these factors influence the structural and thermal behavior of MBCs.

1.4.1 Mechanical response to processing methods

Appels et al. (2019) investigated the effects of cold and hot pressing on thermo-physical properties. The results indicate that the tensile strength and elastic modulus of these materials increase significantly under hot pressing compared to cold pressing. The resulting densification shifted the stress–strain behavior from foam-like to cork- and wood-like profiles, underscoring

its impact on mechanical performance (Figure 1.11). The study also suggested that enhancing colonization in the composite's core; e.g., through air injection, could improve consistency and internal bonding.

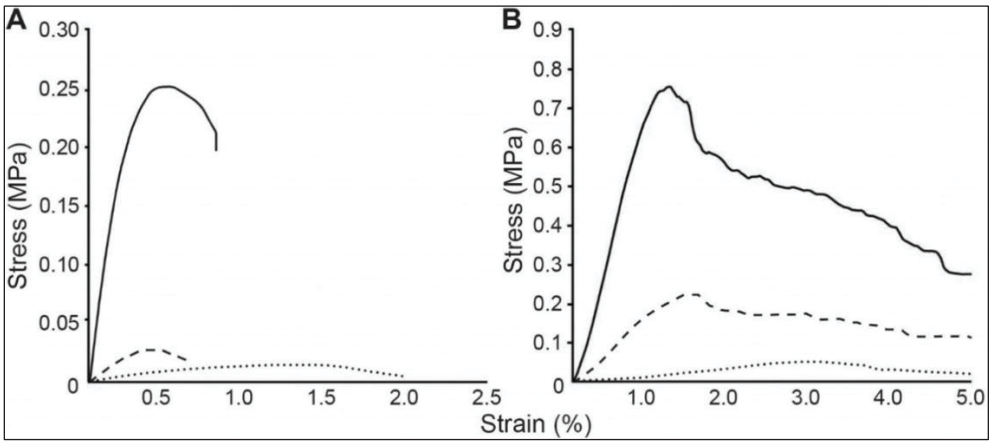

Figure 1.11 Tensile (A) and bending (B) tests of P. ostreatus grown on rapeseed straw without pressing (dotted line), with cold (striped line) or with hot (solid line) pressing
Taken from Appels et al. (2019, p. 68)

Karana et al. (2018) evaluated six mycelium-based composites fabricated under varying levels of compression and compared them to conventional materials such as MDF and cork. Heat-compressed samples exhibited the highest tensile strength, demonstrating that fabrication technique plays a critical role in mechanical optimization (Figure 1.12). Similarly, Lingam et al. (2023) conducted a comprehensive analysis of engineered MBCs, reporting that hot-pressed composites displayed superior compressive and flexural strength, directly attributed to increased density and microstructural integrity.

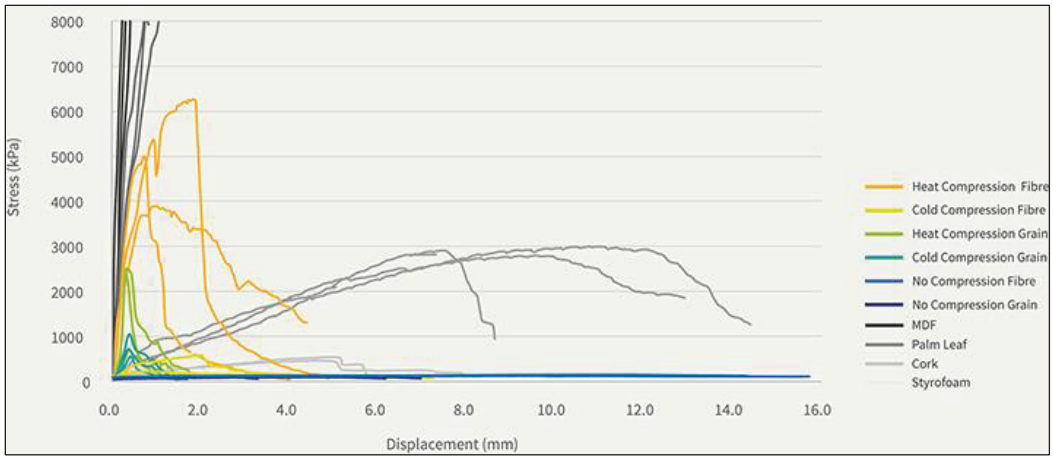

Figure 1.12 Tensile test results of mycelium composites in comparison to the reference materials
Taken from Karana et al. (2018, p. 127)

M. Islam et al. (2018) characterized the mechanical response of MBCs under cyclic compressive loads. The study developed a multiscale model, employing a random fiber network at the microscale, and a continuum model at the macroscale, to investigate density variation and capture its rate of change. The non-linear compressive behavior of the material was successfully characterized through the integration of the two modeling approaches. The results depicted in Figure 1.12 (right hand-side) show strong agreement with experimental measurements.

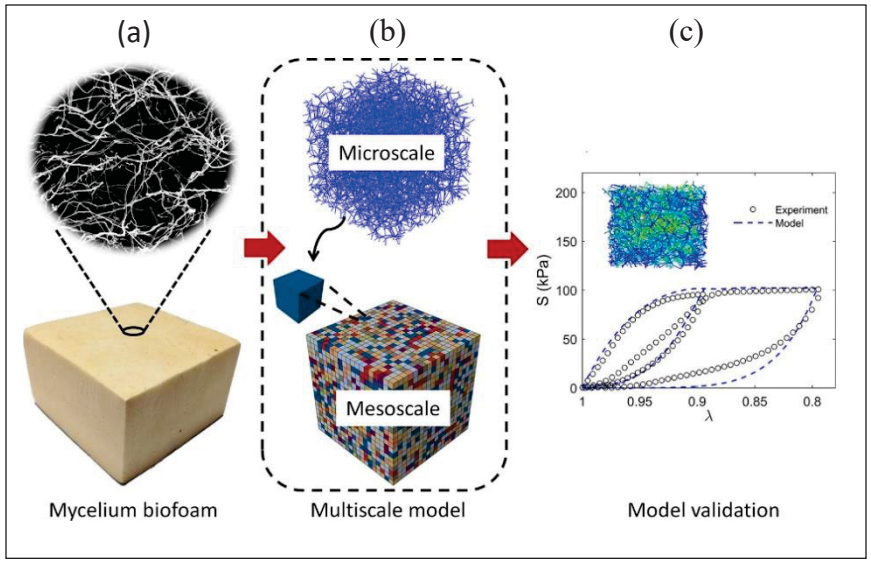

Figure 1.13 (a) Scanning electron micrograph of mycelium biofoam showing its filamentous hyphal network; (b) Multiscale modeling framework linking a microscale fiber network to a mesoscale stochastic continuum representation; (c) Model validation: simulated stress–stretch response (dashed blue line) compared to experimental data (black circles), with inset showing a mesoscale simulation snapshot
Taken from M. Islam et al. (2018, p. 549)

1.4.2 Hygrothermal behavior

Water absorption and vapor permeability are critical factors influencing both the durability and insulation performance of MBCs. Attias et al. (2019) measured water adsorption capacity (Figure 1.14) across three MBCs produced using different fungal species grown on vine and apple wood substrates. Their comparative analysis revealed that the pairing of fungal strain and substrate significantly impacts both density and water absorption behavior, emphasizing that tailored biological inputs can be used to optimize the hygrothermal performance of MBCs for specific building applications.

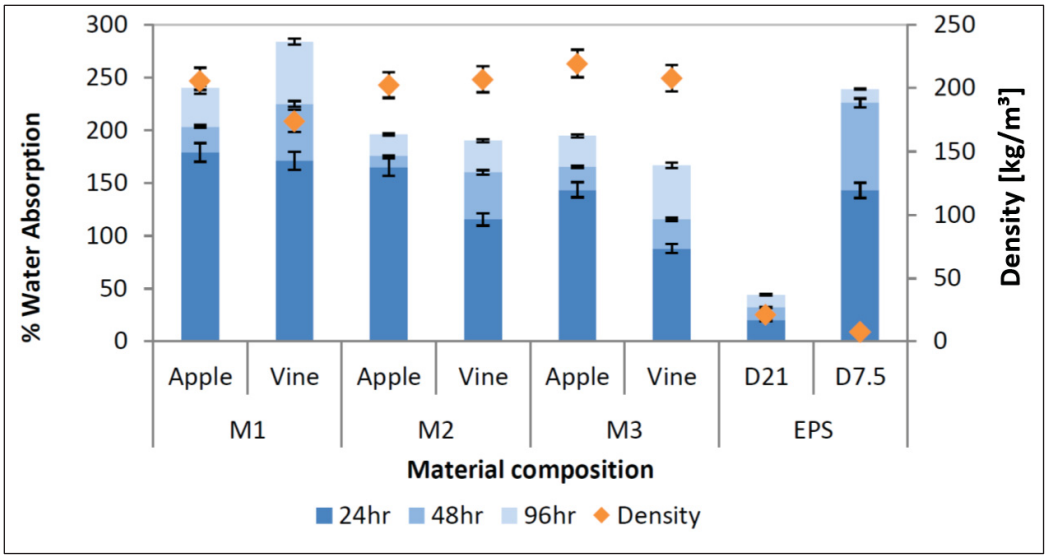

Figure 1.14 Comparative analysis to evaluate the effect of material composition and incubation method on density and water absorbance performance
Taken from Attias et al. (2019, p. 1654)

This figure shows the variation in water absorption over time and corresponding density across different mycelium-based composites. In general, higher-density samples tend to demonstrate lower water absorption, indicating an inverse relationship between density and hygroscopic behavior. These results highlight how composition and growth conditions directly influence MBC hygrothermal performance.

Elsacker et al. (2019) similarly demonstrated that densified, pre-compressed substrates reduce both water uptake and thermal conductivity (Figure 1.15, Table 1.2), reinforcing broader findings that mechanical densification generally enhances hygrothermal resilience. Results in Table 1.2 demonstrate that mycelium-based materials exhibit insulating properties comparable to those of traditional construction materials. Yang et al. (2021) further emphasized the importance of fungal strain and pore architecture in enhancing both thermal and moisture performance. Nguyen et al. (2017) provided benchmark hygrothermal data for bio-insulation materials made from bamboo fibers and natural binders, illustrating that mycelium-based materials perform comparably or better in terms of moisture buffering capacity and thermal conductivity, further supporting their viability for sustainable building envelopes.

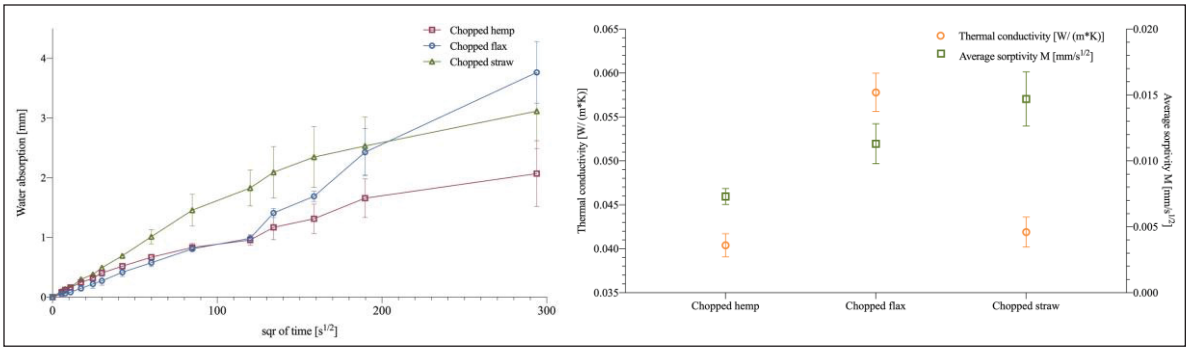

Figure 1.15 Hygric and mechanical characterization of mycelium with different substrate processing
Adapted from Elsacker et. Al (2019, pp. 11-12)

Table 1.2 Comparison of mycelium bio-composite's conductivity with traditional insulation materials (Letters indicate significant differences based on Tukey's family error rate at $p \leq 0.05$ for sample-specific ANOVA (Analysis of Variance))
Adapted from Elsacker et al. (2019, p. 10)

Insulating Material	**Thermal Conductivity ($W \cdot m^{-1} \cdot K^{-1}$)**	**Density ($kg \cdot m^{-3}$)**
Mycelium–flax composite—a	0.0578 ± 0.002^{bc}	135
Mycelium–hemp composite—b	0.0404 ± 0.001^{a}	99
Mycelium–straw composite—c	0.0419 ± 0.0002^{b}	94
Rock wool	0.044	470–2250
Glass wool	0.033–0.045	13–100
Extruded polystyrene	0.025–0.035	18–50
Kenaf	0.034–0.043	30–180
Sheep wool plates	0.038–0.054	10–25

Figure 1.15 shows that chopped straw yields the lowest thermal conductivity and water absorption among the tested substrates, whereas flax performs the worst. These trends reflect substrate-dependent differences in porosity and moisture affinity. Table 1.2 further highlights that mycelium-hemp and straw composites offer thermal conductivity comparable to conventional insulators like glass wool, despite their much lower density—underscoring their potential as efficient, lightweight, bio-based insulation materials.

Farrera-Vázquez et al. (2022) studied MBCs made from *Trametes elegans* and measured hygrothermal parameters including moisture sorption and buffering capacity. Their findings confirm that MBCs contribute to regulating indoor humidity while maintaining thermal insulation, supporting passive building strategies. Pittau et al. (2022) and Babenko et al. (2024) also conducted comparative assessments of MBCs with plant-fiber composites. Both studies found that MBCs exhibit competitive or superior performance in thermal conductivity, moisture buffering, and biodegradability, positioning them as effective alternatives for environmentally responsive building envelopes.

Thermal insulation performance is a key property in evaluating mycelium-based composites in building applications, and recent studies have shown that fabrication parameters directly influence their effectiveness. A detailed exploration of thermal insulation performance was provided by Sağlam and Özgünler (2024), who evaluated mycelium composites fabricated from *Ganoderma lucidum*. The study found that both incubation time and substrate choice significantly influenced thermal conductivity, which ranged from 0.036–0.048 $W \cdot m^{-1} \cdot K^{-1}$, comparable to those of commercial insulation products. Jin et al. (2024) examined *Pleurotus ostreatus* grown on straw, showing that thermal performance improved with increased incubation time and optimized fiber packing density. These findings suggest that fine-tuning growth parameters can significantly enhance insulation performance.

However, comprehensive hygrothermal characterization of MBCs remains limited. Koh et al. explicitly measured both moisture sorption isotherms and coupled heat-moisture behavior in MBCs. In this work, equilibrium moisture sorption isotherms were obtained for mycelium-based composites alongside other plant-based insulations (Figure 1.16), and the dependence of thermal conductivity on relative humidity was quantified (Figure 1.17). This study provided one of the first quantitative link between hygric and thermal properties in mycelium materials.

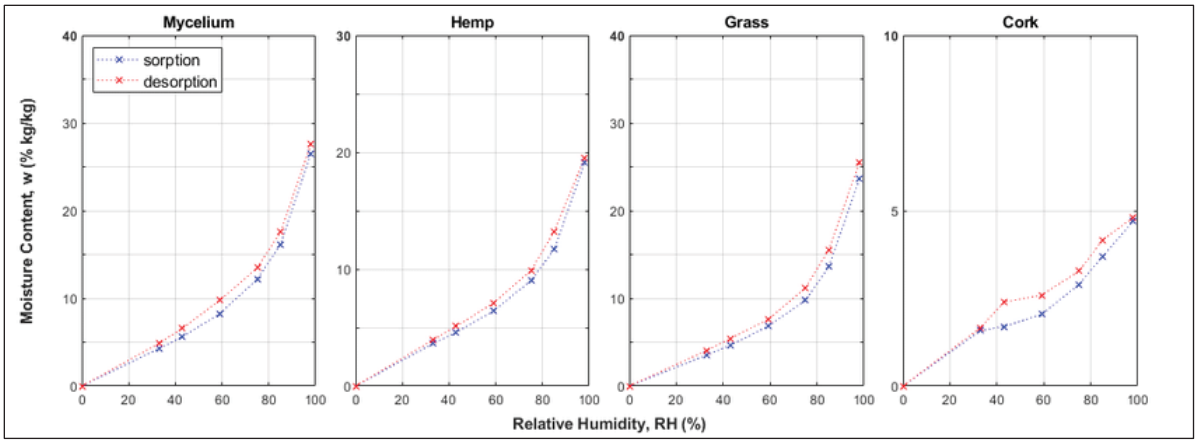

Figure 1.16 Sorption isotherms for mycelium, hemp, grass and cork composites
Taken from Koh et al. (2022, p. 7)

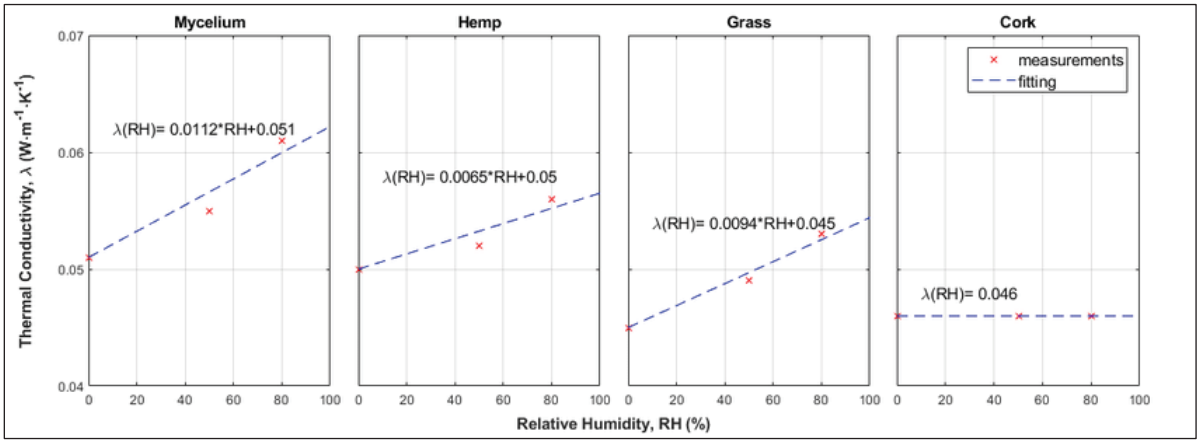

Figure 1.17 Thermal conductivity against RH for mycelium, hemp, grass and cork composites
Taken from Koh et al. (2022, p. 7)

Hemp, grass, and mycelium exhibit comparable thermo-hygric performance in the presented data. However, cork (on the right-hand side) shows the lowest thermal conductivity and sorption capacity among the tested materials.

Subsequent studies have built upon these findings by examining the direct correlation between thermal and hygric properties and the role of microstructure in MBC performance. Wildman et al. (2024) reaffirmed that moisture content is a critical extrinsic factor influencing the effective thermal conductivity of mycelium composites. In practical terms, absorbed moisture

within the pore network increases thermal conductivity because water conducts heat more readily than air. Song et al. (2025) addressed this issue by applying a hydrophobic alkyl ketene dimer (AKD) treatment to mycelium-based insulation materials. The AKD treatment significantly reduced the water absorption of the composites and improved their mold resistance, thereby preserving low thermal conductivity under humid conditions. This modification underscores that limiting moisture ingress (for instance, via surface hydrophobization) can substantially enhance the hygrothermal stability and durability of MBCs.

These findings collectively underscore that both formulation and microstructure critically influence MBC hygrothermal performance.

1.4.3 Environmental impact of MBCs

Owing to their favorable hygrothermal performance—characterized by low thermal conductivity, high vapor permeability, and effective moisture buffering—mycelium-based composites (MBCs) can significantly reduce operational energy demand for heating and cooling in buildings. Beyond these operational benefits, recent life cycle assessment (LCA) studies also highlight their low embodied carbon, positioning MBCs as promising materials for environmentally sustainable and low-impact construction.

Recent studies assessing the environmental impact of mycelium-based composites (MBCs) consistently demonstrate their potential as low-carbon or even carbon-negative building materials, especially when produced under optimized conditions. Stelzer et al. (2021) conducted a cradle-to-gate life cycle assessment (LCA) of fungal composite bricks and reported emissions of approximately 0.49 kg CO_2-eq per brick at laboratory scale, which could be reduced by up to 68 % in an industrialized scenario. The study highlighted electricity consumption during sterilization, incubation, and drying as the dominant contributor to greenhouse gas (GHG) emissions. Compared to conventional bricks, MBCs showed 2.5 to 6 times lower emissions, though they performed worse in categories such as eutrophication and

land use due to the agricultural origin of substrates. Similarly, Volk et al. (2024) evaluated mycelium insulation produced in Germany and found its embodied carbon to be around 0.37 kg·CO_2-eq·kg^{-1} lower than many synthetic insulations like XPS and PIR. However, they noted that bio-based insulations such as strawboard and wood fiber still outperform MBCs in terms of overall climate impact when end-of-life phases are considered.

Other LCA studies reinforce these findings, while also pointing to key trade-offs. Alaux et al. (2024) found that mycelium insulation blocks could achieve lower emissions than petroleum-based foam insulation, but did not outperform mineral wool in most impact categories. They emphasized that electricity use during manufacturing remains the most significant environmental hotspot. In a carbon sequestration-focused study, Livne et al. (2022a) demonstrated that MBCs could act as carbon sinks, reporting a net negative embodied carbon of −39.5 kg·CO_2-eq·m^{-3} due to biogenic carbon storage in the fungal matrix. Akromah et al. (2024) showed that in African contexts, mycelium bricks produced with renewable energy could emit five times less GHG than concrete bricks, but with fossil-fuel-based electricity, their impact could exceed that of concrete. These studies collectively indicate that while MBCs are promising environmentally, their actual carbon performance is highly sensitive to energy sourcing, processing methods, and regional context.

1.4.4 Fire resistance and safety of MBCs

Fire performance testing over the past decade indicates that MBCs can exhibit favorable fire behavior compared to conventional synthetic and wood-based materials. Cone calorimetry studies report that MBCs have competitive or lower flammability metrics, including delayed ignition and reduced heat release. For example, Irbe et al. (2024) found peak heat release rates (pHRR) of roughly 134–243 kW·m^{-2} for various mycelium-based insulation boards – values significantly below those of expanded polystyrene (EPS) foam or plywood (which typically reach 240–280 kW·m^{-2}) (Irbe et al., 2024). Correspondingly, total heat release (THR) from mycelium composites (often <~30 kW·m^{-2}) was much lower than that of wood-based panels (98–127 kW·m^{-2}) (Irbe et al., 2024). Such improvements are largely attributed to the

mycelium's propensity to char. Under fire, the fungal biomass forms an insulating char layer that slows thermal decomposition and inhibits volatile fuel release. Jones et al. (2018) demonstrated via thermogravimetry and pyrolysis combustion flow calorimetry that pure mycelium has a significantly lower combustion propensity than common polymers (PMMA or PLA), making it noticeably less prone to ignition and flaming. In cone calorimetry, even a modest mycelial content in composites was shown to reduce the heat release rate by promoting char formation which acts as a thermal barrier. Notably, the charring tendency of mycelium-rich composites does not substantially benefit from extended growth time (beyond a certain point), meaning even relatively short-grown mycelium can impart inherent fire-resistance to the material (Jones et al., 2018). Decomposition of mycelium generally starts around 250 °C – overlapping with hemicellulose and lignin breakdown – but yields a high char residue (aided by the fungi's natural chitin/protein content) (Irbe et al., 2024). This robust char network in turn delays combustion and reduces peak temperatures, explaining why MBCs often outperform high-density foams and wood in fire tests (Irbe et al., 2024).

Other fire-relevant behaviors of MBCs have also been documented through standardized lab-scale tests. In cone calorimeter experiments (ISO 5660), mycelium composites consistently showed lower smoke production than petrochemical foams: Irbe et al. (2024) observed total smoke release values of 7–281 $m^2 \cdot m^{-2}$ for MBC specimens, compared to hundreds for polyurethane or polyisocyanurate insulations. The lowest-smoke MBC formulations (e.g. dense waste-fiber/mycelium boards) yielded an order-of-magnitude less smoke than typical rigid foam, suggesting a potential safety advantage in reducing toxic fire effluents. Flame-spread performance has been evaluated with small-scale flame tests as well. Chulikavit et al. (2023) incorporated mycelium into an epoxy polymer and found that UL-94 vertical burn tests exhibited slower flame spread and shorter burn lengths in the mycelium-infused samples relative to neat epoxy. In practice, many mycelium composites tend to self-extinguish once the ignition source is removed, due to the protective char layer starving the flame of fuel and oxygen (Jones et al., 2018). Even at sustained heat flux (e.g. 35 $kW \cdot m^{-2}$ in cone tests), mycelium-based panels often burn out with smaller THR and leave substantial char residue (Irbe et al., 2024). Overall, recent validated fire tests – including cone calorimetry,

thermogravimetric analysis, and UL 94 classifications – concur that mycelium bio-composites exhibit reduced flammability, slower flame spread, high char yield, and lower smoke generation compared to many conventional building materials (Jones, 2019). These properties underscore the promise of MBCs as an inherently fire-resilient, sustainable material class for applications like insulation and cladding in buildings.

1.4.5 Influence of microstructure on the hygrothermal performance of MBCs

As MBC research progresses, increasing attention is placed on how microstructural features affect thermal insulation and moisture control. New research have shown that the microstructure of MBCs plays a pivotal role in governing their thermal–hygrothermal performance. Zhang et al. (2023) fabricated an ultra-light mycelium composite (approximately 94% porosity) with a hierarchical pore architecture, achieving a thermal conductivity as low as 0.044 $W \cdot m^{-1} \cdot K^{-1}$. This performance, comparable to conventional foam insulations, highlights that tailoring the pore size distribution (e.g., combining micro- and macro-pores in an optimal ratio) can markedly improve insulation effectiveness.

Verhelst et al. (2024) further demonstrated that the intrinsic mycelial network structure, shaped by fungal strain and growth conditions, directly influences both thermal and hygric outcomes. In their study, composites produced by fungi that developed denser, more homogenously colonized mycelium networks showed lower bulk density and enhanced thermal insulation capacity. This seemingly counterintuitive result, where denser fungal growth leads to reduced thermal conductivity, is attributed to microstructural transformation: the fungal colonization partially consumes and binds the lignocellulosic substrate, reducing solid mass while maintaining volume. This process generates more small, air-filled pores and reduces the size and connectivity of larger voids. As a result, the material contains a higher fraction of insulating micropores and fewer interconnected macro-pores, thus impeding convective heat transfer and lowering the effective thermal conductivity.

Moreover, a well-developed mycelial “skin” and network tend to increase surface hydrophobicity of the composite. In dense mycelium composites, this inherent hydrophobic character helps resist moisture uptake, allowing air pockets to remain dry and effective for insulation even under high humidity. Verhelst et al. (2024) observed that all their mycelium samples exhibited considerable hydrophobicity, with water contact angles ranging from approximately 105° to 122°.As a result, only subtle inter-strain differences in moisture sorption could be detected. Consequently, no strong statistical correlation between contact angle and thermal conductivity emerged among those samples; nevertheless, the concept that moisture incurs a thermal penalty was evident.

Motamedi et al. (2025) systematically evaluated the coupled heat and moisture behavior of MBCs fabricated from hemp and straw substrates colonized by *Ganoderma lucidum* and *Trametes versicolor*, using a multi-scale experimental protocol. Notably, their study includes one of the rare experimental characterizations of sorption isotherms for MBCs, showing moisture contents reaching up to 30 % at 90 % RH and confirming the influence of additives, substrate type, and fungal species on hygroscopic behavior. Additive-enriched composites exhibited up to 21.8 % higher moisture uptake at 90 % RH, while straw-based composites reached free water saturation values up to 704 $kg \cdot m^{-3}$, indicating greater moisture sensitivity. In contrast, hemp–*Ganoderma* composites exhibited lower vapor permeability and a moisture sensitivity coefficient thirty times lower than *Trametes*-based samples in thermal conductivity response. Thermal conductivity ranged from 0.045 to 0.08 $W \cdot m^{-1} \cdot K^{-1}$, increasing nonlinearly with relative humidity and temperature. These findings confirm that dense, interconnected hyphal networks suppress capillary condensation and vapor transport, enhancing moisture buffering and thermal stability. A comparison of the average thermal conductivities obtained in this study with various EPS grades is presented in Figure 1.18.

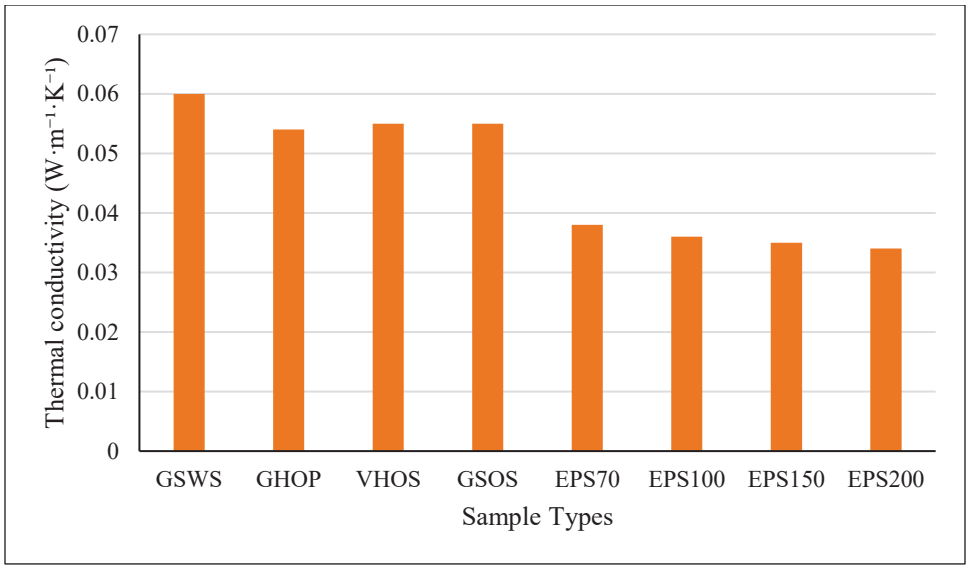

Figure 1.18 Comparison of average thermal conductivity values of selected mycelium-based composites with conventional expanded polystyrene (EPS) insulation materials (EPS70–EPS200)

The sample codes in the figure above represent specific combinations of fungal species, substrates, additives, and treatment methods, following a standardized naming convention. Full definitions of these abbreviations are provided in the Nomenclature section. The results highlight the competitive insulation performance of MBCs, with thermal conductivity values ranging from 0.054 to 0.06 $W \cdot m^{-1} \cdot K^{-1}$, approaching those of conventional EPS products, particularly in denser, well-structured formulations like GHOP.

Recent studies confirm that optimizing pore architecture and controlling moisture interaction are vital for maximizing MBC insulation performance. Overall, the integration of mechanical, thermal, and hygric characterization, alongside by microstructural analysis, provides a more holistic understanding of MBC performance. By leveraging these insights, researchers and practitioners can better design mycelium-based composites with balanced mechanical strength, enhanced insulation value, and robust moisture resistance for sustainable building applications. In conclusion, the performance of MBCs is closely tied to the interplay between fabrication parameters and microstructural development. Mechanical strength, thermal insulation, and moisture buffering can be improved through densification, fungal selection, and surface treatments. Environmental and safety evaluations further reinforce the suitability of MBCs as

sustainable alternatives to conventional insulation materials. The main findings are summarized below:

- Mechanical performance improves significantly with densification techniques such as hot pressing, which reduce porosity and enhance strength.
- Hygrothermal performance is strongly influenced by fungal strain, substrate, and microstructure; denser mycelial networks yield better insulation and lower water uptake.
- MBCs exhibit thermal conductivities (0.036–0.048 $W \cdot m^{-1} \cdot K^{-1}$) comparable to commercial insulation while offering biodegradability and carbon negativity.
- Life cycle assessments confirm MBCs' low embodied carbon, though results vary based on region, energy sourcing, and end-of-life treatment.
- MBCs demonstrate promising fire resistance and self-extinguishing behavior due to char formation and low combustion rates, enhancing safety for building applications.

1.5 Discussion

This review aimed to move beyond cataloging the properties of mycelium bio-composites (MBCs) by synthesizing observed relationships between fabrication methods, microstructural development, and performance characteristics, particularly in relation to real-world feasibility. Its central contribution lies in structuring a fragmented body of experimental data into a cohesive framework that explains how MBCs can transition from lab-scale innovations to scalable, application-ready materials. To that end, we categorized the literature into eight thematic domains and evaluated each with respect to fabrication techniques, resulting properties, and performance outcomes.

1.5.1 Fabrication methods

MBCs are produced using mold-based growth, additive manufacturing techniques such as direct ink writing (DIW) and paste extrusion, and hybrid methods combining biological growth

with textiles or cellulose nanofibrils. Mold-based techniques offer reproducibility (Elsacker et al., 2019; Stelzer et al., 2021), while additive manufacturing enables complex geometries and tailored microstructures (Luo et al., 2025; Soh et al., 2023; Teoh et al., 2024). However, these approaches face challenges with contamination, growth variability, and process standardization (Camilleri et al., 2025; Mohseni et al., 2023). Emerging robotic fabrication and modular strategies (Attias et al., 2020; Elsacker, Søndergaard, et al., 2021) show promise for scalable production. Despite innovation in additive manufacturing and robotic methods, fabrication processes remain highly variable due to inconsistent sterilization, contamination risks, and lack of standardized protocols, which limits reproducibility and comparability across studies (Camilleri et al., 2025; Jones et al., 2017; Mohseni et al., 2023).

1.5.2 Mechanical and hygrothermal properties

MBCs exhibit thermal conductivity values between 0.036 and 0.06 $W \cdot m^{-1} \cdot K^{-1}$, comparable to materials like mineral wool, hempcrete, and cork (Babenko et al., 2024; Koh et al.; Motamedi et al., 2025). Mechanical strength, particularly tensile and compressive properties, is significantly improved through densification processes such as hot pressing (Appels et al., 2019; Karana et al., 2018; Lingam et al., 2023). Performance varies with fungal strain, substrate, and processing: dense mycelial networks reduce water uptake and enhance insulation, while loosely structured composites offer better moisture buffering (Attias et al., 2019; Farrera-Vázquez et al., 2022; Verhelst et al., 2024; Yang et al., 2021).

Recent studies have characterized sorption isotherms and demonstrated the impact of relative humidity on thermal conductivity (Koh et al.; Motamedi et al., 2025). Moisture uptake increases effective conductivity, emphasizing the importance of microstructural control. Motamedi et al. (2025) also quantified vapor permeability and moisture sensitivity across fungal–substrate combinations, highlighting hyphal density as a key determinant. Additionally, multi-scale models have been used to describe compressive behavior in relation to density and pore architecture, bridging microstructure with mechanical response (M. Islam et al., 2018). These findings underscore the potential to tailor MBCs for both structural and hygrothermal

applications through process and material optimization. However, maintaining consistent performance remains challenging due to sensitivity to ambient humidity and the variability introduced by fungal strain and substrate heterogeneity.

1.5.3 Environmental impact and life cycle performance

Several LCA studies demonstrate the environmental benefits of MBCs, including low embodied energy and carbon-negative performance under optimal conditions (Livne et al., 2022a; Stelzer et al., 2021). Carbon footprints range from 0.37 kg CO_2-eq·kg^{-1} to −39.5 kg CO_2-eq·m^{-3} depending on the production method and energy source (Akromah et al., 2024; Volk et al., 2024). However, high electricity demand for sterilization and drying remains a key impact driver (Alaux et al., 2024). Compared to petroleum-based materials like XPS and PIR, MBCs offer a favorable emissions profile, but trade-offs exist in categories such as eutrophication and land use. While MBCs have low embodied carbon, their environmental footprint is highly dependent on energy-intensive steps such as sterilization and drying. Regional variation in electricity sourcing significantly affects LCA outcomes.

1.5.4 Fire resistance and safety

MBCs demonstrate intrinsic fire resistance via formation of a char layer that slows flame spread and reduces heat release and smoke generation (Irbe et al., 2024; Jones et al., 2018). Cone calorimetry and UL-94 vertical burn tests confirm that certain formulations not only resist ignition but also self-extinguish once the heat source is removed (Chulikavit et al., 2023). These properties make MBCs promising candidates for safe insulation applications, although further validation under standardized conditions is needed. Fire performance testing of MBCs remains limited to lab-scale studies; standardized certification procedures for fire safety are still lacking, which hinders integration into building codes.

1.5.5 Durability and long-term performance

As bio-derived materials, MBCs are inherently biodegradable, making moisture exposure a critical concern. Without treatment, samples may lose up to 43% of their mass after 16 weeks in soil (Van Wylick et al., 2022). However, post-treatments such as beeswax–coconut oil coatings (Farrahnoor et al., 2024) and hot pressing (Alemu et al., 2022; Nussbaumer et al., 2023) significantly enhance moisture resistance and delay microbial decay. Strain selection for dense, hydrophobic hyphae (e.g., *Trametes hirsuta*) has also been shown to improve performance under wet conditions (Gauvin et al., 2022; Kuribayashi et al., 2022). Despite these advances, long-term exposure to UV, freeze-thaw cycles, and microbial attack still warrants further study (Gan et al., 2022; Schultz et al., 2024). Another challenge is that uncoated MBCs degrade rapidly under outdoor or high-humidity conditions, while protective treatments that enhance durability may compromise their inherent compostability (Gan et al., 2022; Gauvin & Vette, 2020; Van Wylick et al., 2022).

1.5.6 Scalability and real-world implementation

Pilot-scale installations such as the Growing Pavilion and MycoTree highlight the architectural potential of MBCs (Es-sakali et al., 2023), but full-scale commercialization remains limited. Scaling is challenged by batch variability, growth inconsistency, and the absence of standardized, reproducible fabrication protocols (Alaneme et al., 2023; Bitting et al., 2022; Shin et al., 2025). Many fabrication techniques remain proprietary, limiting transparency and broader adoption. A synthesis of the literature also points to systemic barriers: the lack of open-source methods hinders collaborative development, and the absence of certification pathways restricts integration into regulatory frameworks. Despite these constraints, advances in genetic engineering, robotic automation, and modular bio-hybrid strategies offer promising routes toward scalable and consistent production (Attias et al., 2020; Elsacker, Søndergaard, et al., 2021; Wattanavichean et al., 2025).

1.5.7 Innovation landscape

Beyond academic exploration, the development of MBCs is increasingly influenced by industrial innovation and intellectual property strategies. Cerimi et al. (2019) identified a growing number of patents related to mycelium applications, including structural panels, fire-resistant boards, and packaging systems. These findings confirm that fungal composites are attracting commercial interest, particularly for low-carbon material applications. However, much of the innovation remains proprietary, and access to these fabrication technologies is limited—posing a challenge for standardization, open-source collaboration, and certification alignment.

1.5.8 Comparative bio-based materials

Several studies have benchmarked MBCs against other bio-based insulators such as hempcrete, cork, straw, and bamboo fiber composites. While MBCs offer comparable or superior thermal conductivity and biodegradability (Koh et al.; Nguyen et al., 2017; Verhelst et al., 2024), they often underperform in mechanical durability and moisture resistance unless treated (Song et al., 2025; Yang et al., 2021). In general, MBCs benefit from tunable composition and locally sourced lignocellulosic feedstocks, supporting material circularity and regional adaptability. However, further optimization is needed to match the long-term performance of more established bio-based materials in demanding building environments.

To complement this thematic synthesis, Table 1.3 presents an overview of the main constituents and technological approaches reported across the reviewed studies. This classification reflects the diversity of substrates, fungal strains, and fabrication strategies employed, along with the specific innovations or performance goals pursued in each case. These distinctions help situate the thematic insights within the broader context of material configurations and research directions observed in the field.

Table 1.3 Overview of constituent materials and technological approaches used across the reviewed MBC studies

Author	Type	Fiber	Fungi	Technology / Initiative / Novelty
(Appels et al., 2019)	Article	Rapeseed straw Beech sawdust Cotton	*T. multicolor* *P. Ostreatus*	Non-pressed Heat-pressed Cold-pressed
(Attias et al., 2019)	Article	Vine and apple woodchips (residues of pruning)	*Colorius sp.* *Trametes sp.* *Gonoderma sp.*	The effect of further inoculation inside perforated bags on the quality of the material
(Babenko et al., 2024)	Article	Wheat straw Hemp straw Flax straw	*Ganoderma lucidum*	Comparative study on thermal performance and biodegradability
(Bhardwaj et al., 2020)	Article	Rice straw Hemp	*Not mentioned*	3d Printing
(Cerimi et al., 2019)	Patent review	Wheat straw, wheat bran, maize straw, rice straw bagasse, wood, saw dust, wood chips, wool, hemp, silk, corncobs,	*Agrocybe aegerita, Agrocybe brasiliensis, Coprinus comatus, Flammulina velutipes, Hypholoma capnoides, Hypholoma, Sublateritium, Lentinula edodes, Macrolepiota procera, Pleurotus djamor, Pleurotus eryngii, Pleurotus ostreatus, Pleurotus ostreatus var. columbines, Polyporales, Fomes fomentarius, Ganoderma tsugae, Ganoderma*	Organic packaging material, fire proof composites, dehydrated mycelium elements, mycelium panels for construction, dehydrated mycelium elements using molding system, stiff engineered composite, roll-to-roll production of dehydrated mycelium, vehicle interieur outfit, bulk fungal materials (fillings), self-supporting composites,

Author	Type	Fiber	Fungi	Technology / Initiative / Novelty
			lucidum, Ganoderma orogenese, Grifola frondesa, Piptoporous betulina, Polyporus mylittae, Pycnoporus cinnabarinus, Trametes versicolor, Russulales Hericium erinaceus, Ascomycota, Pezizales, Morchella Angusticeps, Xylariales Xylaria Polymorpha, Xylaria hypoxylon, Xylaria filiformis, Xylaria longipes	ultrasonic treatment, vehicle parts, sound attenuating materials, electric circuits composed of fungal mycelium
(Chutimanukul et al., 2023)	Article	soybean meal	*H. erinaceus*	Medical applications
(Elsacker, Søndergaard, et al., 2021)	Article	Hemp hurd Beachwood sawdust	*Ganoderma resinaceum* *Trametes versicolor*	Scalability of the fabrication practices - Growing large blocks - on-site robotic wire cutting - multi-functional framework usage of mycelium - Self healing of fungal organisms
(Elsacker et al., 2019)	Article	Hemp Flax Flax waste Soft wood Wheat straw	*Trametes versicolor*	The effect of substrate type and pre-processing of the substrate on the hygrothermal properties

Author	Type	Fiber	Fungi	Technology / Initiative / Novelty
(Farrera-Vázquez et al., 2022)	Article	Corn stalk	*Trametes elegans*	Development of bio-insulation from T. elegans and cornstalk with hygrothermal testing
(Gauvin & Vette, 2020)	Thesis	Rapeseed straw Cellulose	*G. lucidum*	Prolonging inoculation phase
(Holt et al., 2012)	Article	Cotton plant biomass (CPB)		Proprietary information of Ecovative
(M. Islam et al., 2018)	Article	Ecovative supplied bio composite		Multi scale stochastic analysis
(Jiang et al., 2017)	Article	Jute Hemp Cellulose	Mycelium-bound agricultural waste (core) Bioresin (matrix)	Manufacturing of biocomposite sandwich structure
(Karana et al., 2018)	Product design journey	Fiber Grain	Not Mentioned	Non-pressed Heat-pressed Cold-pressed
(Koh et al.)	Article	Straw Miscanthus Flax	Not mentioned	-Hygrothermal characterization -comparison of mycelium-based composites with other type of bio-based building materials
(Pittau et al., 2022)	Conference	Hemp shiv Lagarosiphon major fibres	Not mentioned	Use of invasive aquatic plant fibres with mycelium for insulation
(Rahman et al., 2022)	Article	Not mentioned	Not mentioned	3d Printing

Author	Type	Fiber	Fungi	Technology / Initiative / Novelty
(Scott et al., 2022)	Article	Mixed fiber (straw, wood shavings, plain flour)	*Pleurotus ostreatus*	- Knitting living textiles as scaffolds - Incorporation of bacteria and mycelium
(Sisti et al., 2021)	Article	bran/cotton, bran/hemp Additive: wheat bran	Proprietary information of Mogu	Investigation of wheat bran as an upgrading filler to the base substrate
(Soh et al., 2020)	Article	Bamboo culms	*Ganoderma lucidum*	3d Printing
(Soh et al., 2023)	Article	Coffee grounds	*Pleurotus ostreatus*	3d Printing
(Song et al., 2025)	Article	Grass	Not mentioned	Application of AKD hydrophobization to reduce water uptake
(Stelzer et al., 2021)	Article	Hemp shiv	Fomes fomentarius	LCA for fungal-based composite bricks
(Sun et al., 2019)	Article	Soft wood	White-rot basidiomycete	Cellulose nanofabrils
(Verhelst et al., 2024)	Article	Mixture of hemp shives and flax shives	*Ganoderma lucidum* *Pleurotus ostreatus* *Trametes versicolor* *Trametes hirsuta* *Schizophyllum commune* *Coprinus comatus* *Lentinula edodes* *Hericium erinaceus* *Fomes fomentarius*	Comparative study of fungal strain impact on insulation properties
(Zhang et al., 2023)	Article	Poplar and birch sawdust	*Trametes versicolor*	Lightweight, hydrophobic mycelium composites with hierarchical structures

Building on the diverse approaches and material strategies observed across the literature, future research should prioritize the development of standardized, reproducible fabrication protocols, particularly for additive and hybrid manufacturing, to improve consistency and enable certification. Further investigation is needed to optimize mechanical and hygrothermal performance under variable environmental conditions, with emphasis on coupled heat and moisture behavior, sorption isotherms, and long-term exposure. Expanding life cycle assessments to include diverse climatic regions and energy contexts will improve the comparability and robustness of environmental impact evaluations. Fire safety research should advance beyond laboratory-scale testing toward standardized assessments aligned with building codes. Addressing the durability and compostability trade-off remains essential, especially through bio-based treatments that preserve circularity. For real-world adoption, efforts must also target scalable, modular production systems and open-access knowledge sharing. Lastly, benchmarking MBCs against other bio-based materials under unified criteria will help position them more clearly within the broader landscape of sustainable construction options.

1.6 Conclusion

This review synthesizes a decade of experimental and applied research on mycelium bio-composites (MBCs), highlighting how fabrication methods directly influence mechanical and hygrothermal performance. Key findings include:

Fabrication methods such as mold-based, 3D printing, and hybrid techniques significantly impact consistency, scalability, and microstructure.
Mechanical and hygrothermal properties are strongly dependent on fungal strain, substrate, and densification techniques, with densified MBCs showing better insulation and moisture resistance.

- Environmental performance is promising, with several LCA studies confirming low or even negative embodied carbon under optimized conditions.

- Durability remains a critical limitation, especially under prolonged humidity; however, post-treatment and material hybridization strategies show potential.
- Fire resistance is generally favorable due to high char formation and low smoke release, making MBCs safer than many synthetic insulations.

Based on this synthesis, we recommend the following future research directions:

- Standardizing fabrication protocols to enable reproducibility and certification, especially for 3D printing and modular assembly.
- Advancing bio-hybrid strategies, including robotic manufacturing and self-healing systems, to improve scalability and reliability.
- Extending durability studies across diverse climates and building types, focusing on long-term moisture, UV, and biodegradation performance.
- Quantitative coupling of microstructure with thermal and moisture behavior, to enable predictive material design.
- Comprehensive LCA and end-of-life studies in various regional contexts to inform policy and market adoption.

Collectively, these findings provide a technical foundation for scaling MBCs as viable components in high-performance, low-carbon buildings.

CHAPTER 2

FABRICATION PRACTICE OF MYCELIUM BIO COMPOSITES

Abstract

This chapter investigates tailored fabrication methods for mycelium-based composites (MBCs) through iterative adjustments of substrates, fungal strains, and additives. Systematic fabrication trials were conducted using hemp shiv and wheat straw in combination with *Ganoderma lucidum*, *Trametes versicolor*, and *Pleurotus ostreatus*. Comparative growth assessments revealed distinct substrate–fungus interactions: straw exhibited superior moisture-buffering capacity, making it suitable for interior layers, while hemp, especially when consolidated with a dense mycelial surface, performed effectively for exterior hygric insulation. Material hydrophobicity was shown to depend on moisture adsorption and release during fabrication. Among the tested fungi, *G. lucidum* demonstrated consistent compatibility with both substrates, while *T. versicolor* adapted well to hemp-based composites. *P. ostreatus* showed weaker performance under the present conditions, likely due to spawn-quality variability, and was therefore excluded from the final sample set despite its strong potential reported in the literature. Additionally, mold material strongly influenced growth outcomes: PVC supported uniform mycelial layers, whereas cast iron compromised internal cohesion. These findings establish fabrication parameters that inform the subsequent quantitative characterization of hygrothermal properties presented in Chapter 3.

2.1 Introduction

Mycelium-based composites (MBCs) have emerged as promising sustainable alternatives to conventional materials in construction, packaging, and design (Alaneme et al., 2023; Jiang et al., 2013; Madusanka et al., 2024). These biocomposites are produced by growing fungal mycelium through lignocellulosic substrates—typically agricultural residues or industrial by-products—forming a continuous hyphal network that binds particles into a cohesive solid

(Peng et al., 2023; Sydor et al., 2022). Resulting materials are lightweight, biodegradable, and environmentally benign, attributes that have broadened their appeal for circular and low-carbon applications (Alaneme et al., 2023; Girometta et al., 2019).

The fabrication of MBCs is governed by a coupled set of variables spanning fungal species, substrate composition, and processing conditions (Madusanka et al., 2024; Peng et al., 2023). A wide range of lignocellulosic feedstocks—e.g., rice husks, sawdust, straw, and corn residues—have been explored to tune density, porosity, and interfacial bonding (Aiduang et al., 2022; Elsacker et al., 2019). Inoculation strategy and growth control (spawn type/ratio, temperature–humidity regimes, gas exchange) strongly influence colonization kinetics and network uniformity (Vandelook et al., 2021). Post-growth treatments—cold/hot pressing, drying, or thermal curing—affect dimensional stability and moisture response and are therefore central to process design (Appels et al., 2019; M. R. Islam et al., 2018)

Among strains most relevant to fabrication practices, *Ganoderma lucidum* and *Trametes versicolor* (white-rot basidiomycetes) exhibit distinct growth morphologies and substrate interactions that shape process design. *G. lucidum* typically develops dense, cohesive mycelial mats with a multi-hyphal network that binds lignocellulosic particles effectively; its strong ligninolytic system (e.g., laccases, peroxidases) facilitates penetration into stiff cereal straws and woody residues (Aiduang et al., 2022), and alkaline pretreatments that open the straw surface (e.g., desilication) have been shown to improve colonization uniformity and interparticle bonding during growth in molds (Gezer & Kuştaş, 2024; Kuştaş & Gezer, 2024).

T. versicolor is frequently reported to advance rapidly over the substrate surface and through pore networks, forming a continuous outer mycelial layer that bridges particles—behavior that supports clean demolding and enables secondary growth phases (e.g., short regrowth after demolding) before drying; in wood-flour and sawdust matrices, this species establishes continuous sheaths that can be further consolidated by moderate pressing (Nussbaumer et al., 2023) without fully suppressing oxygen supply (Elsacker et al., 2019). Across both species, fabrication choices that govern access to oxygen and nutrients—spawn type and dose, particle

size distribution and packing, substrate conditioning (pasteurization/pretreatment), and the breathability of molds and coverings—largely determine colonization rate, depth of penetration, and the formation of a robust mycelial “skin” prior to curing (Aiduang et al., 2022; Elsacker et al., 2019; Jones et al., 2017; Vandelook et al., 2021).

Despite clear progress, fabrication practices remain heterogeneous and predominantly empirical. Systematic frameworks that relate substrate formulation, inoculation/growth parameters, and post-processing choices to hygrothermal and mechanical performance remain limited, constraining predictability and scalability. Moreover, many studies emphasize lab-scale protocols without fully addressing moisture durability, shrinkage control, and process standardization required for consistent, application-ready products.

This chapter develops and evaluates a reproducible fabrication methodology for MBCs using agricultural residues (wheat straw and hemp shiv) combined with selected fungal species (*G. lucidum*, *T. versicolor*) and supplementary additives to optimize colonization, microstructural cohesion, and dimensional stability. Key stages—inoculation, molding, demolding, and drying/curing—are systematically varied and assessed via mass/volume evolution, water uptake/loss, and qualitative mycelial network development. The resulting evidence base links fabrication decisions to observable physical outcomes, providing guidance for consistent preparation of specimens intended for subsequent hygrothermal characterization in chapter 3.

In this chapter Section 2.2 details the formulation of the samples (substrates, fungi types, and supplementary additives). Section 2.3 presents the fabrication practice, including inoculation, molding, demolding, and drying procedures. Section 2.4 provides the conclusion, synthesizing implications for subsequent experimental work.

2.2 Formulation of the samples

2.2.1 Substrates

Following the literature survey, two distinct substrates for sample fabrication are chosen, each of which demonstrate contradictory characteristics in terms of their hygric efficiency and thermal performance. These substrates are primarily composed of lignocellulosic materials, which consist of three key elements. This characterization is instrumental in determining the most suitable fungi to be mixed with these substrates, ensuring the development of a fully colonized mycelial layer throughout the material's cross-sections. Chemical composition of the base filler (substrate) is critical in the choice of fungi and the composition's subsequent application. Table 2.1 details substrates' chemical composition for wheat straw and hemp shiv.

Table 2.1 Chemical composition of the substrate (median percentage reported)

Substrate Type	Cellulose (%)	Hemicellulose (%)	Lignin (%)	Reference
Wheat straw	35-45	20-30	15-40	(Carvalheiro et al., 2009)
Hemp shiv	44-51.6	6.4-27	8-28	(Diakité et al., 2021)

Wheat straw and hemp shives exhibit notable differences in their chemical composition. A wide spectrum of compositions for hemp shiv and wheat straw is reported in the literature. Despite variations, both substrates are generally regarded as rich in cellulose. On the other hand, hemp shives have a more rigid structure, partially caused by the higher lignin content, compared to the wheat straw.

Additionally, hemp exhibits a hydrophobic waxy outer layer, known as the 'cuticle,' which acts as a natural barrier, hindering water absorption into the material. This unique property enhances hemp's resistance to moisture, making it advantageous for applications requiring durability and moisture resistance, such as the production of specific myco materials and building products. In contrast, wheat straw-based composites are primarily used in materials

adjacent to low humidity indoor spaces within the building envelope. In these applications, the material's moisture buffering capacity is essential for regulating indoor relative humidity and enhancing occupant comfort.

2.2.2 Fungi types

The choice of mycelium strain for use in mycelium-based materials depends on various factors, one of which is the specific chemical composition of the substrate (e.g., hemp shivs or wheat straw). Different mycelium strains have varying preferences for substrates, and the choice of mycelium should align with the composition of the substrate for optimal growth and colonization.

Due to higher lignin content in hemp shives, mycelium strains that are efficient in breaking down hemicellulose and lignin are often a good match for hemp shives. Some strains of the genus *Pleurotus* (e.g., oyster mushrooms), *Agaricus bisporus* (button mushrooms), and *Trametes versicolor* have been known to work well with hemp shives. Wheat straw on the other hand contains lower lignin, and therefore mycelium strains that excel at breaking down cellulose-rich substrates are more suitable for wheat straw. *Trichoderma reesei* and some *Ganoderma* species are examples of strains that can efficiently colonize cellulose-rich materials. Among these mycelium species, *Ganoderma lucidum* excels in working with both lignin-rich and cellulose-rich materials, although forming a particularly rigid structure when used with hemp (a lignin-rich substrate).

In this study, as illustrated in the Table 2.2 three types of fungi were identified for mixtures: *Ganoderma lucidum* and *Trametes versicolor*, both sourced from Mycelia in Belgium, and *Pleurotus* from Odyssey mushrooms in France. The mycelium is obtained in the form of spawn rather than liquid culture. Liquid culture is primarily suited for inoculating grain-based substrates like rye or millet, while spawn is more commonly used for fibrous substrates such as hemp, straw, and flax. It is essential to ensure that the acquired mycelium is intended for myco material production. Spawn designed for mushroom farming or indoor cultivation

usually has a lower concentration of colonized mycelium and is therefore unsuitable for myco material production.

Table 2.2 Description of the utilized fungi types

	Type of fungi	Description
	*Ganoderma lucidum*	Renowned for its lignin-degrading abilities, ideal for creating robust and long-lasting myco materials. Most common strain used in commercial and research mycomaterials.
	*Trametes versicolor*	Reliable, strong white network
	*Pleurotus ostreatus*	Faster growth, good flexibility, but lower overall biocomposite strength

From the aforementioned fungal species, during the growth trials, *P. ostreatus* showed slower colonization and incomplete binding compared to *G. lucidum* and *T. versicolor*. These results should be interpreted cautiously, as the observed underperformance is consistent with spawn-quality variability rather than the biological potential of the species. Some commercial strains are primarily optimized for agricultural or culinary use rather than composite fabrication, which may also explain the reduced performance observed here. Consequently, *P. ostreatus* was excluded from the final set of samples, although its effectiveness for MBC fabrication is well documented in prior studies.

2.2.3 Supplementary additives

Soybean meal and wheat bran are used as additives to bolster the nutritional content of the substrate. These additives serve as supplementary nutrient sources that support mycelium

growth and ultimately the development of robust myco materials. Their inclusion is particularly valuable when working with substrates like hemp and straw, which may lack certain essential nutrients required for optimal mycelial colonization.

Soybean meal, a byproduct of soybean processing, is a valuable nitrogen source for mycelium due to its high protein, amino acid, and nitrogen content. The protein content in soybean meal serves as a readily available nutrient source, complementing carbon-rich substrates like hemp and straw. Conversely, wheat bran contributes additional carbohydrates, vitamins, and minerals to the substrate. Its complex carbohydrate composition enhances the overall nutrient profile and helps maintain a balanced carbon-to-nitrogen ratio, a critical factor for mycelium growth. The combined use of soybean meal and wheat bran as additives creates a substrate that not only provides essential structural support but also establishes a nutrient-rich environment conducive to mycelial colonization and maturation. (Chutimanukul et al., 2023; Sisti et al., 2021)

Straw-based composites develop better mycelial structure using additive in their specimen recipe. Between utilized fungi *versicolor* and *Pleurotus* reacting better to the added supplements. As depicted in Figure 2.1, the disparity between two samples VHWS and VHOS (the nomenclature and the composition of samples are listed in the Table 2.3), is rooted in the compositions of wheat straw and *versicolor* with and without additives, which underscores the augmented growth of the mycelial layer on the surfaces as a result of incorporating additives in the mixture.

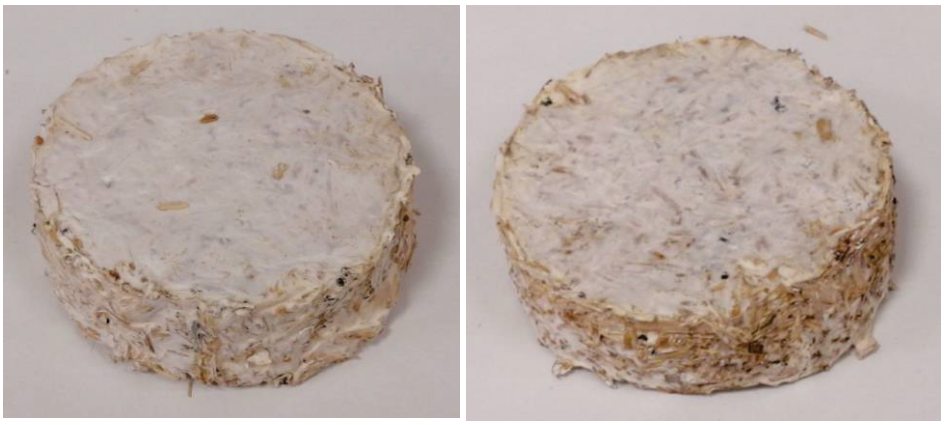

(a) (b)

Figure 2.1 The comparison of hemp and *T. versicolor* mixture; (a) with additive; (b) without additive

Wrapping up the combination of aforementioned ingredients out of the viable mixtures, Table 2.3 presents the selected samples' names, the type of mycelium embedded, the presence of additives, a note on the pasteurization process, particle size, distinctive label, sample count and respective mould size. As mentioned in Section 2.2, in practice, *P. ostreatus* exhibited slower colonization and weaker binding compared to the other strains tested. Substrate penetration was inconsistent, with incomplete formation of a cohesive mycelial skin. While these trials indicated limitations under the present conditions, the underperformance is attributed to spawn-related variability rather than species characteristics, as *P. ostreatus* is widely recognized in the literature for its strong colonization potential. For this reason, it was excluded from the final sample set but remains relevant for future fabrication studies when high-quality spawn is secured.

Table 2.3 Summary of fiber types, processing, type of fungi with the corresponding labels

Critical Parameters				**Specifications**		
Substrate	**Mycelium Type**	**Additives**	**Processing**	**Label**	**Sample Count**	**Mould Size**
Hemp shiv (H)	*Ganorderma*	with additives (w)	Unpasteurized (U)	GHWU	3	35*35*162 (mm)
Wheat straw (S)	*Ganorderma*	with additives (w)	Pasteurized (P)	GSWP	6	35*35*162 (mm)
Hemp shiv	*Ganorderma*	w/o additives (o)	Pasteurized	GHOP	3	35*90*162 (mm)
Hemp shiv	*Versicolor*	w additives	Pasteurized	GHWP	3	35*90*162 (mm)
Hemp shiv	*Ganorderma*	w/o additives	Pasteurized	GHOU	1	500*500*30 (mm)
Hemp shiv	*Ganorderma*	w/o additives	Unpasteurized	GHOP	1	500*500*30 (mm)
Hemp shiv	*Versicolor*	w/o additives	Pasteurized	VHOP	3	Cylindrical D103 mm
Hemp shiv	*Ganorderma*	w/o additives	Pasteurized	GHOP	3	Cylindrical D118 mm
Hemp shiv	*Ganorderma*	w/o additives	Pasteurized	GHOP	3	Cylindrical D103 mm
Wheat straw	*Ganorderma*	w additives	Pasteurized	GSWP	3	Cylindrical D103 mm
Hemp shiv	*Ganorderma*	w additives	Unpasteurized	GHWU	3	Cylindrical D103 mm
Hemp shiv	*Ganorderma*	w/o additives	Unpasteurized	GHOU	2	Cylindrical D103 mm

Critical Parameters				Specifications		
Substrate	**Mycelium Type**	**Additives**	**Processing**	**Label**	**Sample Count**	**Mould Size**
Wheat straw	*Versicolor*	w/o additives	Pasteurized	VSOP	3	Cylindrical D103 mm
Hemp shiv	*Versicolor*	w/o additives	Sterilized	VHOS	3	Cylindrical D103 mm
Hemp shiv	*Versicolor*	w additives	Sterilized	VHWS	3	Cylindrical D103 mm
Wheat straw	*Versicolor*	w/o additives	Sterilized	VSOS	3	Cylindrical D103 mm
Hemp shiv	*Ganorderma*	w additives	Sterilized	GHWS	3	Cylindrical D103 mm
Wheat straw	*Ganorderma*	w additives	Sterilized	GSWS	3	Cylindrical D103 mm
Hemp shiv	*Ganorderma*	w/o additives	Sterilized	GHOS	3	Cylindrical D103 mm
Wheat straw	*Ganorderma*	w/o additives	Sterilized	GSOS	3	Cylindrical D103 mm
Miscanthus	*Ganorderma*	w/o additives	Sterilized	GMOS	1	Cylindrical D103 mm
Miscanthus	*Ganorderma*	w additives	Sterilized	GMWS	1	Cylindrical D103 mm

2.3 Fabrication practice

The application of myco materials in buildings is crucial, with key attributes including thermal conductivity, hygric efficiency, and mechanical strength. However, achieving these properties can involve trade-offs. For instance, increased porosity can lower thermal conductivity but leads to higher moisture absorption. Additionally, open porosity can diminish mechanical resistance, but certain mycelium strains can enhance it. Hence, production should be tailored to the specific building application, engineering the final characteristics accordingly.

Establishing universally applicable practices for all mycelium bio-composites remains an ongoing challenge. While certain parameters, such as temperature and relative humidity, are widely documented for the incubation and growth phases, the customization of various factors for each mycelium-substrate-additive combination is crucial. Within the scope of this study, our focus centers on optimizing material ingredients among fabrication parameters. This section will elaborate on the optimal fabrication conditions to achieve the most desirable properties, based on qualitative analyses of the effects of various fabrication parameters in each mixture.

2.3.1 Inoculation

In this phase, substrate pretreatment and disinfection, eliminates other fungi, leaving the incorporated fungi as the dominant species. To perform a valid test of the effect of fungi on the substrate, it must undergo either pasteurization (heating in water between 80 to 100 °C) or sterilization (at 121 °C under 2 bars of pressure).

To evaluate hyphal growth quality under various conditions, trials were conducted by varying the fabrication parameters while cultivating mycelium on pure substrate without any disinfection pretreatment. The results revealed that *Ganoderma*, known for its strong adaptability, can thrive in both unpasteurized and pasteurized/sterilized substrates. However, its growth on sterilized substrates is significantly more uniform and results in a more homogenous structure. Conversely, *T. versicolor* and *Pleurotus* must be inoculated under sterile conditions, as these substrates are highly sensitive to the presence of bacteria in the medium.

The preparation of the substrate-fungi mixture, involving water and additives, can be implemented using various methods. One approach utilizes autoclaves, where the substrate is sterilized within autoclave bags. Another method involves placing the substrate into the autoclave using metal containers. In the first approach, water can be introduced into the

substrate-additive mixture and then placed in the autoclave, facilitating the complete absorption of water into the substrate fibers during the sterilization process. The required mass for the molds can be estimated using the final dry density and the average adsorbed moisture content as initial data for the calculation of the required mass of the dry substrate, additive, water, and mycelium, all of which are detailed in Table 2.4. It should be noted that the nomenclatures presented in Table 2.4 (see Abbreviations section of the thesis) differ from those in Table 2.3, as they are intended not only to identify the formulation and composition of the mycelium bio-composites, but also to distinguish the shape of the built samples. This distinction arises because the nomenclatures excluding sample shape are primarily used in Chapter 3 to report hygrothermal properties, whereas the nomenclatures including sample shape—also applied in Figure 2.6 and Figure 2.10—are essential for elaborating the influence of geometry on the fabrication process.

Conversely, in the second method, the substrate-additive mixture requires a different water incorporation process. In our specific protocol, substrate was immersed in the demineralized water for a duration of 24 h. Then, the substrate was sterilized in autoclave-equipped metal plates. Immersing the substrate in water is a crucial step in both sterilized and non-sterilized methods to ensure uniform distribution of water within the substrate. Mixing the substrate, additives, and water immediately before inoculation can result in the accumulation of water at the bottom of the inoculation bag. As a consequence, the upper substrate layers may lack sufficient water, while the lower layers become submerged, leading to an inadequate formation of the mycelial layer. This methodological consideration is pivotal to achieve optimal mycelial growth and homogenous substrate conditions.

Table 2.4 Adsorption characterization of the mycelium bio-composites

Sample	Dry mass (g)	Moisture content (%wt.)	Final Dimension (mm)				Dry density ($kg \cdot m^{-3}$)
			Cylindrical	Rectangular			
			Diameter	Length	Width	Height	
GHWUR	29.4	270.5		152	35	34	162.8
GSWPR	29.7	336.5		151	35	35	160.4
GHOPR	69.3	224.6		151	85	35	154.3
GHWPR	60.3	369.3		151	85	35	134.3
GHOUR-L	1170.0	330.9		477	475	41	125.9
GHOPR-L	1351.0	428.7		473	480	47	126.6
VHOPC	20.0	450.0	93.5			27.5	105.9
GHOPC-MBV	62.0	251.9	110			44	148.3
GHOPC	25.3	408.8	90			25	159.3
GSWPC	25.0	424.0	90			24	163.7
GHWUC	27.0	385.2	90			25	169.8
GHOUC	27.0	395.1	89			25	173.6
VSOPC	21.3	520.0	90			25	134.1

In laboratory-scale experiments, the initial inoculation is primarily carried out within plastic bags to facilitate the preliminary growth of mycelium before molding. In this study, non-filtered bags are opted, specifically employing standard zip-lock bags for the inoculation of samples. Subsequently, these bags were manually perforated with sterilized needles and then placed in a climatic chamber, (shown in Figure 2.2), maintained in a temperature range of 26-28 °C and a relative humidity level of 65-75 %. The maintenance of laminar airflow within the climatic chamber is essential to mitigate the risk of bacterial contamination within the samples. It is advisable to target an inoculation duration of 7-8 days for most samples. Prolonging the inoculation beyond the 10-day mark tends to result in desiccation of the inoculated mycelial

mat, compromising the final sample's quality. Conversely, an inoculation period of fewer than 5 days fails to promote sufficient mycelium growth within the substrate, leading to weakened mycelial development during the subsequent molding phase.

Figure 2.2. Exterior and interior view of the large-scale climatic chamber used in our experiments

2.3.2 Molding

PVC molds have demonstrated superior performance when compared to metal molds, as indicated in the Figure 2.3. This is attributed to the absence of chemical interactions between PVC and mycelium, whereas cast iron exhibited detrimental interaction. Consequently, when molding in PVC molds, a consistently dense mycelial layer forms in layers adjacent to the mold, often exceeding the quality of the layer in contact with the surrounding air. To maintain a favorable environment during molding, it is advisable to employ a perforated and disinfected plastic sheet covering the top of the sample. This practice helps preserve high relative humidity within the molding space. However, as shown in Figure 2.4, it is crucial to note that condensation on the plastic sheet, with subsequent water droplets falling onto the sample, can adversely affect the sample's visual attributes.

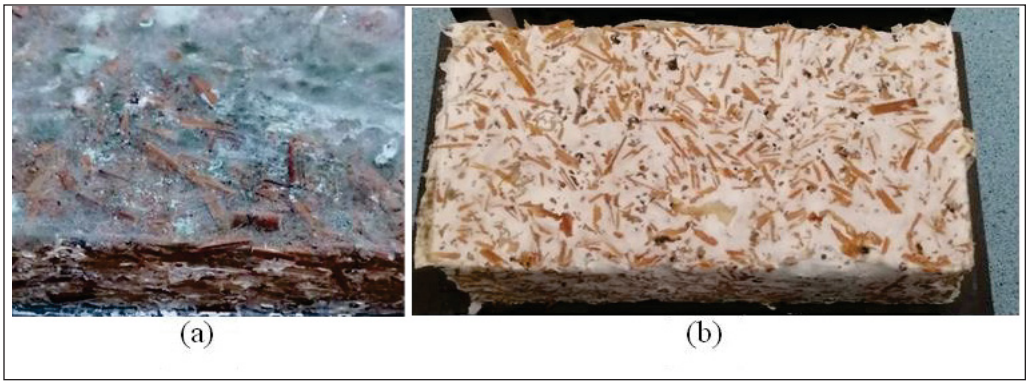

Figure 2.3. The comparison between; (a) Metal-molded samples; (b) PVC-molded samples

To mitigate this issue, it is mandatory to ensure that the plastic sheet does not come into direct contact with the uppermost layer of the sample, thereby averting condensation on the sample's exterior surface. Moreover, positioning the plastic sheet close to the top layer of the sample, within the perforated, oxygen-rich areas, may lead to undesired growth. This can disrupt the molding process if allowed to continue beyond 5 days. As a result, it is advisable to select molds with greater height than the thickness of the samples to prevent such interruptions and ensure smooth molding operations.

Molds are positioned under the same conditions as the inoculation bags. For all sample mixtures, a molding period of 7-8 days has proven to be the most effective practice. Nevertheless, extending the molding duration may be considered for mycelium types with slower growth rates or when enhanced inoculation is required. It's important to note, however, that an extended molding phase can result in the previously mentioned issue of unintended mushroom growth due to the elevated moisture content within the plastic sheet. Positioning molds in close proximity to each other with varying fungi contents can have adverse consequences, as the emitted spores from different fungi may interact harmfully, potentially neutralizing specific fungi types or causing spoilage in certain instances. In this project, a large climatic chamber is employed to ensure sufficient spacing between molded samples featuring distinct fungi types, even though they were not segregated into separate environmental zones.

(a) (b) (c)

Figure 2.4 Condensation as a result of direct contact of plastic sheet and sample; (a) dense molding in PVC; (b) condensation due to close contact of sheet with sample; (c) effective molding in larger heights molds

Given the compressibility of fibers, applying sufficient pressure during the molding process can yield an improved microstructure in the final product. Inoculated sample are initially crushed into fiber pieces and subsequently pressed by applying manual pressure by hand. This practice results in a denser molded sample, as shown in the Figure 2.4.a, which is necessary for optimal growth. The small size of the molds precluded the use of an industrial press. Ensuring uniform pressure across all areas of the mold, as well as across different molds, is essential for achieving a more accurate comparison between samples. To the best of the authors' knowledge, no specific reference has previously addressed the influence of pressure during the molding phase. The relevant references studied the effect of mechanical press during the material's drying phase. In the investigation conducted by Elsacker, Søndergaard, et al. (2021) a mechanical press, situated within an oven at 100 °C, exerted a maximum force of 30 kN at a rate of 2 $kN \cdot min^{-1}$ during cold pressing.

This procedure was found to enhance the overall mechanical strength of dried mycelium composites. Additionally, Appels et al. (2019) explored the substitution of the drying phase with hot pressing at 150 °C and cold pressing at 20 °C. This study also limited the applied force to 30 kN. However, during the molding phase, given that the hyphal structure remains a living organism, the applied pressure must be carefully adjusted to preserve the inherent properties of the mycelial structure. The denser molded mat will result in less space between

fibrous structure, which enables hyphae to grow denser within the filler, as depicted in Figure 2.5.

Figure 2.5 Complete mycelial development within densely compressed specimens

As shown in Figure 2.5, dense molding facilitates more complete and uniform mycelial colonization. The application of sufficient pressure compresses the fibrous substrate, reducing void space and enabling hyphae to form a compact, interconnected structure throughout the specimen. This structural density is essential for improving mechanical integrity and restricting moisture pathways. The image illustrates how compression enhances mycelial development, particularly in central regions of the sample, confirming the effectiveness of manual pressure in achieving homogeneous growth and structural cohesion.

In the case of straw-based samples, high initial substrate moisture content presents a significant challenge during the molding phase due to its rapid adsorption rate. Subsequently, in the drying phase a higher degree of shrinkage and a reduction in the final sample's size occurs, compared to hemp bio-composites. Therefore, application of manual pressure during the molding phase in substrate-based samples is crucial for maintaining the integrated physical structure of the final product. This pressure can be tailored to specific applications based on the required balance between porosity and mechanical resistance, which often function in opposite directions. The comparison between the adsorbed average moisture content (in color) and the average shrinkage (in hatched lines) of selected composites is illustrated in Figure 2.6.

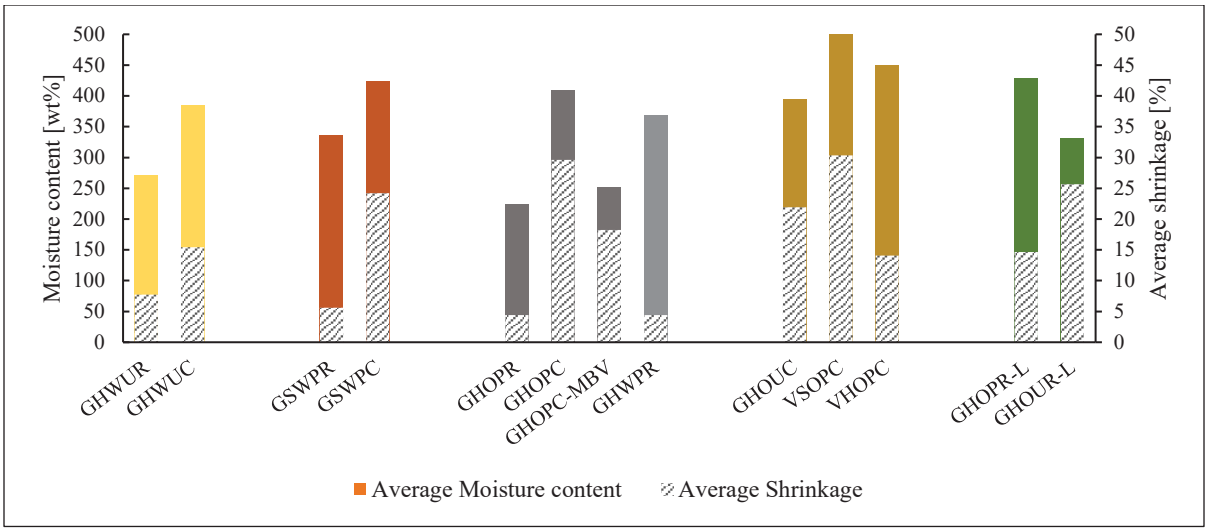

Figure 2.6 Moisture content and shrinkage of the samples during the drying process

The study analyzes five material categories, comparing their moisture content and subsequent drying shrinkage. The first two categories (including the comparison between GHWUR and GHWUC, as well as GSWPR and GSWPC) contrast rectangular and cylindrical molds, with rectangular molds exhibiting higher density (due to the ease of increased compaction during the molding phase), resulting in significantly lower moisture adsorption during growth and less shrinkage in the drying phase.

The third category includes both dense and light samples, along with larger samples customized for MBV testing (Annex II). The difference in the density of these samples is due to variations in material compaction during fabrication, not the constituents themselves. Rectangular samples, despite absorbing more moisture due to their higher hemp content, exhibit lower shrinkage because of greater compaction. This suggests that the durability of these samples, which is closely linked to shrinkage rate, is highly dependent on the compaction process during fabrication.

The fourth category examines different substrates with the same fungi and the same substrate with different fungi types, investigating their resulting shrinkage behavior. Due to the cylindrical shape of the samples in this category, the compaction rate is assumed to be nearly uniform across samples. Comparing GHOUC and VHOPC, the more rigid and dense structure

of *G. lucidum* in GHOUC, along with its hydrophobicity, results in lower moisture absorption and consequently less shrinkage. Between VSOPC and GHOPC, the straw exhibits a high and rapid adsorption rate, leading to greater shrinkage during the drying phase, as previously discussed.

The fifth category focuses on large-size samples, which share the same substrate and fungi but differ in pasteurization methods. In comparing the large and small sizes of GHOP (both rectangular and cylindrical), the small size shows a higher shrinkage rate during drying, despite having the same moisture content. This is because manual compression of the larger samples is easier and more efficient, resulting in a denser structure. However, the comparison between larger samples is inconclusive due to inconsistent density across different spots within each sample and between samples, preventing reliable comparative results.

2.3.3 Demolding

The objective of the demolding process is to promote homogeneous mycelial growth across all parts of the samples, particularly those in proximity to the mold surfaces. In contrast to the molding phase, which maintained a uniform duration for all samples, the demolding phase can be tailored to enhance the quality of the mycelial layer, contingent upon the intended applications. For robust mycelium types, like *Ganoderma*, the optimal demolding time is typically 2-3 days.

Beyond this period, as illustrated in Figure 2.7, the samples begin to exhibit a brownish hue, indicating the onset of mushroom fruiting, and a degradation in mycelium quality. The circled (a) zones of the sample represent fruiting bodies formed due to excess molding time. In contrast, the circled (b) spot in the photo on the right shows the effect of contact between the plastic sheet and the sample during the fabrication process.

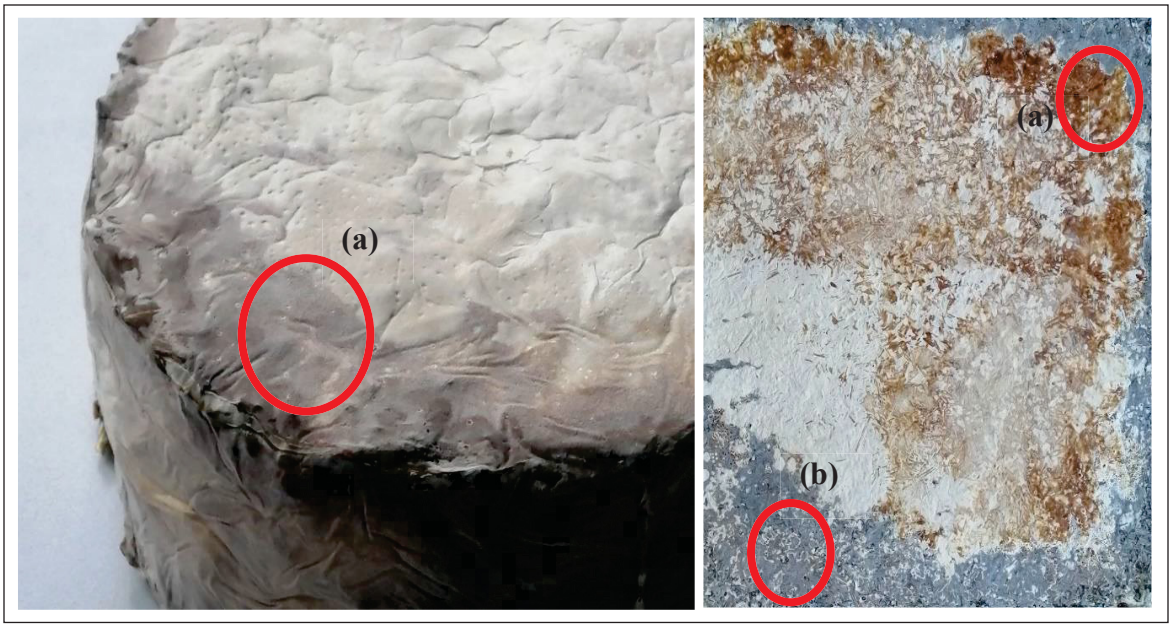

Figure 2.7 Anomalies on the mycelial layer; (a) fruiting bodies; (b) the effect of plastic sheet condensation and direct touch

Conversely, for less resilient fungi such as *Pleurotus* and *versicolor*, a demolding duration of 7-8 days has proven suitable for facilitating optimal mycelium colonization on the surfaces. To prevent condensation on the caps, it is advisable to place the samples in a spacious container, while maintaining similar relative humidity and temperature levels as in the molding phase. As previously noted, the utilization of PVC molds facilitates mycelial growth on surfaces contiguous to the mold. As depicted in Figure 2.8, this robust surface growth diminishes the requirement for prolonged demolding periods exceeding 7 days.

Figure 2.8 Perfect growth of mycelium in the surfaces adjacent to the PVC mold

2.3.4 Drying

The drying of the samples is carried out at 60℃ to 65℃ until a stable mass is achieved in the last one hour (For small size samples it was occurred in the 50hrs. The duration of this process varies depending on the sample and their initial moisture content, ranging from 48 to 96 hours in certain cases. The drying setup for small (left side) and large size ovens (right side) are shown in Figure 2.9.

Figure 2.9 Samples' drying setup for small (left) and large (right) ovens

The drying curves of the samples illustrate notable moisture adsorption characteristics in both hemp-based and straw-based composites. Figure 2.10 indicates the adsorption and desorption of the moisture and the subsequent evaporation rate in the drying process. As can be seen, in the large sized samples the evaporation rate is approximately four times less than the small-sized samples.

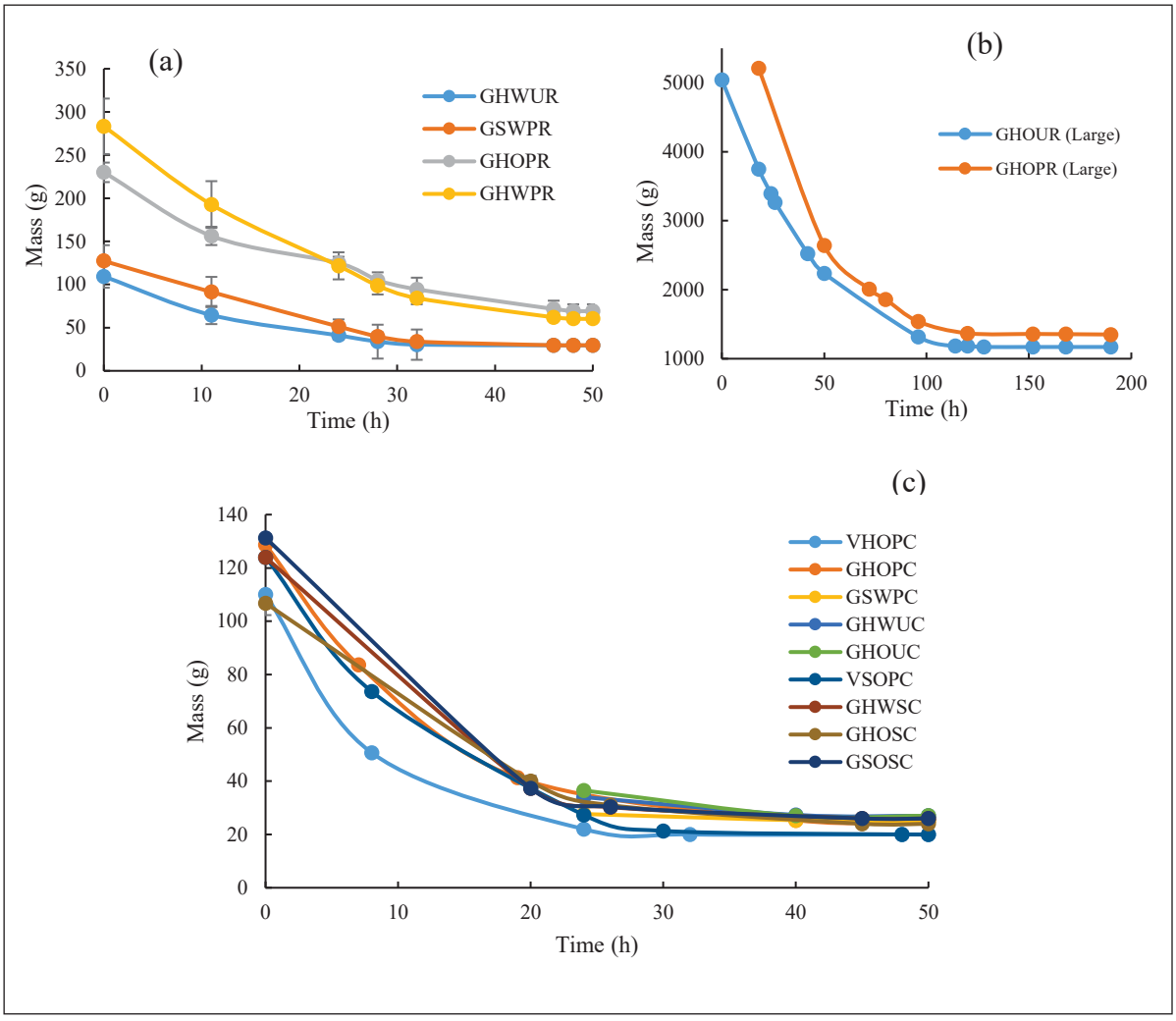

Figure 2.10 Mass reduction of samples in the drying process: (a) small rectangular samples (b) Large samples (c) cylindrical samples

Based on the mass change shown in Figure 2.10, although the initial wet masses of the molded samples vary due to differences in water uptake capacity, the final dry masses show close

proximity because the amount of mixed substrate and fungi is constant. The differences in drying curves across samples are attributed to their distinct adsorption and drying behaviors.

2.4 Conclusion

The research presented in this chapter focuses on developing and optimizing fabrication methods for MBCs. The primary objective was to identify effective combinations of agricultural residues as substrates, specific fungal species, and additives to enhance the properties of MBCs. Employing a systematic trial-and-error methodology, the study meticulously analyzed the physical and appearance characteristics of various samples. Key metrics such as weight changes, water dynamics during the fabrication process, and the extent of mycelial growth within the substrate matrix were evaluated. These efforts aim to contribute to customizing and improving the fabrication techniques of MBCs for building insulation applications.

In the fabrication procedure, hemp and straw exhibited distinct characteristics in water absorption, evaporation, and shrinkage during their drying process. Based on the comparison between hemp-based and straw-based samples in Figure 2.6 straw exhibited higher moisture adsorption and therefore is ideal for applications requiring a moisture buffer, particularly in layers close to interior spaces to regulate indoor humidity. Hemp is more efficient for hygric insulation near the outer surface, with lower water uptake, especially when a dense mycelium layer is engineered on the material's surface. It is noteworthy that the material's hydrophobicity is determined by its ability to adsorb and release moisture during fabrication. For a more precise and quantified discussion on water vapor permeability and moisture buffer, our next study is dedicated to characterizing these hygric properties.

The compatibility of three fungi types, representing distinct mycelium categories, with straw and hemp was explored. G. lucidum demonstrated consistency with both materials, while they contrasted in terms of cellulose, hemicellulose, and lignin content. *P. ostreatus* and *T. versicolor* exhibited mostly adaptable behavior with hemp-based composites in the study.

However, the addition of nitrogen-rich additives significantly enhanced mycelium growth on the straw-based substrates.

Given that mycelium is a living organism, its interaction with mold materials is crucial in the selection process. In the fabrication tests, PVC led to the perfect formation of a fungi layer adjacent to the mold, whereas cast iron adversely affected mycelium interaction, damaging the inner structure and compromising the entire content. Mycelium growth engineering is crucial in designing the fabrication process of MBC. Through precise adjustment of additives, careful selection of fungi-substrate pairing, use of PVC molds, and controlling mycelium growth duration during molding and demolding phases, a tailored mycelium layer can be crafted for diverse applications, including building, packaging, acoustic insulation, and other viable uses for MBC.

These findings highlight the importance of tailoring fabrication parameters to the intended application, as substrate–fungus interactions directly influence moisture management, structural cohesion, and surface properties. While this chapter focused on qualitative optimization, further quantitative characterization (Chapter 3) is essential to validate performance under standardized conditions. The limitations observed with spawn variability, particularly for *P. ostreatus*, underscore the need for consistent material inputs to ensure reproducibility in fabrication trials and reliability in future upscaling efforts.

CHAPTER 3

EXPERIMENTAL CHARACTERIZATION OF MYCELIUM-BASED COMPOSITES

Abstract

This study investigates the coupled hygrothermal behavior of mycelium-based composites (MBCs) as a function of their microstructural organization, governed by fungal species, substrate type, additive incorporation, and treatment method. Eleven composite formulations were selected and characterized using a multi-scale experimental approach, combining scanning electron microscopy, dynamic vapor sorption, vapor permeability tests, capillary uptake measurements, and transient thermal conductivity analysis. Scanning Electron Microscopy (SEM) analysis revealed that *Ganoderma lucidum* forms dense and interconnected hyphal networks, whereas *Trametes versicolor* generates looser, localized structures. These morphological differences directly influence water vapor transport and heat conduction. Additive-enriched composites exhibited up to 21.8% higher moisture uptake at 90% RH, while straw-based composites demonstrated higher capillary uptake and free water saturation (up to 704 $kg \cdot m^{-3}$), indicating enhanced moisture sensitivity, relative to hemp–Ganoderma composites, indicating greater overall moisture sensitivity. In contrast, hemp-based formulations with *Ganoderma lucidum* showed reduced sorption and vapor permeability due to limited pore interconnectivity. Thermal conductivity varied nonlinearly with temperature and moisture content. Fitting the experimental data with an exponential model revealed a moisture sensitivity coefficient thirty times lower for GHOP compared to VHOP, highlighting the stabilizing effect of a compact microstructure. The distinction between total and effective porosity emerged as a key factor in explaining discrepancies between apparent and functional moisture behavior. These findings demonstrate that hygric and thermal properties in MBCs are governed not by porosity alone, but by the geometry and connectivity of the internal fungal network. Optimizing these structural features enables fine control over heat and mass transfer, laying the groundwork for the development of high-performance, bio-based insulation materials.

3.1 Introduction

The construction industry, contributing approximately 38% of global carbon emissions (Hamilton et al., 2020), faces mounting pressure to adopt sustainable materials that address both embodied and operational carbon. In Canada, commercial and institutional buildings account for 18% of total energy demand, with the residential sector adding 33% (Jones & Brischke, 2017). Embodied energy, which is often overlooked, constitutes 10–30% of a building's carbon emissions (Beccali et al., 2013; Cuéllar-Franca & Azapagic, 2012; Lawrence, 2015), emphasizing the need to transition from zero-energy buildings (ZEB) to life-cycle zero-energy buildings (LCZEB) (Dutil et al., 2011). Mycelium-based composites (MBCs) are sustainable insulation alternatives produced through the colonization of agricultural by-products by fungal mycelium. Mycelium acts as a natural binder, replacing chemical binders such as lime, and offers sustainability benefits due to its low carbon footprint, biodegradability, and carbon sequestration ability during growth (Alaux et al., 2023; Cerimi et al., 2019; Livne et al., 2022b). These qualities position MBCs as viable alternatives to energy-intensive insulation materials like expanded polystyrene (EPS).

Recent research has advanced MBC property understanding, yet hygrothermal studies remain limited. Elsacker et al. (2021) explored moisture uptake in extruded MBCs, showing resilience under different hygric conditions (Elsacker, Søndergaard, et al., 2021). Koh et al. measured thermal conductivity (0.06–0.08 $W \cdot m^{-1} \cdot K^{-1}$) and moisture uptake in mycelium-based insulation composites, highlighting substrate influence in their physical properties. Yang et al. (2021) reviewed MBC functionality, noting thermal insulation potential akin to EPS. Gauvin et al. (2022) reported low thermal conductivity (0.05–0.07 $W \cdot m^{-1} \cdot K^{-1}$) and good moisture buffer capacity in MBCs as foam-like insulation. Schultz et al. (2024) demonstrated thermal stability (0.06 $W \cdot m^{-1} \cdot K^{-1}$ post-weathering) under simulated conditions. Farrahnoor et al. (2024) improved water barrier properties of MBCs with beeswax coatings, aiding thermal performance. Additionally, in terms of carbon emission, Alaux et al. (2023) and Stelzer et al. (2021) quantified environmental benefits, with the latter reporting a carbon footprint of 0.3–0.7 kg $CO_2e \cdot kg^{-1}$ for MBC bricks.

Recent studies on mycelium-based composites (MBCs) leverage scanning electron microscopy (SEM) to elucidate how microstructural features govern hygrothermal performance. Haneef et al. (2017) utilized cryo-SEM to examine MBCs from *Ganoderma lucidum* and *Pleurotus ostreatus* grown on cellulose-based substrates, demonstrating that substrate-driven variations in hyphal morphology and composition, such as increased chitin content, directly enhance water absorption rates, a key hygrothermal property. Gauvin et al. (2022) reported that extended fungal growth forms a denser mycelium layer, improving water resistance and influencing thermal conductivity, with microstructural insights supported by SEM-based studies they reference, such as Elsacker et al. (2019). Yang et al. (2021) reviewed SEM analyses of species like *Trametes versicolor* and *Ganoderma lucidum*, linking species-specific structural variations, particularly porosity, to thermal insulation and moisture buffering capacity.

Despite recent advancements in the study of MBCs, significant research gaps remain, particularly regarding the correlation between their microstructure and comprehensive hygrothermal properties. The existing literature has predominantly focused on basic parameters such as thermal conductivity, moisture uptake, and mechanical strength, while more detailed hygrothermal characteristics, such as sorption isotherms, vapor permeability, and moisture buffer values, have been largely overlooked. Furthermore, the lack of an established link between microstructural features and hygrothermal performance hinders the optimization of MBCs for practical applications in sustainable building insulation.

To address these research gaps, this study systematically characterizes the microstructural and hygrothermal properties of MBCs, fabricated from hemp and straw substrates colonized by *Ganoderma lucidum* and *Trametes versicolor*. The study evaluates how variations in substrate–fungus combinations and fabrication parameters influence the microstructure of samples. Accordingly, this study entails the characterization of key insulation properties, including moisture adsorption, vapor permeability, water uptake and thermal conductivity. By integrating scanning electron microscopy (SEM) with hygrothermal analysis, the research seeks to establish a direct correlation between microstructural characteristics and material

performance, offering valuable insights into fungal–substrate interactions and optimizing MBC design for sustainable building insulation.

This chapter is organized to present the investigation of MBCs as sustainable insulation materials. Section 2 outlines the materials and experimental methods alongside the governing equation used for the calculation of physical properties. It encompasses the fabrication of MBCs and the protocols for microstructural and hygrothermal characterization. Section 3 reports the findings, detailing microstructural analysis via scanning electron microscopy (SEM), alongside hygric and thermal property assessments. The discussions are included in this section alongside the presented results. Section 4 summarizes the key outcomes, their implications for sustainable building insulation and proposes directions for future research. To provide a comprehensive understanding of these effects, a detailed experimental approach is necessary to isolate the influence of fungal species, substrates, and processing conditions on microstructural and hygrothermal outcomes.

3.2 Materials and methods

This section presents the materials used and the procedures followed for fabricating and testing MBCs, allowing for the systematic characterization of their structural, hygric, and thermal behavior.

Tested MBCs were fabricated using two fungal species: *Ganoderma lucidum* and *Trametes versicolor* and two types of agricultural substrates, hemp shiv and wheat straw. Substrates were sourced locally, cleaned, and sieved to particle sizes between 2 mm and 10 mm to achieve consistent composite textures. Two organic nutritional additives, wheat bran and soybean meal, were utilized to enhance fungal colonization. Each composite mixture comprised substrate, fungal spawn, and additives in specific weight ratios detailed below. Three disinfection methods were examined: unpasteurized (ambient), pasteurized (80 °C for 60 min), and sterilized (121 °C, 15 psi for one hour), to evaluate their effect on fungal growth and composite properties.

Formulations followed these ratios:

- Substrate (hemp or straw): 50 % dry mass;
- Fungal spawn: 33 % dry mass;
- Nutritional additive (wheat bran or soybean meal): 17 % dry mass (only for specific formulations indicated below);
- Water content adjusted to 233 % of dry mass using distilled water.

The prepared mixtures were then inoculated for 7 days in plastic bags at controlled conditions (temperature: 26–28 °C, relative humidity: 65–75 %) for 7–8 days. Inoculated samples were then placed into rectangular and cylindrical molds with dimensions adjusted for planned hygrothermal tests (R1: 35 × 35 × 162 mm³; R2: 35 × 90 × 162 mm³; R3: 500 × 500 × 30 mm³; C1: Cylindrical D103, H30 mm; C2: Cylindrical D118, H30 mm). For each formulation in each test, three samples were fabricated to ensure the repeatability of the experimental results. The samples were then covered with plastic and incubated at the same controlled conditions for another 7–8 days. Samples were demolded and left for an additional 7 days of incubation for the edges of the samples to be fully colonized by mycelium. The process was then followed by drying process at 60 °C to 65 °C until mass stabilization, which is typically achieved within 48 to 96 h.

3.2.1 Sample nomenclature

Sample naming conventions consistently follow substrate–fungus–additive–disinfection order:

- Fungus species: *Ganoderma lucidum* (G), *Trametes versicolor* (V);
- Substrate: Hemp (H), Straw (S);
- Additive: With additive (W), Without additive (O);
- Disinfection method: Unpasteurized (U), Pasteurized (P), Sterilized (S).

Thus, for instance, the sample “GHOP” denotes *Ganoderma lucidum* colonized on Hemp substrate, withOut additives, and Pasteurized. Using this mixture to systematically investigate the influence of compositional and processing variables on the hygrothermal performance of

mycelium-based composites (MBCs), a total of 11 formulations were prepared. These formulations vary in terms of fungal species, substrate type, presence of additives, and processing treatments. This variety was designed to account for a realistic range of material conditions encountered in MBCs fabrication methods. The selection of specific formulations for each test was guided by the suitability of the sample for the target property being measured. For example, for microstructural analysis, two samples were chosen to highlight the differences resulting from the use of different fungal species; for thermal conductivity measurements, the most cohesive specimens with the lowest densities and highest porosity were selected; and for hygric tests, a representative subset was selected to encompass variation across all major fabrication parameters, supporting a more comprehensive interpretation of moisture-related behavior.

3.2.2 Microstructural characterization

Scanning Electron Microscopy (SEM) was performed using selected representative samples (GHOP and VHOP) to qualitatively analyze fungal colonization, network density, substrate interaction, and internal morphology. SEM imaging was conducted following specimen preparation and imaging practices consistent with ISO 16700 recommendations. Samples were prepared by slicing small segments ($1 \times 1 \times 5$ mm^3) from the center of cured composites, mounted on SEM stubs, and gold-coated for 120s using sputter coating. Images were captured at magnifications ranging from 30x to 7000x, providing insights into microstructural differences associated with fungal species and substrates.

3.2.3 Hygric characterization

Sorption isotherm analysis was performed using a Dynamic Vapor Sorption (DVS) device. Sorption isotherms were measured in accordance with ISO 12571. The ProUmid DVS device, is manufactured by ProUmid GmbH & Co. KG, which is headquarters in Ulm, Baden-Württemberg, Germany. This device is used for these measurements offers a mass precision of 0.01 mg with an uncertainty of ±0.005% for moisture content, and controls relative humidity with a precision of ±0.1 % and an uncertainty of ±1% to ±1.5 %. The device was programmed

to vary the relative humidity (RH) over the range of 0 to 90 % RH in 10 % humidity range steps. Sorption isotherms are characterized at five different temperatures to assess the temperature's influence on the adsorption behavior. Five samples are characterized including GHOP, GHOU, GHWU, GSWP, and VHOP (see Nomenclature for definitions).

The GAB model is employed to characterize the hygric behavior of the tested composites during adsorption. It enables the modeling of a material's hygroscopic behavior across the entire spectrum of relative humidity from 0 % to 100 %. The relationship between the moisture content (u) and the relative humidity (ϕ) based on this equation is as follows:

$$u(\phi) = \frac{w_m C K \phi}{(1 - K\phi)(1 - K\phi + CK\phi)} \tag{3.1}$$

where w_m represents the moisture content associated with an adsorbed monolayer, while C and K are coefficients dependent on the molar heat of absorption and the latent heat of condensation, respectively. The DVS device provides sorption isotherms in terms of the equilibrium moisture content on a mass basis, u ($kg \cdot kg^{-1}$), as a function of the applied relative humidity. In order to use these data in transport equations, where the volumetric moisture content w ($kg \cdot m^{-3}$) is required, the conversion is carried out by multiplying u with the bulk density of the dry material or, alternatively, with the free water saturation w_f. In this way, the sorption results can be consistently integrated with the hygrothermal model parameters. The constant parameters of the GAB model are then obtained by regression on the measured DVS data.

Water vapor permeability was measured using the cup method in accordance with ISO 12572 (and ASTM E96/E96M for comparison). The dry cup method involves creating a dry environment beneath the sample and subjecting the top to controlled environmental condition of 50 % relative humidity in the climatic chamber. The successive mass variations in the last five measurements should be less than 5% of the difference in the initial and final moisture content of the sample. The diffusion coefficients for vapor transfer using the dry methods are

calculated based on Equation (3.2) as a function of relative humidity or moisture content. The tested samples in the permeability test are VSOP, GSWP, and GHWU.

$$g_v = -\delta_p \nabla P_v = -\delta_p P_{v,sat} \nabla \phi = -D_{v,\varphi} \nabla \phi = -D_{v,w} \nabla w = -\frac{\delta_p P_{v,sat}}{\xi_\phi} \nabla w \tag{3.2}$$

where g_v is the vapor flux, δ_p represents the water vapor permeability, and P_v denotes the partial vapor pressure, $P_{v,sat}$, corresponds to the saturation vapor pressure, while ϕ represents the relative humidity. The vapor diffusion coefficient as a function of relative humidity and moisture content are denoted by $D_{v,\varphi}$ and $D_{v,w}$, respectively. w indicates the moisture content, and ξ_ϕ is the slope of the sorption isotherm. Accordingly, the resistance factor is calculated as follows:

$$\delta_p = \frac{\delta}{\mu} \tag{3.3}$$

where δ_p is the vapor permeability of the material, and μ is the water vapor diffusion resistance factor. By applying a capillary boundary condition, the capillary diffusion coefficient can be determined, representing the liquid moisture transport within the material at elevated moisture contents. The capillary coefficient will be calculated as a function of moisture content.

$$g_w = -D_{l,w}(w) \nabla w \tag{3.4}$$

where g_w represents the liquid water flux and $D_{l,w}$ is the liquid water diffusivity. The liquid diffusivity is obtained from the following equation (Künzel, 1995):

$$D_{l,w} = \frac{\delta_p}{\rho_w} \frac{dp_v}{dw} \tag{3.5}$$

where δ_p is the vapor permeability of the material, ρ_w is the density of water, and $\frac{dp_v}{dw}$ comes from the slope of the sorption isotherm. Additionally, Künzel (1995) established an approximation to define a liquid transport coefficient, as follows:

$$D_{ws} = 3.8 \times (\frac{A_c}{w_f})^2 \times 1000^{(\frac{w}{w_f}-1)} \quad (3.6)$$

where D_{ws} is the capillary transport coefficient, specifically referring to diffusivity under saturation conditions. A_c is absorption coefficient of water, w_f is the free water saturation, and w is the actual moisture content. By plotting mass per unit area against the square root of time, A_c is determined from the slope of the capillary sorption graphs. The capillary water absorption coefficient of the mycelium-based composite samples was determined using the partial immersion method in accordance with ISO 15148, which specifies the procedure for measuring liquid water uptake in porous building materials under controlled conditions. The principle of the test is to measure the mass evolution of samples that are in contact with water. This condition is achieved by placing the samples on a grid and immersing them to a depth of approximately 3 mm. The tested samples are of dimensions 38 × 31 × 100 mm^3. Three different samples from the mixtures of Straw and Hemp with *Ganoderma lucidum* (GSWP, GHOU, and GHOP) are tested. For each type of composite, three samples were prepared. The specimens are cut to eliminate the layer that was in contact with the mold. The samples are then dried in an oven at 70 °C, which is the maximum permissible temperature to prevent MBC decomposition, until the mass stabilizes. The lateral faces of the samples are isolated using cellophane and aluminum foil tape. At the beginning of the test, mass measurements were taken at 30 s intervals, followed by measurements at 1 min, 5 min, 10 min, 20 min, and 1 h. Before each measurement, the specimen is superficially drained and wiped.

The measurement of the free water saturation samples are measured through submerging cylindrical samples with the dimensions D90 mm and H25 mm. The samples are initially placed in a sealed chamber and vacuumed for 2 h to remove the air trapped in the open pores of the material. The chamber is then filled with water and resealed, with samples submerged

in the water. The same vacuum pump is used to ensure that the cavities of the samples are effectively filled with water. The weight is monitored hourly until the mass of the samples stabilizes. The weight of water adsorbed by the sample was measured in 0.1g increments until the weight stabilized over three consecutive measurements. Three samples of each type of bio-composite were utilized. Free water saturation in Equation (3.7) indicates the open porosity of the material, while the maximum water content, denoted as w_{max}, reflects the filling of all cavities (open and closed) in the material, representing total porosity. Measuring the maximum water content is often impractical because closed porosity requires pycnometry tests, which involve crushing the material into powder, a challenging process due to the material's compressible nature and resistance to pulverization. Therefore, free water saturation substitutes this parameter in the equations. Additionally, as shown later in this paper, the majority of the material's porosity is open, so this assumption does not compromise the accuracy of the results. It is noteworthy that based on this study's findings, the majority of material porosity is open, thereby minimally affecting the results.

$$w_f = \rho_w \cdot n \tag{3.7}$$

where w_f represents the free water saturation as previously discussed, ρ_w is the density of water, and n denotes the porosity of the material.

3.2.4 Thermal characterization

Thermal conductivity and specific heat capacity are measured as the basic thermal properties. Thermal conductivity was measured using the transient plane source (TPS) method following ISO 22007-2 guidelines. The TPS device operates by employing a transient heat source to measure thermal conductivity. It consists of a sensor with a flat, thin, and round probe that is heated for a short duration. The temperature response of the material undergoing testing is then monitored, and the thermal conductivity is determined based on the rate at which heat is transferred through the sample. This method allows for quick and accurate measurements of thermal conductivity across a wide range of materials.

Using TPS, thermal conductivity is measured for three relative humidities (0, 50 and 80 percent) and three different temperatures (10 °C, 20 °C and 30 °C). The relative humidity and temperature conditions are adjusted by placing both the TPS device and the test sample inside a climatic chamber throughout the duration of the measurement. Four samples are characterized, including GHOP, GSWS, GSOS, and VHOS. Relative humidity causes fluctuations in material moisture content, thereby directly impacting thermal conductivity. Increasing temperature can partially increase pore diameters, thus directly affecting thermal conductivity. However, its primary influence indirectly occurs by changing saturation pressure as follows (Promis et al., 2018):

$$p_v^{sat} = \exp\left[23.5771 - \frac{4042.9}{T - 37.58}\right], \tag{3.8}$$

where p_v^{sat} is the saturation vapor pressure, and T represents the temperature.

With a robust experimental protocol in place, the results derived from SEM analysis and hygrothermal testing now offer insights into the material's behavior and performance trends. The extension of the testing procedures described is summarized in Table 3.1, which details the test types, number of replicates, sample formulations, and corresponding dimensions.

Table 3.1 Summary of sample types, formulations, and dimensions used

Test Type	**Number of Samples for Each Formulation**	**Sample Formulations**	**Sample Dimensions**
Microstructural Characterization	3	VHOP, GHOP	1 × 1 × 5 (mm)
Sorption Isotherms (DVS)	3	GHOP, GHOU, GHWU, GSWP, VHOP	30 × 40 × 50 (mm)
Water Vapor Permeability	3	VSOP, GSWP, GHWU	Cylindrical D103, H30 (mm)
Water Absorption	3	GSWP, GHOU, GHOP	Cylindrical D103, H30 (mm)
Thermal Conductivity	3	GHOP, GSWS, GSOS, VHOS	Cylindrical D103, H30 (mm)

The capillary water absorption coefficient of the mycelium-based composite samples was determined using the partial immersion method in accordance with ISO 15148, which specifies the procedure for measuring liquid water uptake in porous building materials under controlled conditions.

To enable direct comparison with conventional insulation materials, the thermal resistance (R-value) of the tested samples was calculated from the measured thermal conductivity values using the following equation. This approach provides a standardized performance indicator relevant to building envelope applications.

$$R = \frac{e}{\lambda} \tag{3.9}$$

$$R_{US} = 5.678 \, . \, R_{SI} \tag{3.10}$$

where R_{SI} denotes the thermal resistance expressed in SI units ($m^2 \cdot K \cdot W^{-1}$), e is the specimen thickness (0.03 m for all tested samples), λ represents the measured thermal conductivity, and R_{US} is the corresponding thermal resistance expressed in Imperial units ($ft^2 \cdot °F \cdot h \cdot BTU^{-1}$).

3.3 Results and discussion

The following section presents and interprets the key find ings from structural, hygric, and thermal characterization, linking them to the underlying material formulations and microstructural features.

3.3.1 Microstructural Characterization

This analysis aimed to examine the interaction between fungal mycelium and hemp substrate, the formation of hyphal networks, and the overall material morphology. Understanding these microstructural features is essential, as they directly influence the mechanical integrity, porosity, and interfacial bonding within the composite. The analysis focused on two selected samples: GHOP and VHOP.

By analyzing high- and low-magnification images, SEM provides insights into the extent of mycelial colonization, fiber–matrix adhesion, and the presence of microstructural voids or reinforcements. These observations help assess how fungal growth patterns contribute to the composite's structure, potentially impacting its mechanical and moisture-related properties. The following section presents the microstructural observations derived from SEM imaging.

Both mycelium species form a network of filamentous structures called hyphae (Figure 3.1). These networks exhibit similar morphology, consisting of numerous branches. Each filamentous hypha elongates outward, fusing with other growing filaments to form a large "fractal network" structure. According to A. Farrahnoor et al. (2024) mycelium develops by consuming nutrients from substrates, decomposing organic matter, and converting it into compounds for its growth.

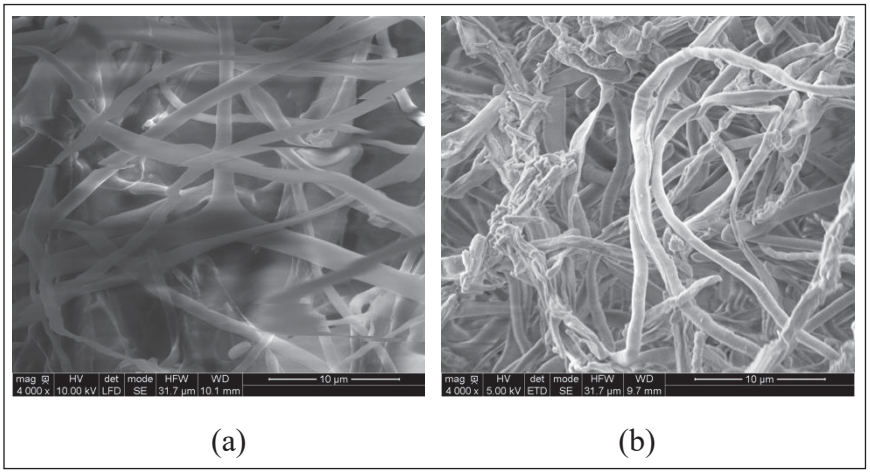

Figure 3.1 High-magnification (G = 4000) observation of mycelium development in the material: (a) GHOP; (b) VHOP

The interwoven structure of the hyphae indicates a dense network, suggesting effective substrate colonization, which is crucial for the formation of MBCs. According to Yang et al. (2021) the elongated and thin appearance of the hyphae likely results from shrinkage during the drying process, as the hyphae lose water content. The observed filament diameters range from 1 to 3 µm for GHOP and approximately 1 µm for VHOP, aligning with the lower range of white mycelium filament dimensions (1–30 µm) reported by Yang et al. (2021).

Based on the interaction between mycelium and substrate observed in the images, the multi-scale fiber effect between mycelium and granules might have influenced the composite's mechanical properties. This effect refers to how the mycelium's filamentous network (hyphae) intertwines with and binds the hemp granules at different scales. Such an interaction can enhance impact resistance, as demonstrated by Cai et al. (2023). The dense, interconnected mycelial network likely strengthens bonding between granules, distributes stress more effectively, and improves energy dissipation upon impact, contributing to greater durability.

At lower magnification, the mycelium network appears denser in *Ganoderma lucidum* (Figure 3.2). Given that the substrate is the same in both samples, this suggests that hemp shiv granules may not support the development of *Trametes versicolor* as effectively. The denser fungal growth in *Ganoderma*-based sample results in less porosity of that is further discussed in the next section with respect to its effects on hygric and thermal properties.

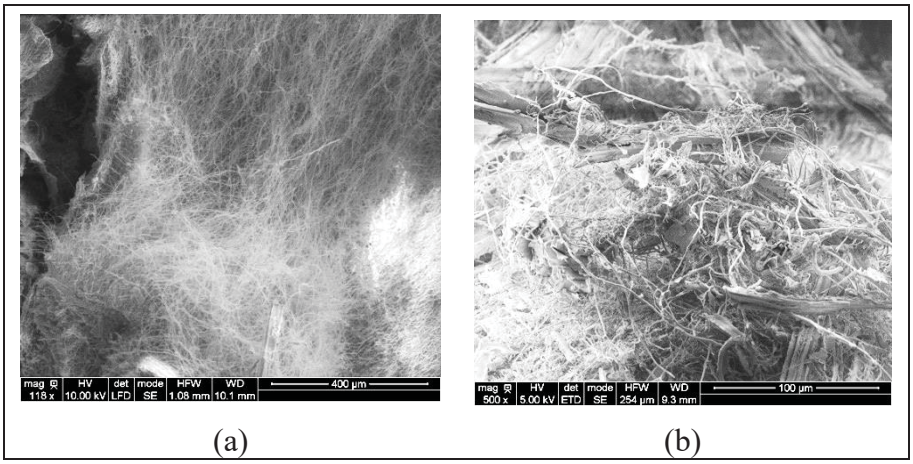

(a) (b)

Figure 3.2 Low-magnification (120 < G < 500) observation of mycelium network: (a) GHOP (118×); (b) VHOP (500×).

While still at a low magnification, the mycelial distribution within the composite appears more extensive and interconnected in the case of *Ganoderma lucidum* (Figure 3.3c). The denser, tightly interwoven filaments effectively fill voids between hemp granules, creating a more cohesive matrix. This suggests that *Ganoderma lucidum* exhibits stronger substrate colonization, enhancing particle adhesion and overall composite integrity compared to

Trametes versicolor. However, it is important to note that the samples were observed at different magnifications, which may influence the perceived differences in network density.

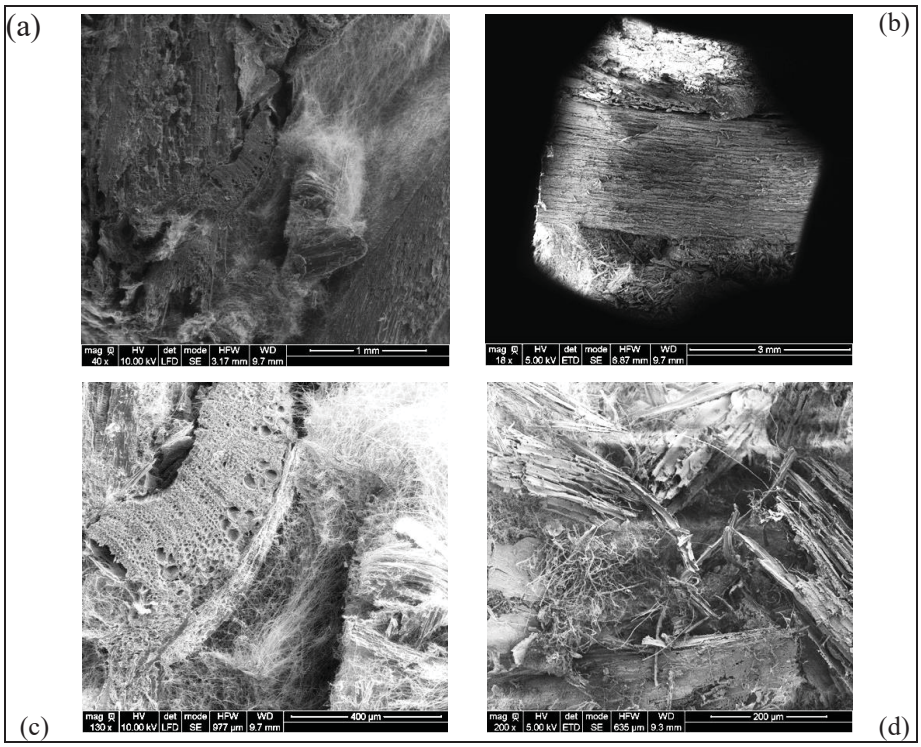

Figure 3.3 Low-magnification distribution of mycelium throughout the substrate: (a) GHOP (30×); (b) VHOP (18×); (c) GHOP (130x); (d) VHOP (200×)

While *Ganoderma lucidum* shows a higher concentration of mycelial filaments, both samples exhibit variations in mycelium distribution across different regions. The mycelial growth is notably denser along the edges of the aggregates (Figure 3.4), suggesting uneven colonization within the composite structure.

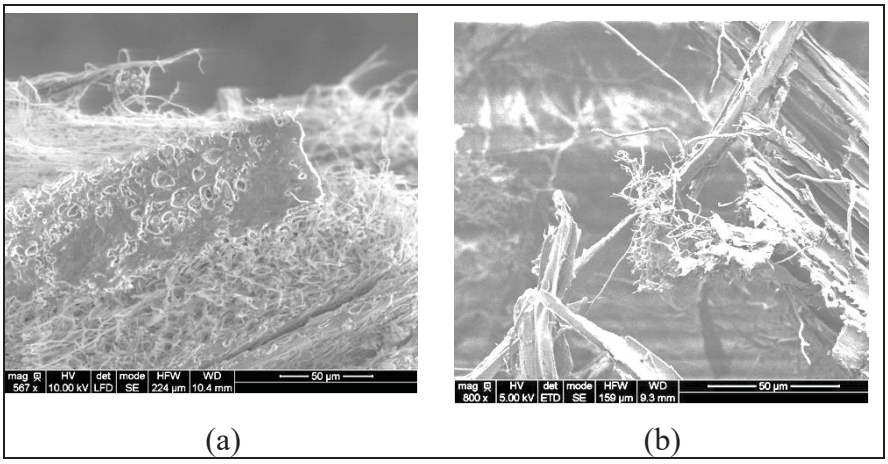

(a) (b)

Figure 3.4 High-magnification distribution of mycelium throughout the substrate: (a) GHOP (567×); (b) VHOP (800×)

It is also observed that the mycelium does not penetrate the internal structure of the aggregates (Figure 3.5). This is beneficial, as the retained voids enhance the material's insulating properties by reducing thermal conductivity.

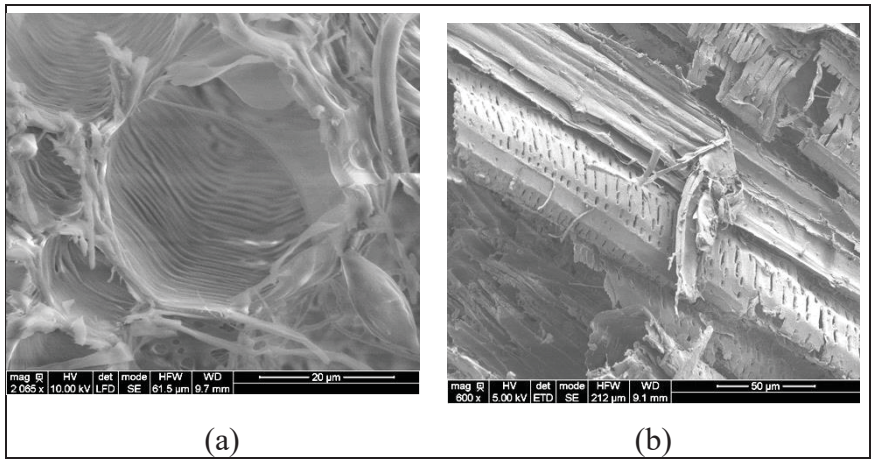

(a) (b)

Figure 3.5 Penetration of mycelium into the substrate in high magnification ratio: (a) GHOP (2065×); (b) VHOP (600×)

Additionally, at high magnifications, as shown in Figure 3.6, the presence of mycelium on the surface of the granules suggests partial lignocellulose digestion by the fungus. This interaction indicates the fungus' ability to break down and adhere to the substrate, potentially influencing the material's mechanical properties. The presence of mycelium is notably more pronounced

in *Ganoderma lucidum*, suggesting a stronger enzymatic activity or surface colonization compared to *Trametes versicolor*.

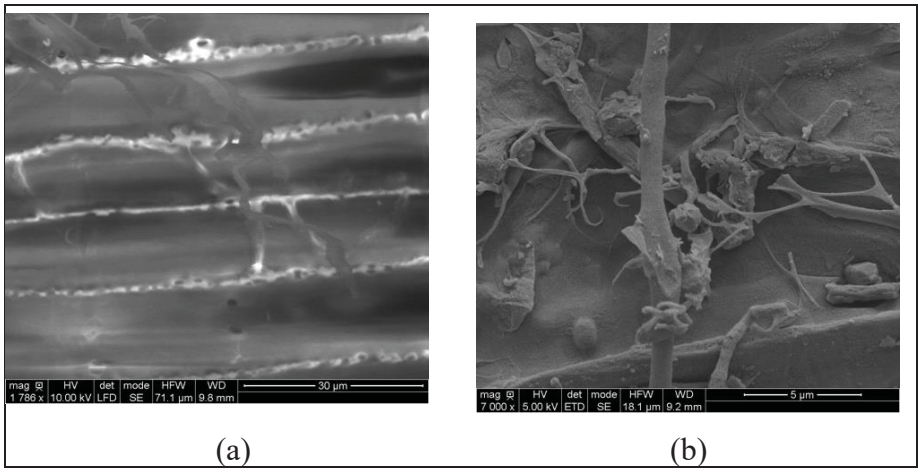

Figure 3.6 Observation of the surface of hemp substrate: (a) GHOP (1786×); (b) VHOP (7000×)

Additionally, partially spherical or granular structures observed on the granules appear to be part of the mycelium network. According to Adaskaveg and Gilbertson (1986), and Gaff et al. (2024), these formations are likely chlamydospores, specialized fungal structures known for their resistance to harsh conditions such as drought and high temperatures. Their presence suggests a potential adaptation mechanism that enhances the mycelium's ability to survive in challenging environmental conditions. Despite this fungal activity, the substrate's cell walls retain their fundamental morphology, indicating that while the mycelium interacts with the substrate, it does not significantly alter its structural integrity.

While these SEM observations reveal clear differences in network formation and substrate colonization, their functional implications on moisture-related behavior warrant further analysis.

3.3.2 Hygric Characterization

To evaluate how these structural differences influence the material's response to humidity, we now examine the hygric behavior of MBCs through sorption, permeability, and water uptake tests.

3.3.2.1 Sorption Isotherms

This test aimed to evaluate moisture sorption behavior, using five formulations (GHOP, GHOU, GHWU, GSWP, and VHOP), using the DVS device. Additionally, adsorption isotherms are tested separately for five temperatures. The sorption isotherms indicate the evolution of moisture content as a function of relative humidity. Figure 3.7 illustrates Sorption isotherms measured at 23 °C, comparing the effects of mycelium, treatment, substrate, and additive types on sorption across relative humidity levels for the tested formulations.

The four sorption isotherm graphs reveal that the additive type has the most significant impact on hygroscopic behavior, with GHWU (with additives) showing a 21.82 % higher moisture uptake than GHOU (without additives) at 90 % RH, followed by substrate type, where GHWU (hemp-based) exhibits an 11.38 % higher uptake than GSWP (straw-based) at 90 % RH. Treatment type (GHOP vs. GHOU) has a smaller effect, with a maximum difference of 5.28% at 80 % RH, while mycelium type (GHOP vs. VHOP) shows the least impact, with GHOP's uptake only 4.34 % higher than VHOP's at 60 % RH.

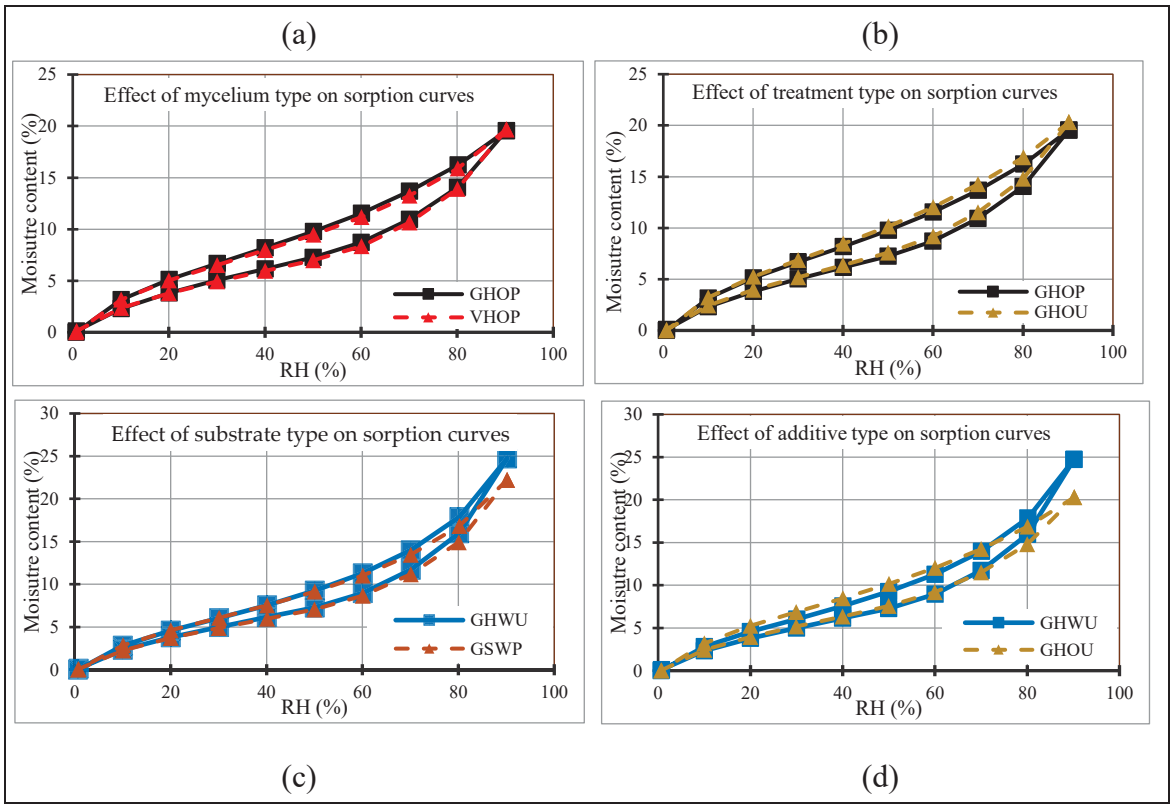

Figure 3.7 The effect of fabrication parameters on sorption isotherms including: (a) mycelium type; (b) treatment type; (c) substrate type; (d) additive types

An initial interpretation of the negligible sorption difference observed between GHOP and VHOP can be drawn from SEM images, which show strong surface colonization by both species. The presence of chitin in the mycelial structures may increase surface hydrophobicity, potentially resulting in similar moisture interactions under the low-pressure, laminar airflow conditions of the DVS device. However, a more detailed analysis of the internal microstructure provides deeper insight into this behavior.

These findings can be further understood by referring to the microstructural observations presented before. Although the difference in moisture uptake between GHOP and VHOP is quantitatively small (4.34 % at 60 % RH), the structural analysis provides valuable insights into this behavior. SEM images (Figures Figure 3.2–Figure 3.4) revealed that *Ganoderma lucidum* forms a denser and more interconnected hyphal network compared to *Trametes versicolor*, which tends to produce a looser and more localized structure. The denser network

in GHOP likely enhances connectivity between internal pores while simultaneously limiting their volume, thus reducing capillary condensation at high RH. Conversely, the more porous VHOP structure may offer more adsorption sites but with reduced interconnectivity, leading to localized saturation that does not lead to an increased total moisture content under DVS conditions.

Furthermore, the relatively higher sorption observed in hemp-based composites (e.g., GHWU) compared to straw-based ones (e.g., GSWP) is consistent with differences in fungal colonization efficiency. SEM images showed more homogeneous mycelial development in hemp composites, whereas straw-based composites exhibited anisotropic colonization and incomplete coverage of intergranular spaces. This results in less effective moisture transport pathways and a reduced capacity for homogeneous moisture distribution throughout the material volume, despite higher open porosity values.

The pronounced effect of additives, as observed in GHWU, also aligns with microstructural trends. Nutritional supplements enhance fungal activity and hyphal proliferation, increasing the overall surface area available for moisture interaction. This may also contribute to more complex capillary networks within the composite, leading to increased moisture retention at higher RH levels. These relationships between structure and moisture response are summarized in Figure 3.8 below, where the correlation between microstructure and hygroscopic behavior in mycelium-based composites is highlighted. The SEM micrographs show the dense, interconnected hyphal network of *Ganoderma lucidum* (top) and the more porous, localized structure of *Trametes versicolor* (bottom). The corresponding sorption isotherms illustrate slightly higher moisture uptake in GHOP due to network interconnectedness, and significantly increased uptake with additive use (GHWU), indicating a higher hygroscopic capacity associated with enhanced surface area.

In light of these correlations, it becomes evident that sorption behavior in mycelium-based composites is governed not only by the total porosity or fungal species but by the spatial configuration and connectivity of the hyphal network formed during colonization. Integrating

microstructural features into the interpretation of hygric measurements offers a more comprehensive understanding of moisture dynamics and supports the hypothesis that controlling fungal morphology through fabrication parameters is key to tailoring MBC performance for building applications.

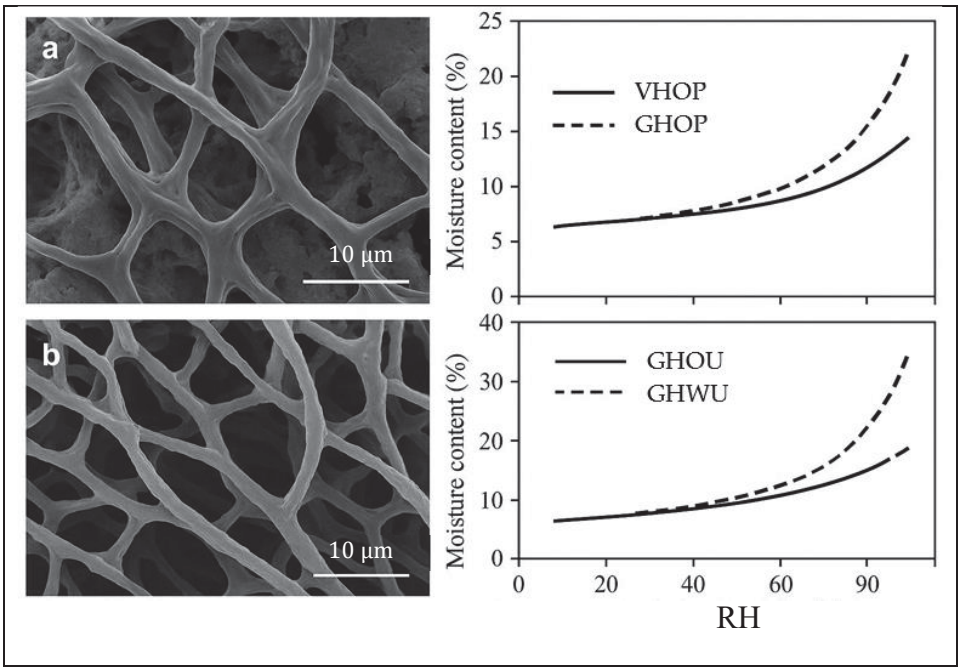

Figure 3.8 Correlation between microstructure of (a) *Ganoderma lucidum* and (b) *Trametes versicolor* and hygroscopic behavior in mycelium-based composite

GAB model was applied to fit the experimental adsorption isotherms of formulations enabling a quantitative assessment of their hygroscopic behavior across the full range of relative humidity at 23 °C. According to Equation (1), the calculated values of the GAB parameters are presented in Table 3.2 as follows.

Table 3.2 Fitting constants of GAB equation for sorption isotherms at 23 °C

Sample	Type	Fitted GAB Parameters		
		w (kg·kg⁻¹)	c	k
GHWU	Adsorption	0.053	8.701	0.877
GSWP	Adsorption	0.054	8.727	0.848
GHOP	Adsorption	0.062	8.412	0.772
VHOP	Adsorption	0.057	9.596	0.798
GHOU	Adsorption	0.066	7.825	0.768

The GAB model parameters also reveal significant distinctions: GHOP and GHOU exhibit higher monolayer moisture content values than VHOP, indicating a stronger initial affinity for moisture. This supports the hypothesis that the presence of chitin in *Ganoderma lucidum* (as confirmed by Yang et al. (2021)) increases surface hydrophobicity, while also creating internal zones that favor multilayer adsorption under high relative humidity conditions.

Figure 3.9 compares the GAB equation fittings with experimental adsorption isotherms, evaluating the effects of mycelium, substrate, treatment, and additive types on moisture content as a function of relative humidity. The GAB equation effectively captures the hygroscopic behavior of the tested MBC formulations, as demonstrated by high R-squared values (0.9678–0.9849) and low sum of squared errors (SSE ranging from 1.108×10^{-5} to 1.956×10^{-5}), indicating a strong fit between the model and experimental data across all relative humidity levels.

Figure 3.10 compares the adsorption isotherms for the GHWU formulation at five temperatures (15 °C, 23 °C, 30 °C, 35 °C, and 40 °C) to assess the impact of temperature on moisture storage capacity across relative humidity levels. The DVS device restricts high RH measurements at elevated temperatures because generating and controlling high humidity becomes technically unstable and physically constrained due to the exponential increase in vapor pressure, risk of condensation, and sensor limitations. This is a common constraint across most gravimetric sorption analyzers.

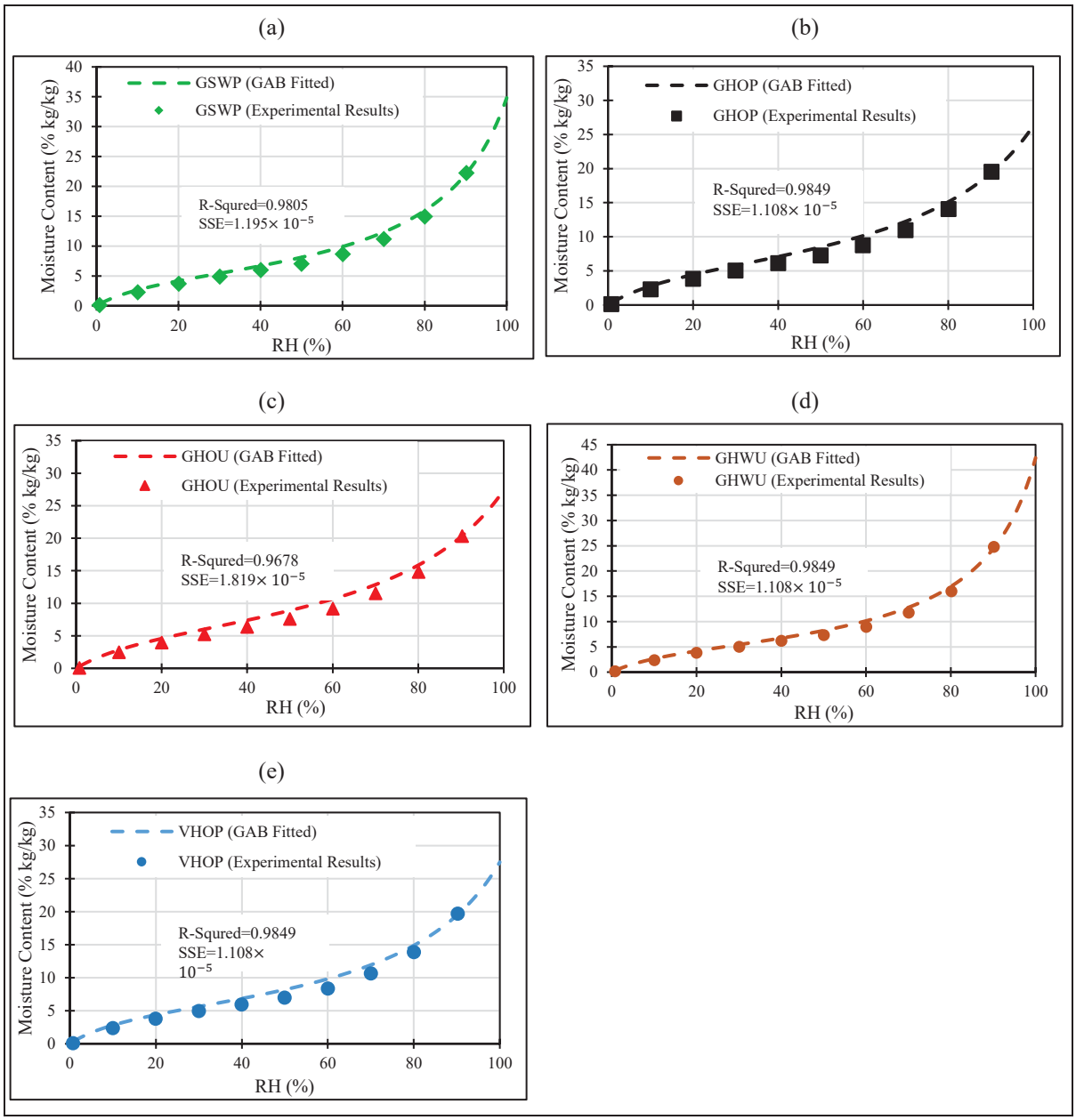

Figure 3.9 Comparison of GAB equations fitting with experimental adsorption isotherms: (a) GSWP; (b) GHOP; (c) GHOU; (d) GHWU; (e) VHOP

The isotherms show moisture content stable at 0–5 % up to 60 % RH, rising to 25–30 % at 90 % RH across all temperatures, indicating that temperature has minimal impact on storage capacity (kg·kg^{-1}). Generally, at higher temperatures (35 °C and 40 °C), there is a slight increase in adsorbed moisture, possibly due to the small widening of pores. However, since this material is already highly porous, temperature does not significantly alter its internal

structure, resulting in only minor changes in moisture adsorption. This finding differs from the hygric behavior of other insulation materials, where temperature typically affects moisture sorption more significantly, suggesting the need for further validation tests with additional formulations to confirm this behavior. The substantial rise in sorption isotherms at higher relative humidity levels is primarily attributed to the increased availability of moisture content, in the air at higher temperatures.

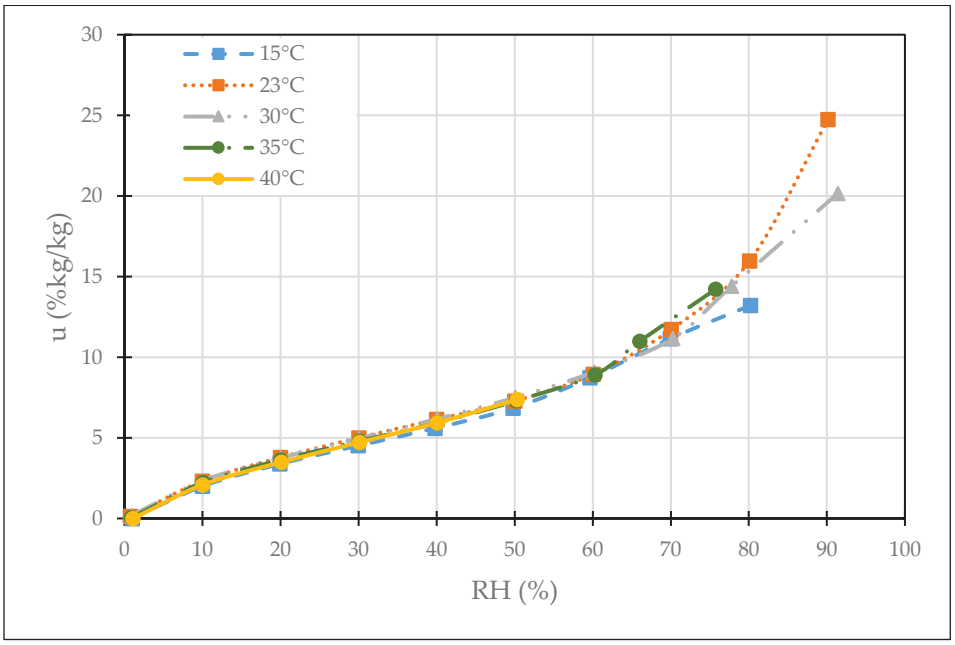

Figure 3.10 Experimental adsorption isotherms' comparison in different temperature for GHWU

3.3.2.2 Permeability

This test aimed to assess vapor permeability under 0/50 % and 0/80 % RH gradients using three formulations (GSWP, GHWU, and VSOP). For each mixture, three samples were tested, and the results are illustrated in Figure 3.11. A linear curve fitting is performed to indicate the evolution of moisture within the materials. Although the steady state was reached at the 150h mark of the test, the test continued until the 315th hour. Consequently, a linear curve fit was applied to the data from this point onward, excluding the initial steep increase in moisture observed during the first 20 h.

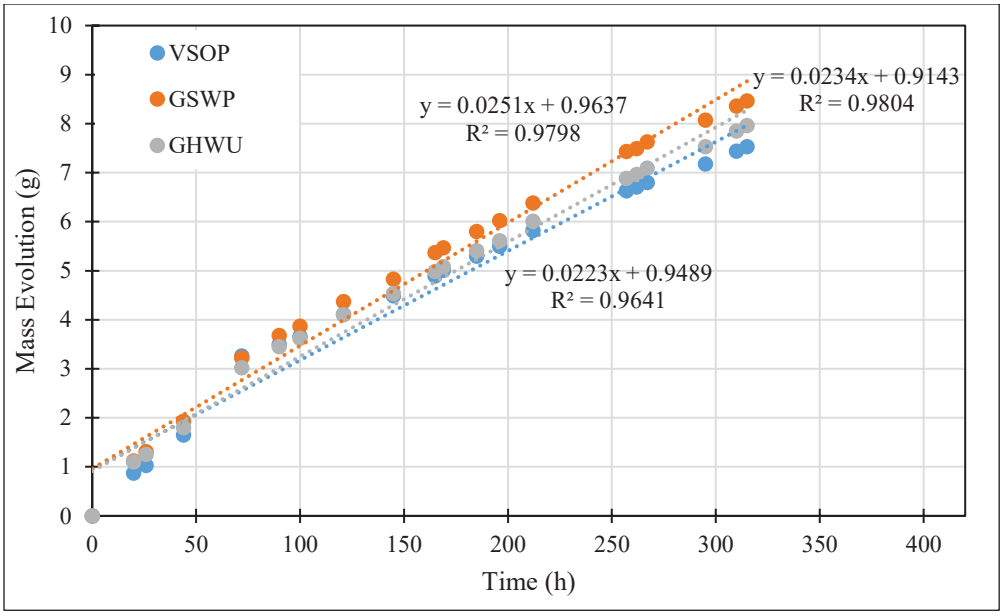

Figure 3.11 Adsorbed moisture evolution in the dry cup condition (0/50%)

Using Equations (2) and (3), the vapor permeability and resistance factors are calculated from known vapor pressure and mass flow rate values, as shown in Table 3.3.

Table 3.3 Water vapor permeability and resistance factors

Composite	**RH [%]**	$g_v \times 10^6$ [kg·m⁻²·s⁻¹]	$\delta_p \times 10^{11}$ [kg·m⁻¹·s⁻¹·Pa⁻¹]	μ
GHWU	0/50	1.097	1.57	12.73
	0/80	1.57	2.25	8.91
GSWP	0/50	1.223	1.74	11.50
	0/80	1.70	2.42	8.29
VSOP	0/50	1.022	1.45	13.77
	0/80	1.34	1.87	10.68

This result confirms the higher permeability in the composition of straw and *Ganoderma lucidum* (GSWP) compared to straw and *Trametes versicolor* (VSOP) as well as hemp and *Ganoderma lucidum* (GHWU) samples, although their values remain very close. For the 0/80 % relative humidity gradient case, the resistance factor decreased by approximately 22%

for VSOP, 28 % for GSWP, and 30 % for GHWU. These results can be further interpreted in light of the aforementioned microstructural observations. While vapor permeability is commonly associated with overall porosity, the pore connectivity and hyphal architecture could play an equally critical role in driving moisture vapor transport through mycelium-based composites.

SEM imaging revealed that *Ganoderma lucidum* develops a dense, continuous hyphal network that forms highly connected pathways between substrate particles. In the case of straw-based composites like GSWP, this structure not only preserves pore interconnectivity but also stabilizes the pore geometry, preventing collapse during drying and thereby supporting efficient vapor diffusion. This explains the relatively high permeability observed in GSWP, despite the potentially lower overall porosity compared to VSOP.

Conversely, *Trametes versicolor* exhibits a more fragmented and localized colonization pattern, as shown in Figure 3.3, which leads to discrete pore zones that are poorly interconnected. Although this may result in a higher total porosity (as inferred from VHOS free water saturation results), the lack of continuity between voids severely limits vapor transfer, increasing the vapor diffusion resistance factor μ. This supports the idea that "effective porosity"—i.e., the fraction of pore space that contributes to bulk transport, is more relevant than absolute porosity when interpreting vapor permeability in bio-based composites.

Moreover, the combination of straw substrate and nutritional additives in GSWP likely enhanced both fungal growth intensity and structural uniformity, further contributing to an optimal balance between pore size, distribution, and connectivity. This may explain why GSWP shows not only higher vapor permeability than VSOP but also a sharper decrease in μ under 0/80% RH conditions, reflecting improved moisture transport even under elevated humidity gradients.

3.3.2.3 Capillary transport coefficient

This test aimed to determine the capillary adsorption behavior of mycelium bio-composites and calculate the subsequent liquid conduction coefficients, using three formulations (GSWP, GHOU, GHOP) with three samples per formulation. Figure 3.12 shows the capillary adsorption of these composites by plotting the average mass difference against the square root of time.

As capillary absorption phenomena are diffusive in nature, Figure 3.12 demonstrates that the initial evolution follows a linear trend relative to the square root of time. The coefficients of capillary adsorption (A_C) correspond to the slopes of the fitted trend lines. These coefficients are quite different for the straw and *Ganoderma* (GSWP) composite (A_C = 0.16 kg · m^{-2} · s$^{-1/2}$), as the largest value is three times the hemp and *Ganoderma* (GHOP) composite (A_C = 0.0516 kg · m^{-2} · s$^{-1/2}$).

These results corroborate the findings of Rahim et al. (2016), who reported that the capillary coefficient of straw lime concrete (SLC) is four times higher than that of hemp lime concrete (HLC). While the capillary coefficients of SLC and straw-based *Ganoderma* composites (GSOP) are comparable, hemp-based *Ganoderma* composites (GHOP) exhibit higher values than HLC. This increase may be attributed to the robust growth of *Ganoderma* in hemp-based composites compared to lime-based composites, leading to the formation of larger pores within the material, which in turn elevates the capillary coefficient.

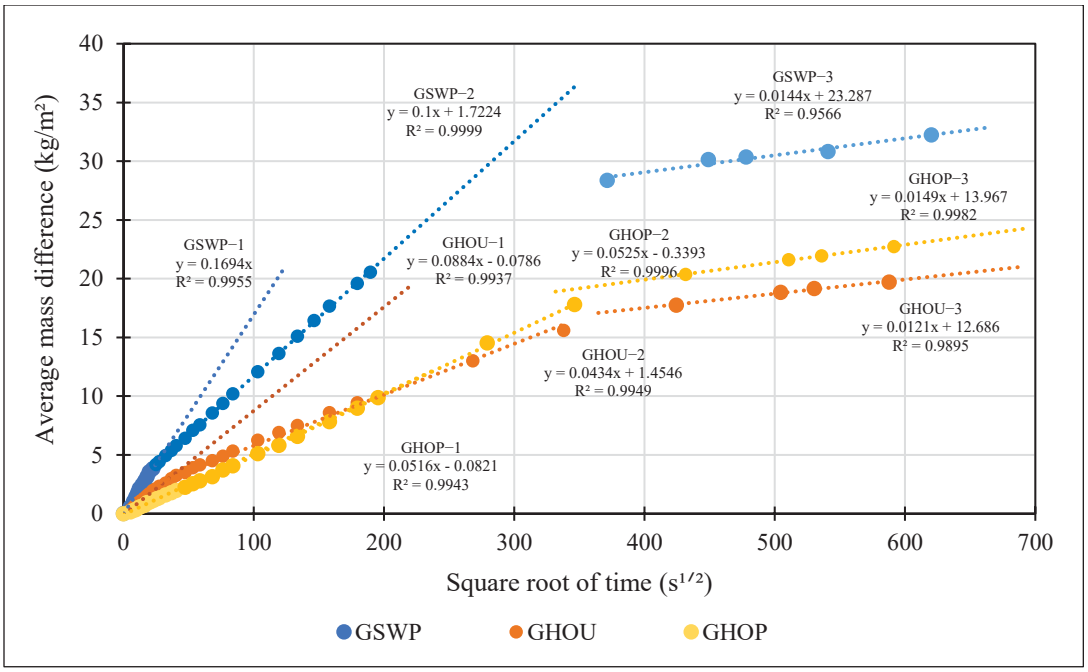

Figure 3.12 Capillary adsorption of mycelium bio-composites

3.3.2.4 Free water saturation

Free water saturation testing was conducted to quantify the open porosity and water retention capacity of the mycelium-based composites. By submerging samples in water under controlled conditions, this test evaluates how effectively each formulation absorbs and retains water, thereby providing critical insights into pore structure and hygrothermal performance. Eight formulations were analyzed to assess the effects of key parameters, including fungal species, substrate type, and treatment, on water uptake. Table 3.4 presents the water content results of the studied materials.

The values reported in Table 3.4 reinforce and contextualize the observed hygrothermal trends by providing insight into the relationship between fungal morphology, substrate structure, and the water storage behavior of MBCs. Formulations such as GHOP (*Ganoderma lucidum* on hemp) display a relatively high dry density (152 kg·m^{-3}) combined with lower open porosity (85 %) and moderate free water saturation (580 %), reflecting the densely interwoven hyphal network observed under SEM (Figures Figure 3.2 and Figure 3.3). This compact structure

minimizes void volume and inhibits water penetration, contributing to low capillary adsorption coefficients (Figure 3.12) and moderate sorption capacity at high RH (Figure 3.7a).

Table 3.4 Physical characteristics of mycelium-based composites

Samples	Density ($kg \cdot m^{-3}$)	Free Water Saturation ($kg \cdot m^{-3}$)	Free Water Saturation (%)	Open Porosity (%)
GHOP	152 ± 3	886 ± 27	580 ± 10	85 ± 0
GHOS	131 ± 0	920 ± 14	701 ± 12	88 ± 0
GHWU	212 ± 4	809 ± 17	382 ± 15	79 ± 1
GSOS	170 ± 4	945 ± 35	556 ± 33	85 ± 1
GSWP	223 ± 15	833 ± 15	375 ± 28	79 ± 1
GSWS	188 ± 3	893 ± 12	475 ± 12	83 ± 0
VHOS	142 ± 13	1000 ± 63	704 ± 19	88 ± 0
VSOP	184 ± 13	818 ± 20	447 ± 41	82 ± 1

In contrast, VHOS demonstrates higher open porosity (88 %) and water saturation (704 $kg \cdot m^{-3}$), which aligns with the fragmented and loosely connected hyphal growth observed in and Figure 3.4. This architecture results in numerous isolated or dead-end pores that facilitate high water uptake but offer limited resistance to moisture transport. Despite this high porosity, the sorption isotherms for VHOP (Figure 3.7a) show only moderate moisture content under DVS conditions, indicating that vapor-phase sorption is hindered by the lack of continuous pathways and the localized nature of hyphal development.

Additive-enriched formulations (e.g., GHWU and GSWP) tend to exhibit denser internal organization and reduced capillary sorption behavior (Figure 3.12), likely due to enhanced fungal colonization and greater hyphal branching. These formulations show lower free water saturation levels (375–382 $kg \cdot m^{-3}$) and display more gradual sorption curves, as seen in GHWU (Figure 3.7d). This suggests that while additives increase the surface area for vapor adsorption, they concurrently limit rapid liquid infiltration, likely by reducing large, continuous pore channels.

Straw-based composites such as GSWS and GSOS exhibit both higher porosity (up to 88 %) and elevated free water saturation, indicating a greater susceptibility to capillary water uptake and bulk saturation. This behavior stems from the less compact and more heterogeneous structure of straw particles, which promote uneven fungal growth and larger void spaces. As shown previously, the capillary uptake coefficient for GSWP is more than three times higher than that of GHOP, confirming the dominant influence of substrate morphology on liquid-phase water transport.

Overall, these findings demonstrate that water retention in MBCs is governed not only by open porosity, but by the geometry, connectivity, and functionality of the internal pore network, all of which are shaped by fungal species, substrate type, and processing parameters. A dense, well-integrated hyphal structure minimizes moisture sensitivity and favors stable performance, while porous, loosely organized networks permit high water uptake but compromise material durability. This highlights the necessity of tailoring microstructural features to achieve optimal hygrothermal responses for insulation applications.

Figure 3.13 illustrates the correlation between open porosity and density, revealing a reverse linear relationship in most samples, except for VHOS which exhibits a different pattern. This suggests that a significant portion of the porosity in these materials is open. This is largely due to the fabrication process of mycelium-based samples, where the growth of fungi within the substrate releases gases that can create open pores during formation. Based on this finding, substituting w_{max} with w_f minimally affects the results.

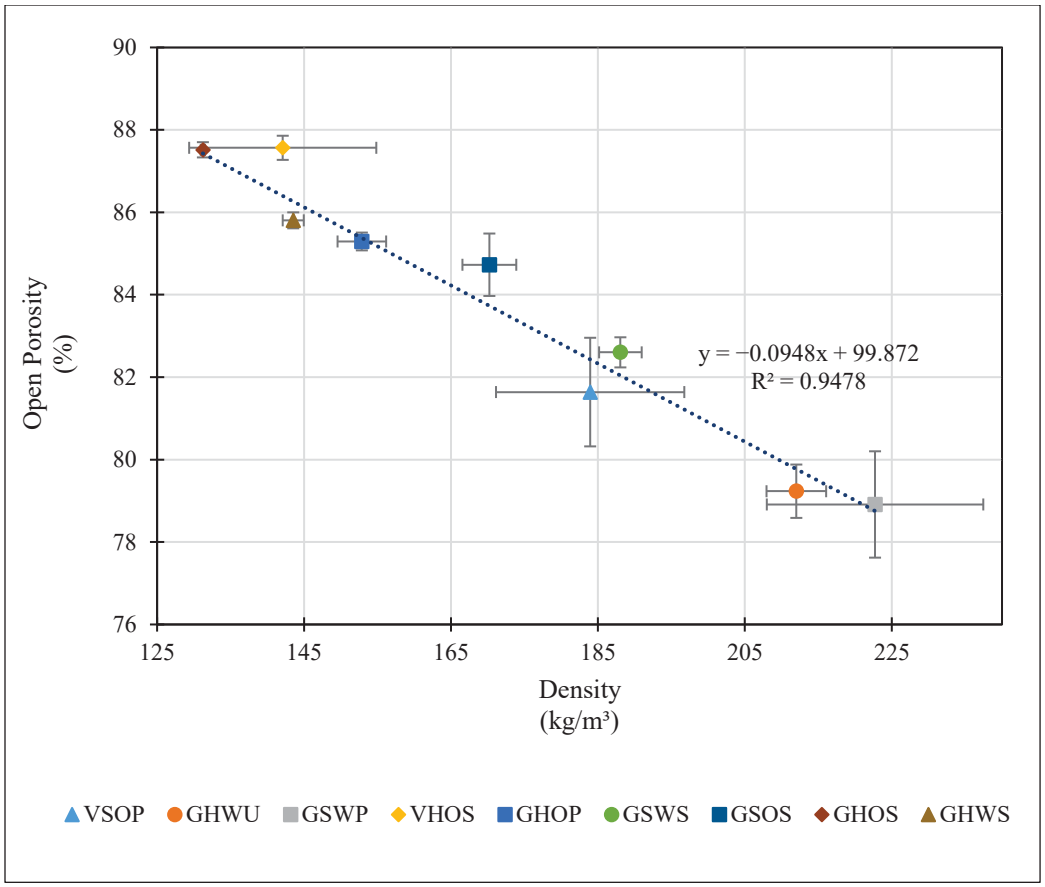

Figure 3.13 Open porosity and density correlation

Figure 3.13 illustrates a general inverse relationship between open porosity and dry density, confirming that denser composites tend to have fewer accessible voids. This trend reflects the effect of fungal colonization: dense hyphal networks, particularly in *Ganoderma lucidum*-based formulations like GHOP and GHWU, enhance particle cohesion and reduce pore volume. However, deviations from this trend, such as in VHOS, suggest that species-specific growth patterns; here, the fragmented colonization by *Trametes versicolor* can produce highly porous but structurally loose composites. These discrepancies highlight that porosity is influenced not only by compaction, but also by pore connectivity and distribution.

The observed structural configurations, shaped by fungal species and substrate interactions, are crucial for interpreting the material's thermal behavior. As moisture retention and transport

directly affect heat flow, understanding these microstructural differences provides a foundation for evaluating the thermal performance of MBCs under realistic environmental conditions.

3.3.3 Thermal characterization

The interplay between density, open porosity, and moisture retention confirms that thermal behavior in MBCs cannot be dissociated from their hygric and microstructural characteristics. The replacement of air by adsorbed or capillary-bound water within the pore network, governed by hyphal morphology, substrate structure, and pore connectivity, directly impacts thermal conductivity. Thermal transport must be interpreted as the outcome of coupled heat and mass transfer processes, modulated by the material's internal architecture.

Thus, thermal characterization was performed to assess the heat transfer properties of the mycelium-based composites as a function of relative humidity, moisture content and temperature to evaluate the individual and combined effects of each parameter on thermal performance. Utilizing the TPS method, key formulations, including GHOP, GSWS, GSOS, and VHOS, were evaluated to establish a quantitative correlation between microstructural features and thermal conductivity.

The correlation between thermal conductivity and temperature across different levels of relative humidity is demonstrated in Figure 3.14 for four samples. This expansion may enhance gaseous conduction within the pores, thereby directly contributing to an increase in thermal conductivity. However, it should be noted that the overall thermal response is also influenced by changes in moisture content and other material properties. As delineated in Equation (8), temperature increase corresponds to an exponential elevation in saturation pressure. Consequently, under constant relative humidity (RH) within the climatic chamber, as a result of temperature increase, vapor pressure experiences a proportional rise. This explains the indirect consequence of temperature elevation, in increasing the moisture content stored within the material.

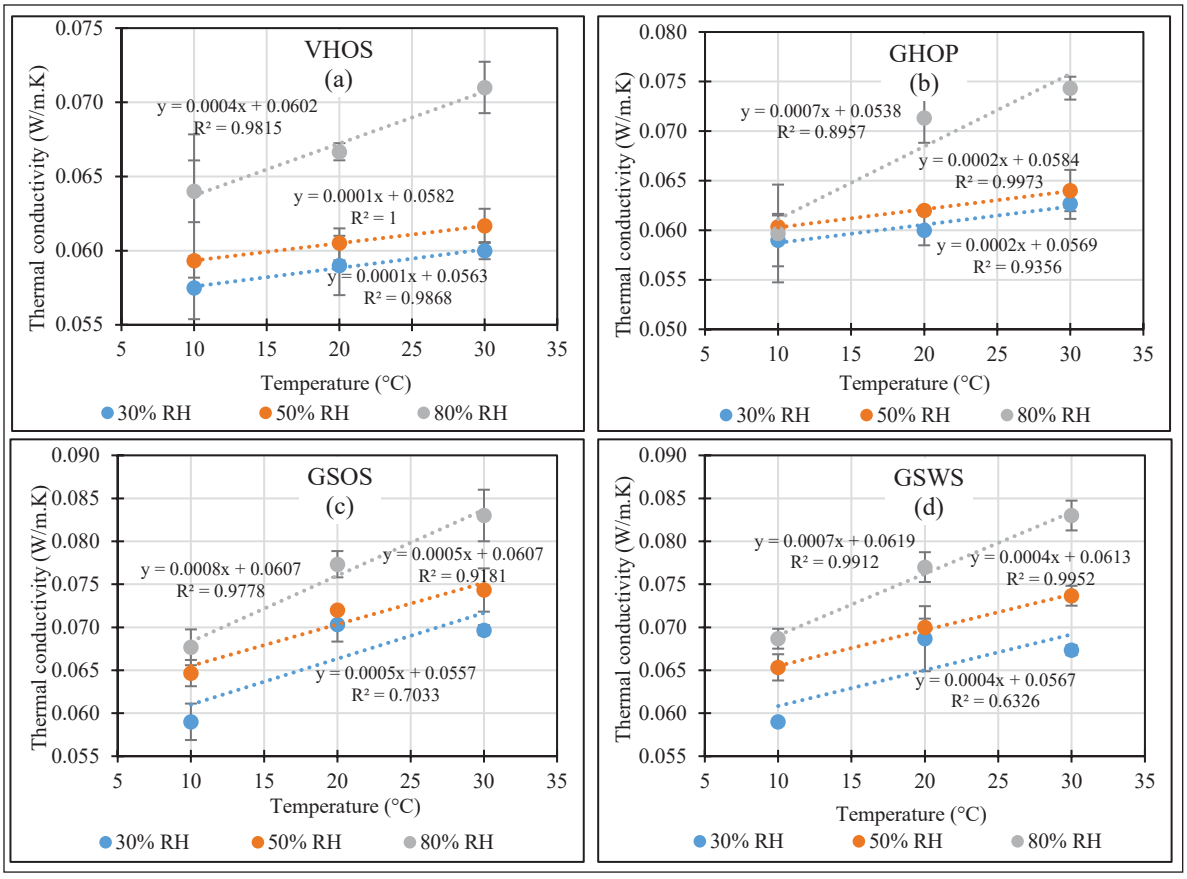

Figure 3.14 Correlation between thermal conductivity and temperature across different relative humidities for: (a) VHOS; (b) GHOP; (c) GSOS; (d) GSWS

In all four composites (VHOS, GHOP, GSOS, and GSWS), thermal conductivity increases with both temperature and relative humidity, confirming the dominant role of moisture in enhancing heat transfer by replacing air within the pore network. However, the magnitude and progression of this increase vary significantly depending on the material's microstructure. GHOP displays the most stable thermal response, with only a modest rise in conductivity. This behavior reflects the dense and cohesive hyphal network observed, which not only limits overall moisture uptake, as confirmed by low capillary absorption and moderate sorption levels, but it also prevents pore dilation under thermal stress. As a result, the pore geometry and gas-filled structure remain largely preserved, maintaining low thermal conductivity even under elevated RH and temperature.

In contrast, VHOS exhibits a steeper and more nonlinear increase in thermal conductivity. This correlates with its high free water saturation and fragmented, porous hyphal morphology (Figure 3.4b), which allows for extensive moisture accumulation and dynamic pore reconfiguration. The loosely organized microstructure lacks the structural rigidity to resist thermal expansion of moisture-laden pores, amplifying the composite's sensitivity to environmental changes.

Straw-based samples such as GSOS and GSWS occupy intermediate positions. Despite also being colonized by *Ganoderma lucidum*, their higher thermal conductivity variation can be attributed to the more heterogeneous and anisotropic colonization of the straw substrate, which creates larger, less confined pores with enhanced moisture transport capacity. This substrate-driven irregularity disrupts the structural integrity of the hyphal matrix, resulting in localized zones of high moisture accumulation and increased conductive pathways as temperature rises. Altering relative humidity causes fluctuations in moisture content, thereby directly impacting thermal conductivity.

The influence of relative humidity on thermal conductivity at various temperatures is illustrated in Figure 3.15. At lower temperatures, there is minimal change in thermal conductivity across different RH levels, due to the low saturation pressure and subsequent low vapor pressure in all RH levels. At 30 % RH, the lowest achievable level within the climatic chamber, thermal conductivity values tend to converge. However, as RH increases up to 80 %, differences between thermal conductivity at various temperatures become more pronounced due to increased disparities in moisture content. Additionally, increasing temperature amplifies the increase in thermal conductivities at constant RH levels by increasing moisture content through higher saturation vapor pressure.

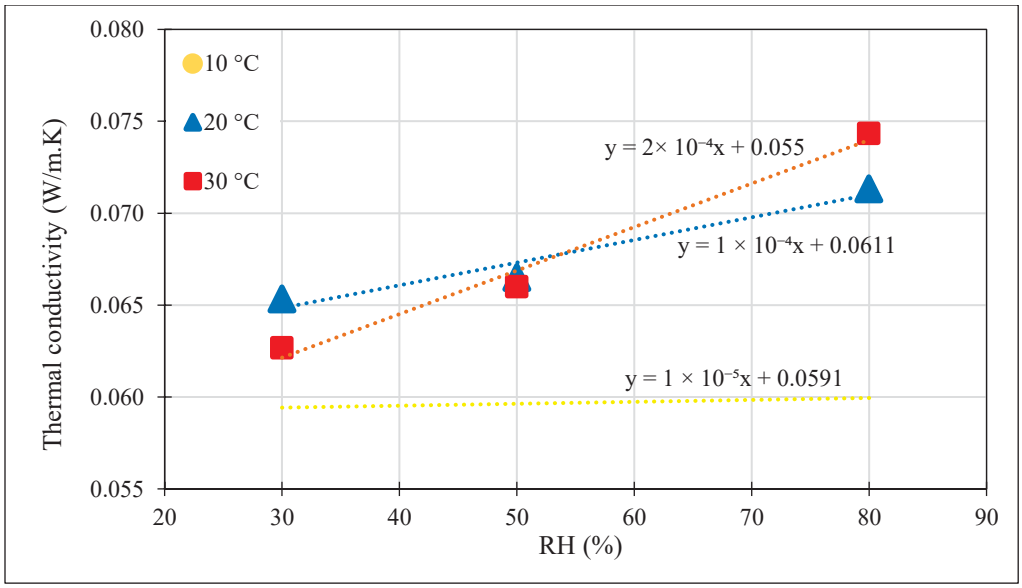

Figure 3.15 Correlation between thermal conductivity and relative humidity in constant temperature for GHOP

In order to better understand the behavior of thermal conductivity as the function of temperature and moisture content, a curve fitting is conducted using MATLAB R2024b. Due to the steeper change in thermal conductivity against moisture content, compared to temperature in the conducted experiments, moisture content is treated as the exponential variable in the correlation, while temperature is considered part of the linear component. The three possible exponential models that could be implemented are as follows:

- $k = a + b \cdot T + c \cdot e^{d \cdot u}$ (Model 1),
- $k = (a + b \cdot T) \cdot e^{c \cdot u}$ (Model 2),
- $k = a + b \cdot T \cdot e^{c \cdot u}$ (Model 3),

where k denotes thermal conductivity, T represents temperature, and u is the moisture content. Model 1 captures the cumulative effects of moisture and temperature. It performs well but slightly underestimates thermal conductivity at higher temperature and moisture content. Models 2 and 3's multiplicative forms better reflect the combined influence of moisture content and temperature. However, Model 2 yields a higher R-Squared and lower RSS, suggesting a

better fit for this dataset. Therefore, Model 2 is chosen for the curve fitting. The resulting curve fitting is depicted in Table 3.5.

Table 3.5 Thermal conductivity correlation as a function of the moisture content ($kg \cdot kg^{-1}$) and temperature (K)

Composite	Curve Fitting	R-Squared	RMSE
GHOP	$y = (0.0008 + 0.0005\mathrm{T}) \times (0.3812 \times \exp(1.2771u)$	0.6883	0.0037
GSWS	$y = (0.0042 + 0.0137\mathrm{T}) \times (0.0155 \times \exp(1.9552u)$	0.8803	0.0031
GSOS	$y = (0.004 + 0.0154\mathrm{T}) \times (0.0139 \times \exp(1.8016u)$	0.8421	0.0035
VHOS	$y = (0.02 + 0.0164\mathrm{T}) \times (0.0118 \times \exp(1.3971u)$	0.8136	0.0023

The exponential fitting parameters presented in Table 3.5 quantify how each composite's thermal conductivity (k) responds to temperature (T) and moisture content (u), which can be directly related to their microstructural organization and moisture dynamics. In porous biocomposites, k is the sum of solid-phase conduction through the hyphal skeleton (k_s), gas-phase conduction in air-filled pores ($k_g \approx 0.026$ $W \cdot m^{-1} \cdot K^{-1}$), bound-/liquid-water conduction ($k_w \approx 0.6$ $W \cdot m^{-1} \cdot K^{-1}$), and a minor radiative term. Rising temperature dilates the average pore diameter and simultaneously raises saturation vapor pressure; these changes increase k_g and k_w, respectively, thus explaining the upward k(T) trends predicted by the exponential model.

GHOP exhibits the lowest sensitivity coefficients for both temperature (0.0005) and moisture content (1.2771), confirming its thermally stable behavior under varying environmental conditions. This reduced sensitivity aligns with the previously observed dense and cohesive hyphal network, which minimizes internal pore volume variation and limits water uptake. Such a compact limits both free-air volume and water uptake. Solid-phase conduction therefore

dominates, and thermal conductivity varies little with either temperature (T) or moisture content (u).

Conversely, VHOP shows significantly higher sensitivity to both parameters, with a moisture coefficient of 1.3971 and a temperature coefficient of 0.0164. These values reflect the more open and disconnected microstructure formed by *Trametes versicolor*. Its high open porosity (~88 % for VHOS; Figure 3.13) produces macropores that (i) dilate upon heating—enhancing gas-phase conduction—and (ii) rapidly fill with water once capillary condensation begins. The exponential fit to k versus u shows a clear inflection in slope at u ≈ 0.15 $kg \cdot kg^{-1}$, marking the transition from multilayer adsorption to capillary water bridges that is consistent with the sorption isotherm of VHOP (Figure 3.7a). Beyond this moisture content, liquid-phase conduction ($k_w \approx 0.6$ $W \cdot m^{-1} \cdot K^{-1}$) dominates, accounting for VHOP's steep k(T,u) response.

This supports the findings of the elevated free water saturation observed in VHOS and its pronounced capillary absorption behavior. Straw-based samples (GSOS, GSWS) colonized by *Ganoderma lucidum* exhibit intermediate sensitivity coefficients and a moderate k(T,u) response, positioning them between the two extremes. Although they share the same fungal species as GHOP, their higher sensitivity coefficients (1.8016–1.9552 for moisture) reflect the influence of the straw substrate's inherent heterogeneity. The longitudinal lumina of the straw fragments introduce anisotropic pore channels that promote moisture transport along the fiber axis. It also contributes to localized pore development and variable moisture distribution, leading to less predictable thermal responses. At elevated moisture contents, these channels facilitate the formation of continuous liquid films, enhancing heat conduction through liquid-phase bridging.

Despite the adequacy of the exponential model in capturing general trends, lower R^2 values, particularly for GHOP, may result from experimental limitations such as uneven sample surfaces affecting probe contact, or reduced measurement stability at low moisture contents. Future work could involve re-testing with a guarded hot plate apparatus under steady-state conditions ($\Delta T \leq 10$ K) and will verify the fitted coefficients and overcome limitations

associated with surface compressibility in TPS measurements. This will also enable the integration of a three-phase (solid–gas–liquid) conduction model that explicitly couples pore-size distribution with the moisture-sorption isotherms. A similar three-phase framework has been shown to predict increases in thermal conductivity in highly porous aerogels when adsorbed water replaces air in mesopores—facilitating capillary condensation and the formation of liquid bridges that enhance heat transfer (Jiang et al., 2025), thereby supporting the mechanism proposed here.

Using the measured minimum thermal conductivity values obtained under dry reference conditions, the corresponding minimum thermal resistance of each formulation was calculated. This comparison provides a direct performance indicator for evaluating the insulation capability of the mycelium-based composites and enables benchmarking against conventional thermal insulation materials.

Table 3.6 Minimum measured thermal conductivity and corresponding thermal resistance of tested mycelium-based composites.

Sample	**Minimum thermal conductivity ($W \cdot m^{-1} \cdot K^{-1}$)**	**Thermal resistance, R_{SI} ($m^2 \cdot K \cdot W^{-1}$)**	**R-value R_{US} ($ft^2 \cdot °F \cdot h$ / BTU)**
GSWS	0.060	0.500	2.84
GHOP	0.054	0.556	3.16
VHOS	0.055	0.545	3.10
GSOS	0.055	0.545	3.10

To place these results in a practical construction context, the measured thermal resistance values were extrapolated to typical insulation thicknesses used in North American wall assemblies. For a standard 2×6 stud wall cavity (nominal depth ≈ 140 mm), the GHOP formulation, which exhibited the highest thermal resistance among the tested samples (R = 3.16 at 30 mm), would correspond to an estimated thermal resistance of approximately R-14.7 (US units), assuming homogeneous material behavior and linear scaling with thickness.

Similarly, for a 2×4 stud wall cavity (nominal depth ≈ 90 mm), the corresponding thermal resistance would be approximately R-9.5. These values fall within the performance range of low-density bio-based insulation materials and approach the lower bound of conventional fiberglass batt insulation typically used in residential construction. While remaining lower than high-performance synthetic foams, the obtained results demonstrate that mycelium-based composites can provide competitive thermal insulation when applied at practical wall thicknesses, particularly when combined with their additional benefits such as moisture buffering capacity and reduced embodied carbon.

3.4 Conclusions and perspective

3.4.1 Conclusions

This study examined the hygrothermal behavior of eleven mycelium-based composites (MBCs) fabricated using various fungal strains, fiber types, sterilization levels, and nutrient additives. Among the tested fungal species, *Ganoderma lucidum*, particularly in the GHOP formulation, demonstrated the lowest k-value (0.045 $W \cdot m^{-1} \cdot K^{-1}$), with minimal moisture content and temperature-induced variation, confirming its robustness for bio-based insulation. Microstructural analysis revealed that *Ganoderma lucidum* forms a compact, interconnected hyphal network, while *Trametes versicolor* produces a more open, porous structure. Extensive hygric and thermal characterizations showed that additives and substrate type had the strongest influence on moisture uptake, whereas fungal species and treatment effects were more modest. GHOP consistently exhibited lower vapor permeability, reduced capillary absorption, and greater thermal stability due to its dense microstructure.

The study highlights a clear relationship between porosity, moisture dynamics, and thermal behavior: denser hyphal networks reduce pore connectivity and moisture ingress, thereby stabilizing thermal conductivity. Elevated open porosity alone did not inherently result in thermal performance; effective insulation was observed when pores were enclosed within a cohesive hyphal matrix, which restricted capillary water uptake and limited temperature-driven increases in thermal conductivity. The exponential model further confirmed that composites

with more porous and disconnected structures were more sensitive to vapor pressure increases. This enabled the GHOP formulation to maintain lowest conductivity values across a wide hygrothermal range (10–30 °C and 0–80 % RH).

In summary, the study established that the hygrothermal performance of MBCs is governed by the geometry and connectivity of their internal structure, shaped by fungal selection and processing parameters. By optimizing these features, MBCs can be tailored for reliable, energy-efficient insulation, supporting their practical adoption in sustainable construction.

3.4.2 Perspectives

The development of a numerical model is essential for predicting the hygrothermal performance of MBCs across varied climatic conditions and building envelope settings. Given the material's highly porous structure and rapid response to hygric changes, integrating a hysteresis model becomes crucial to account for consecutive wetting and drying cycles and their impact on moisture adsorption and retention. Additionally, incorporating non-isothermal models to couple thermal and hygric boundary conditions enhances the practicality of the model across diverse temperature ranges.

Research would benefit from optimizing fabrication processes to reduce variability in mechanical properties, assessing long-term durability under environmental stressors like humidity and temperature fluctuations, and investigating a wider range of substrates and additives to enhance hygrothermal and structural performance. Testing these composites in full-scale building systems and conducting detailed life-cycle assessments to quantify environmental benefits could further support their practical adoption as sustainable insulation materials.

CHAPTER 4

NUMERICAL CHARACTERIZATION OF MYCELIUM-BASED BIO-COMPOSITES

Abstract

This chapter evaluates the hygrothermal behavior of mycelium-based composites through numerical simulations. Using a coupled heat and moisture transfer model, simulations were conducted under both isothermal and non-isothermal conditions to assess the performance of these materials. GAB model is used to model the sorption equations as a function of the moisture content. The function of hysteresis and its effect on the accuracy of isothermal and non-isothermal sorption is included using Mualem II model. This model relies on the definition of the two basic functions of capillary that are used to indirectly calculate sorption equations. Simulation results were compared with experimental data for validation. In isothermal simulations, the hysteresis mode achieved a maximum Mean Absolute Percentage Error (MAPE) of 0.96 %, compared to 7.94 % for the non-hysteresis mode. Average errors in fluctuation amplitude were 0.03% for the non-hysteresis mode and 4.13 % for the hysteresis mode. For non-isothermal simulations, incorporating hysteresis significantly improved accuracy across a range of relative humidity levels, with MAPE values of 17.12 % at 40 °C and 19.27 % at 30 °C. The results demonstrate good agreement with experimental validation under isothermal conditions and highlight the potential of hysteresis-based modeling to enhance accuracy under non-isothermal scenarios. These findings underscore the importance of accurate sorption curve definitions and parameter calibration, while also establishing a foundation for integrating numerical and experimental hygrothermal characterization. This strengthens the predictive reliability of MBCs as sustainable insulation materials in building envelopes.

4.1 Introduction

In the pursuit of sustainable development, the construction industry is increasingly focusing on materials that are not only environmentally friendly but also high-performing in terms of thermal and moisture management. Bio-based materials, such as mycelium bio-composites (MBCs), offer a promising alternative by leveraging natural, renewable resources and potentially reducing the overall environmental impact of buildings. Understanding the hygrothermal properties of these innovative materials is crucial for their successful application in construction. Hygrothermal properties determine how materials interact with heat and moisture, impacting their durability, thermal efficiency, and overall performance in different climatic conditions.

Numerous studies have developed numerical models to simulate coupled heat and moisture transfer within porous building materials under varying environmental conditions. Classical works by Abahri et al. (2011) derived analytical solutions and a 1-D coupled HAM model, showing that thermal diffusion (temperature gradients) can significantly influence moisture migration in walls, thus affecting predicted moisture profiles. Nikitsin and Backiel-Brzozowska (2012) provided methods to determine liquid transfer coefficients (capillary transport parameters) needed to parameterize numerical models of moisture flow in building materials. Knarud and Geving (2015) implements a user-defined 3D coupled heat–moisture (HAM) model for porous building materials in COMSOL Multiphysics and benchmarks it against HAMSTAD benchmarks, showing close agreement and demonstrating COMSOL's viability for 3D hygrothermal analysis. Maliki et al. (2017) presented a transient HAM model in COMSOL for multilayer porous media that solves temperature and capillary pressure simultaneously with nonlinear storage/transport functions, demonstrating 2-D modeling capability for building components. Zhou et al. (2025) examined a straw–alginate panel using coupled heat and moisture (CHM) models. Through parameter calibration via inverse analysis, they demonstrated that models incorporating liquid water transport significantly reduced prediction errors—by 57 % to 61 % depending on sampling depth—compared to models that

only simulate vapor-based moisture transport. This highlights the importance of including both liquid and vapor mechanisms in hygrothermal simulations

Focusing on moisture behavior and sorption hysteresis modeling, Scheffler (2008) conducted validation of hygrothermal material modeling including moisture-storage hysteresis, underscoring the need to represent wetting–drying path dependence in simulations. Tariku et al. (2010) developed a transient coupled heat–air–moisture (HAM) model for multilayered porous media and benchmarked/validated it, establishing a reference framework for whole-assembly simulations. Work by Zhang et al. (2016) proposed a Fickian model of temperature-dependent sorption hysteresis in wood materials, formalizing how temperature shifts hysteresis loops used in hygrothermal models. Moreover, Kwiatkowski et al. (2009) performed numerical analyses of hysteresis effects on mass transfer and implemented a modeling module with sorption-curve hysteresis, demonstrating that hysteresis can alter predicted RH and moisture content fields. Zhang (2014) combined experiments with numerical modeling of sorption hysteresis in cementitious materials and showed that including hysteresis improves agreement with drying/wetting cycles compared to non-hysteresis model. In modeling methodology, Janetti et al. (2016) validated a COMSOL Multiphysics model for drying behavior in calcium silicate specimens—simulating coupled heat and moisture transport—and emphasized the numerical challenges when operating near saturation (100% RH). Their findings suggest that modeling highly hygroscopic materials requires careful handling of nonlinear material functions, especially liquid diffusivity near saturation. Finally, Belleudy et al. (2016) developed a 2-D coupled heat–air–moisture model for porous media in contact with air channels, validated it with 1-D benchmarks, and simulated air-leakage (infiltration/exfiltration) scenarios, showing that exfiltrating indoor air increases moisture storage within materials—an airflow–moisture coupling relevant to hygrothermal risk.

Beyond general porous media, a few studies have focused specifically on predictive modeling of mycelium-based composites (MBCs). Ito (2012) developed a coupled fungal growth–hygrothermal model, integrating WUFI-based heat–moisture transfer with reaction–diffusion dynamics, showing that fungal activity is highly sensitive to relative humidity and requires

calibration with material-specific data. Building on this direction, Koh et al. (2022) carried out transient hygrothermal simulations of wall assemblies that included a mycelium insulation layer, comparing it with hemp, grass, and cork under multiple climate profiles; they reported higher modeled moisture accumulation and mould-growth risk for the mycelium layer than for hemp and grass, underscoring the need for careful envelope design and moisture control when specifying MBCs in practice. More recently, Song et al. (2025) extended this line of work by combining measured material properties with hygrothermal simulations to evaluate mycelium and grass composites before and after alkyl-ketene-dimer (AKD) hydrophobization; their simulations showed reduced moisture uptake and markedly improved modeled mould resistance for the treated materials across different climate profiles, indicating that surface modification can broaden the safe application range of MBC insulation.

Despite significant progress in hygrothermal modeling of porous building materials, the predictive simulation of mycelium-based composites (MBCs) remains underdeveloped. Existing models have demonstrated the potential of integrating fungal growth dynamics and transient hygrothermal analysis into predictive frameworks. However, these studies are limited either to preliminary validation, simplified climate boundary conditions, or a narrow range of fungal species and substrate combinations. Moreover, current models often rely on assumed or literature-based transport parameters without direct experimental calibration, leading to uncertainties in predicting liquid transport, sorption hysteresis, and near-saturation behavior in MBCs. As a result, while the general behavior of bio-based insulations under moisture loading is increasingly understood, the lack of systematically calibrated and experimentally validated numerical models for MBCs restricts their reliable use in hygrothermal risk assessment and building design.

Chapter 4 addresses these gaps by developing and implementing a calibrated numerical simulation framework for the hygrothermal performance of MBCs. Building upon the experimental dataset generated in Chapter 3, the numerical model incorporates material-specific sorption isotherms, vapor diffusion resistance, and liquid transport coefficients derived from laboratory measurements. Using COMSOL Multiphysics, transient simulations are

performed to capture coupled heat and moisture transfer under realistic boundary conditions. The model explicitly integrates hysteresis in sorption behavior and evaluates the influence of fungal species and substrate selection on predicted hygrothermal responses. Through comparison with experimental benchmarks, the study provides validated insights into the moisture buffering, capillary uptake, and vapor diffusion characteristics of MBCs, thereby advancing predictive reliability. This contributes not only to the scientific understanding of MBCs but also establishes a simulation-based toolset that can inform their optimized integration into sustainable building envelopes.

This chapter begins with an introduction that frames the role of modeling in predicting coupled heat and moisture transfer within porous materials. The chapter then outlines the governing equations and the coupled HAM (Heat, Air, Moisture) model, followed by a detailed discussion of sorption hysteresis and the boundary conditions applied to the simulations. The numerical simulation framework is subsequently described, including analytical modeling of sorption isotherms, the influence of temperature on sorption curves, and the definition of heat and mass convection coefficients. Results are presented through both isothermal and non-isothermal simulations, highlighting model calibration and validation against experimental data. The chapter concludes with a synthesis of the findings, discussion of discrepancies, and evaluation of the model's reliability for predicting the hygrothermal performance of MBC.

4.2 Numerical modeling approach

4.2.1 Coupled heat and moisture transfer model in porous material

To accurately represent the hygrothermal behavior of mycelium-based composites, this subsection presents the coupled heat and moisture transfer equations governing fluid flow and thermal transport within porous media.

The Mendes model is based on the theory of Philip and De Vries (1957), where mass transfer through the wall occurs under a vapor pressure gradient for vapor diffusion and under a

capillary pressure gradient for liquid water diffusion. The equations for moisture and energy balance are written as equations (4.1) and (4.2), respectively:

$$\frac{\partial w}{\partial t} = -\frac{\partial g}{\partial x} \tag{4.1}$$

$$(\rho c)_{eff}(T,w)\frac{\partial T}{\partial t} = \frac{\partial}{\partial x}\left(\lambda(T,w)\frac{\partial T}{\partial x}\right) - L_v(T)\frac{\partial}{\partial x}(g_v) \tag{4.2}$$

where w is the volumetric moisture content, g is the total moisture flux, $(\rho c)_{eff}$ is the effective volumetric heat capacity, $\lambda(T,w)$ is the thermal conductivity, T is the temperature, $L_v(T)$ is the latent heat of vaporization, and gv is the vapor flux. According to Philip and De Vries, the equation describing the transfer of water vapor can be written in the following form:

$$g_v = -\delta(\varphi)\frac{\partial p_v}{\partial x} - D_{vT}(T,w)\frac{\partial T}{\partial x} \tag{4.3}$$

where g_v is the vapor flux, $\delta(\varphi)$ is the vapor permeability of the material, $p_v = \varphi p_{sat}(T)$ is the vapor pressure, φ is the relative humidity, $p_{sat}(T)$ is the saturation vapor pressure, and $D_{vT}(T,w)$ is the vapor transport coefficient under a temperature gradient. The vapor diffusion under the influence of a temperature gradient corresponds to the first part of the right-hand side of equation (4.3), while the second part of the equation represents diffusion associated with a water content gradient. The total moisture flux is the sum of vapor and liquid fluxes, expressed as follows:

$$g = g_l + g_v \tag{4.4}$$

where g is the total moisture flux, g_l is the liquid flux, and g_v is the vapor flux. According to De Vries, under non-isothermal conditions, it is given as follows:

$$g_l = -D_w(w)\frac{\partial w}{\partial x} - D_{wT}(T,w)\frac{\partial T}{\partial x} \tag{4.5}$$

where g_l is the liquid flux, $D_w(w)$ is the liquid diffusivity, w is the moisture content, and $D_{wT}(T,w)$ is the liquid transport coefficient under a temperature gradient. By substituting (4.5) and (4.3) into (4.4), we obtain:

$$g = -D_w(w)\frac{\partial w}{\partial x} - [\delta(\varphi)p_{sat}(T)]\frac{\partial \varphi}{\partial x} - (D_{wT} + D_{vT} + \delta(\varphi)\varphi\frac{dp_{sat}}{dT})\frac{\partial T}{\partial x} \tag{4.6}$$

Where $\left(D_{wT} + D_{vT} + \delta(\varphi)\varphi\frac{dp_{sat}}{dT}\right) = D_T$ and $\delta(\varphi)p_{sat}(T) = D_\varphi$. From these equations, mass conservation and heat conservation are reformulated as in equations (4.7) and (4.8), respectively:

$$\frac{\partial w}{\partial t} = \frac{\partial}{\partial x}\left(D_w\frac{\partial w}{\partial x} + D_\varphi\frac{\partial \varphi}{\partial x} + D_T\frac{\partial T}{\partial x}\right) \tag{4.7}$$

$$(\rho c)_{eff}(T,w)\frac{\partial T}{\partial t} = \frac{\partial}{\partial x}\left(\lambda(T,w)\frac{\partial T}{\partial x}\right) - \frac{\partial}{\partial x}(L_v(T)g_v) \tag{4.8}$$

where $\frac{\partial w}{\partial t}$ represents the temporal variation of the moisture content, and $(\rho c)_{eff}(T,w)\frac{\partial T}{\partial t}$ represents the temporal variation of the enthalpy of the porous material. The first term on the right-hand side of Equation (4.7) corresponds to the divergence of the liquid, vapor, and thermal moisture fluxes, while the second term of Equation (4.8) accounts for the divergence of the conductive heat flux. The last term of Equation (4.8) represents the divergence of the latent heat flux linked to vapor transport. The average specific heat can be calculated using equation (4.9:

$$(\rho c)_{eff} = \rho_0 c_{p_0} + w\, c_{p_w} \tag{4.9}$$

where $(\rho c)_{eff}$ is the effective volumetric heat capacity of the material, ρ_0 is the bulk density of the dry solid, c_{p_0} is the specific heat capacity of the dry material, w is the volumetric moisture content, and c_{p_w} is the specific heat capacity of water. The formulation of these coupled equations provides the foundation for subsequent numerical simulations, enabling the prediction of heat and moisture interactions under varying environmental conditions.

4.2.2 Sorption hysteresis

In this subsection, the phenomenon of sorption hysteresis is introduced to account for the distinct differences between adsorption and desorption processes in mycelium-based composites.

In the study of porous materials subjected to repeated wetting-drying cycles, their response is influenced by sorption behavior, as indicated by adsorption and desorption isotherms. Hysteresis, the difference between adsorption and desorption, is observed in this process. During adsorption, starting from low relative humidity, surface adsorption precedes mono-layer and multi-layer adsorption, eventually leading to capillary condensation at high relative humidity. Various phenomena, such as capillary condensation hysteresis, contact angle hysteresis, and the ink-bottle effect, contribute to hysteresis. Several models have been proposed to predict hysteresis, including empirical, conceptual, phenomenological, and Frandsen models. However, these models exhibit limitations, prompting the implementation of the Mualem II model in this context. The Mualem II model, relying on functions dependent on capillary pressure within the porous media, aims to address hysteresis in porous building materials. This model works based on two basic functions that are dependent to the capillary pressure withing the pores as follows:

$$L(P_c) = \int_0^{\bar{\rho}(P_c)} l(\bar{\rho}) d\bar{\rho} \tag{4.10}$$

$$H(P_c) = \int_0^{\bar{r}(P_c)} l(\bar{r}) d\bar{r} \tag{4.11}$$

where $L(P_c)$ and $H(P_c)$ are cumulative functions that depend on the capillary pressure (P_c). The variable $\bar{\rho}$ represents normalized pore bodies, and $\bar{r}$ represents normalized pore necks. These functions describe the distribution of pore sizes inside the material and are linked to the sorption isotherms to model hysteresis effects. The behavior of capillary pressure in porous materials is influenced by the normalized radii of pore necks and pore bodies. By linking these cumulative pore size distribution functions to primary sorption isotherms, calculations can be simplified, as follows:

$$L(P_c) = S_{ads}(P_c) \tag{4.12}$$

$$H(P_c) = \frac{S_{des}(P_c) - S_{ads}(P_c)}{1 - S_{ads}(P_c)} \tag{4.13}$$

where $S_{ads}(P_c)$ is the primary adsorption curve at a given capillary pressure P_c and $S_{des}(P_c)$ is the primary desorption curve. These relations express the cumulative functions $L(P_c)$ and $H(P_c)$directly in terms of the primary sorption isotherms, providing a simplified way to incorporate adsorption–desorption hysteresis into the model.

Manually developed user-defined functions are utilized to measure the derivative of vapor pressure with respect to time. This derivative serves as a determinant for whether the process is in adsorption or desorption, based on whether the derivative is positive or negative, respectively. According to the Promis et al. (2018) the consecutive sorption cycles are implemented using the following sets of equations:

Initially, scanning curve during adsorption (of the first order), commencing from the desorption isotherm at the point $(S_{des}(P_c), P_{c,1})$, can be articulated as follows:

$$S_{ads}(P_c) = S_{des}(P_{c,1}) + [L(P_c) - L(P_{c,1})]H(P_{c,1}) \tag{4.14}$$

where $P_{c,1}$ denotes the reversal point at which the scanning curve starts. This equation defines the scanning adsorption curve originating from that reversal point. Following to that, the drying curve of the order N+1 can be used:

$$S_{ads}(P_c) = S_{des}(P_{c,1}) + [L(P_c) - L(P_{c,1})]H(P_{c,1}) \tag{4.15}$$

Then, wetting curve of order of N+2 will be:

$$S_{des}(P_c) = S_{ads}(P_{c,N}) - [L(P_{c,N}) - L(P_c)] \times [1 - H(P_c)] \tag{4.16}$$

The values of the beginning of the scanning curve are represented by $S(P_{c,N})$, $L(P_{c,N})$, and $H(P_{c,N})$. When comparing drying curves, if $L(P_c)$ is less than or equal to $L(P_{c,N-1})$, then $L(P_{c,N-3})$ should be utilized instead of $L(P_{c,N-1})$. Similarly, in wetting curves, if $L(P_c)$ is greater than or equal to $L(P_{c,N-1})$, then $L(P_{c,N-3})$ should replace $L(P_{c,N-1})$. Hence, it is crucial to maintain a record of the scanning curve history. In incremental calculations, a mathematical series can be developed. For the wetting scanning curve:

$$S_t - S_{t-1} = [L(P_{c,t}) - L(P_{c,t-1})] + H(P_{c,1}) \times [L(P_{c,t-1}) - L(P_{c,t})] \tag{4.17}$$

where S_t and S_{t-1} denote successive values of the scanning curve, and $P_{c,t}$ represents the capillary pressure at the current time step t. This equation defines the incremental update of the wetting scanning curve. Same equation for the drying curves will be:

$$S_t - S_{t-1} = L(P_{c,t}) \times [1 - H(P_{c,t})] - L(P_{c,t-1}) \times [1 - H(P_{c,t-1})] + L(P_{c,1}) \times [H(P_{c,t}) - H(P_{c,t-1})] \tag{4.18}$$

Finally, the calculation of $H(P_{c,1})$ and $L(P_{c,1})$ as the values of the cumulative functions should be recorded as the values corresponding to beginning of the wetting and drying curve.

By integrating sorption hysteresis into the model, the accuracy of numerical predictions is enhanced, particularly in replicating the real hygric behavior of the material under cyclic environmental conditions.

4.2.3 Boundary conditions

This part outlines the boundary conditions applied to the numerical model, detailing the external and internal factors that govern heat and moisture exchanges during simulation. The boundary conditions relevant to the moisture conservation equation manifest between the wall surface and the ambient conditions. The energy balance at the internal and external surfaces of the walls is illustrated in Figure 4.1. The formulation of equations governing the boundary conditions for convective mass transport at both exterior and interior surfaces is presented as follows:

$$g = h_{M,e}(p_{ve,a,e} - p_{ve,s,e}) \ @ \ x = 0, e \tag{4. 19}$$

$$g = h_{M,i}(p_{ve,a,i} - \rho_{ve,s,i}) \ @ \ x = L, i \tag{4. 20}$$

where $h_{M,e}$ and $h_{M,i}$ are the exterior and interior mass transfer coefficients, $p_{ve,a,e}$ and $p_{ve,a,i}$ are the vapor pressures of the ambient air on the exterior and interior sides, and $p_{ve,s,e}$ and $\rho_{ve,s,i}$ are the vapor pressures at the surface on the exterior and interior sides. These relations describe the boundary conditions for convective mass transfer at the two surfaces of the sample. The boundary conditions associated with the energy conservation equation are expressed in the form of:

$$q = h_{T,e}\left(T_{a,e} - T_{s,e}\right) + L_v(T)h_{M,e}\left(p_{ve,a,e} - p_{ve,s,e}\right) + \Phi_{rad,e} \tag{4. 21}$$

$$q = h_{T,i}(T_{a,i} - T_{s,i}) + L_v(T)h_{M,i}(p_{ve,a,i} - p_{ve,s,i}) + \Phi_{rad,i} \quad (4.\ 22)$$

where $h_{T,e}$ and $h_{T,i}$ are the exterior and interior convective heat transfer coefficients, $T_{a,e}$ and $T_{a,i}$ are the ambient air temperatures, $T_{s,e}$ and $T_{s,i}$ are the surface temperatures, and $\Phi_{rad,e}$ and $\Phi_{rad,i}$ represent the exterior and interior radiative heat fluxes. These equations describe the heat balance at the exterior and interior boundaries, combining sensible convection, latent heat exchange due to mass transfer, and radiation.

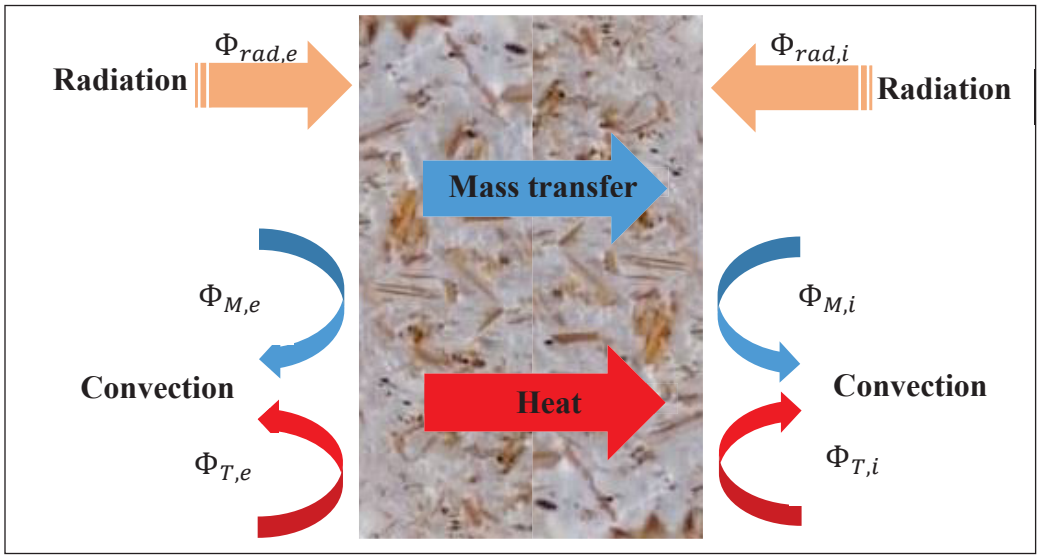

Figure 4.1 Energy and mass balance in sides of the sample

The schematic in Figure 4.1 illustrates the fundamental heat and mass transfer mechanisms governing the hygrothermal behavior of mycelium-based composites. At the material boundaries, radiative fluxes ($\Phi_{rad,e}$, $\Phi_{rad,e}$) interact with convective exchanges ($\Phi_{T,i}$, $\Phi_{T,e}$, $\Phi_{M,i}$, $\Phi_{M,e}$) driving simultaneous heat and moisture transfer across the sample. Internally, conductive heat transfer and vapor diffusion are coupled with mass exchange processes, highlighting the multiphysical nature of the system. This balance of energy and mass fluxes is critical for capturing realistic boundary conditions in the numerical model, ensuring that both isothermal and non-isothermal conditions can be accurately simulated. By accounting for these interactions, the framework provides a reliable basis for evaluating the thermal buffering and moisture regulation potential of mycelium composites in building applications.

Regarding hygric diffusivity, the coefficients can be deduced from the vapor permeability δ_p and the inverse of the slopes of the tangents to the adsorption/desorption isotherms. It is given by:

$$D_\varphi(\varphi, T) = D_{\varphi,v}(\varphi, T) + D_{\varphi,l}(\varphi, T) = \delta_p \, . p_{sat}(T) \tag{4. 23}$$

where D_φ is the diffusion coefficient associated with relative humidity, $D_{\varphi,v}$ and $D_{\varphi,l}$ are its vapor and liquid contributions, δ_p is the vapor permeability, and $p_{sat}(T)$ is the saturation vapor pressure. Regarding hygric diffusion under the influence of a thermal gradient, assuming that thermal diffusion in the liquid phase is negligible, as generally accepted, it is expressed by the vapor diffusion associated with a temperature gradient ΔT_v. Referring to the literature, Abadie et al. (2005) also suggests using the following equation:

$$D_{vT}(\varphi, T) = \delta_p(\varphi)\varphi \frac{\partial p_{sat}(T)}{\partial T} \tag{4. 24}$$

where D_{vT} is the diffusion coefficient describing vapor transport under a temperature gradient, $\delta_p(\varphi)$ is the vapor permeability as a function of relative humidity, φ is the relative humidity, and $\frac{\partial p_{sat}(T)}{\partial T}$ is the derivative of the saturation vapor pressure with respect to temperature. Defining these boundary conditions allows the model to replicate realistic hygrothermal scenarios, thereby increasing the reliability of the predicted results.

4.3 Numerical simulation methods

This section specifies the COMSOL simulation setup and inputs—hygrothermal boundary conditions, sorption isotherms, and the separation of isothermal and non-isothermal cases. The hygrothermal boundary conditions utilized to input the numerical model are detailed in Table 4.1. Alongside the material's physical properties, sorption isotherms serve as inputs for the

numerical simulation. Psychrometric chart indicates that an increase in temperature typically results in higher water content for a given relative humidity.

Consequently, sorption isotherms vary with temperature changes. In the simulation campaign, both isothermal and non-isothermal models are developed and validated using experimental data. The isothermal model predicts the moisture content evolution within the material under constant temperature conditions, while the non-isothermal model considers variations in both temperature and relative humidity as parameters. This study primarily concentrates on modeling the adsorption isotherm as a function of temperature, as elaborated in the following section.

Table 4.1 Hygrothermal boundary condition of the numerical simulation

Isothermal Conditions		
Sample	**Relative humidity**	**Temperature**
GHOP	50 %	23 ℃
Non-isothermal condition		
Sample	**Relative humidity**	**Temperature**
GHOP	0-80 %	15 ℃
GHOP	0-80 %	30 ℃
GHOP	0-80 %	35 ℃
GHOP	0-80 %	40 ℃

4.3.1 Analytical modeling of the sorption isotherms

Sorption behavior is represented with the GAB equation to relate moisture content to relative humidity, using an averaged curve between adsorption and desorption to account for hysteresis. Equation (4.25), previously introduced in Chapter 3, is repeated here for clarity. Moisture content stored within the material (u) is often represented as a function of the surrounding relative humidity (ϕ) in academic research. Typically, these models are developed for specific temperatures, ignoring the influence of temperature variation. In porous materials,

moisture absorption patterns are usually described using the water retention curve. To achieve this, researchers have devised several models, each with its set of parameters known as partial regression coefficients. These coefficients help identify different stages of moisture absorption behavior. The GAB model, derived from the BET model, is widely employed. It enables the modeling of a material's hygroscopic behavior across the entire spectrum of relative humidity from 0% to 100%.

$$u(\phi) = \frac{w_m CK\phi}{(1 - K\phi)(1 - K\phi + CK\phi)} \tag{4. 25}$$

Where w_m represents the moisture content associated with an adsorbed monolayer, while C and K are coefficients dependent on the molar heat of absorption and the latent heat of condensation, respectively. It is important to note that in this equation, two types of moisture content are employed: u, the mass-based equilibrium moisture content, and w (and w_m), the volumetric moisture content. Unless otherwise stated, sorption isotherms are expressed in terms of u, while transport equations are expressed in terms of w.

Consequently, the GAB model was employed to characterize the hygric behavior of building materials during both adsorption and desorption. In order to examine the impact of hygric hysteresis on moisture transfer, an average sorption curve was generated by taking the mean between the GAB curves for adsorption and desorption. Kwiatkowski et al. demonstrate that relying solely on one of the sorption isotherm equations (either adsorption or desorption) results in significant disparities, emphasizing that employing the average of both equations leads to more precise outcomes in the model (Kwiatkowski et al., 2009).

The experimental data for the sorption isotherms for five different mixtures of the fungi and substrate are extracted and plotted and compared in Figure 3.7. Additionally, based on Table 3.4 measured free water saturation (w_f) for GHOP, yielded 886.73 $kg \cdot m^{-3}$ equivalent to 580.01%. Experimental data were analyzed using the GAB model to achieve a fit for absorption and desorption using MATLAB. The fitting process involved meticulous

consideration of the three parameters of the GAB model, focusing particularly on the polymolecular sorption domain corresponding to the building range. Curve fitting parameters for GAB models based on moisture content and moisture contents relative to the free water saturations are separately indicated in Table 4.2.

Table 4.2 Input GAB curve fitting parameters for the input of numerical simulation

Type	**Temperature**	**Fitted GAB parameters**			**R-Squared**	**SSE (*10^{-6})**
		w	**c**	**k**		
Adsorption	23 °C	0.048	9.428	0.844	0.9996	1.116*10^{-5}
Desorption	23 °C	0.081	7.44	0.685	0.9997	1.03*10^{-5}
Type	**Temperature**	**Fitted GAB parameters based on w_f**			**R-Squared**	**SSE (*10^{-6})**
		w	**c**	**k**		
Adsorption	23 °C	0.0076	9.46	0.845	0.9876	1.024*10^{-5}
Desorption	23 °C	0.037	2.636	0.349	0.9876	1.024*10^{-5}

The fitted GAB parameters reported in Table 4.2 serve as direct inputs to the simulation and anchor subsequent comparisons with experiment.

4.3.2 Modeling the effect of temperature on the sorption curve

To capture temperature dependence, the approach derives isosteric heat via the Clausius–Clapeyron relation and Poyet's isostere method, then uses it to generate sorption isotherms at target temperatures. Various approaches have been suggested to offer a physical explanation for the phenomenon, where water content increases with temperature under constant relative humidity. These approaches are grounded in physical phenomena, such as the expansion of the material's pore space due to rising temperature, changes in the thermophysical properties of water, and shifts in thermodynamic equilibrium.

Several models have been developed to understand the impact of temperature on sorption isotherms. Milly (1982) focuses on how temperature influences sorption isotherms by modifying intrinsic water properties. On the other hand, Poyet's model (Poyet & Charles, 2009) emphasizes the inadequacy of solely altering physical properties and pore structure to replicate

concrete's hydric behavior with temperature. Instead, Poyet's model considers the thermodynamic evolution of physio-sorption mechanisms, incorporating the heat released during the exothermic adsorption process (Brunauer et al., 1940).

This phenomenon can be described by the Clausius-Clapeyron equation, which allows for the assessment of the heat involved in a phase change for a system at equilibrium. In the case of adsorption, the heat exchanged by the "water vapor/adsorbed water" system is referred to as the isosteric heat of adsorption. It corresponds to the change in energy for a constant coverage of the adsorbent surface. Using the Clausius-Clapeyron equation, it can be expressed as follows:

$$Q_{st}(u) = -R\left(\frac{\partial \ln\left(p_v\right)}{\partial\left(\frac{1}{T}\right)}\right)_u \tag{4.26}$$

where $Q_{st}(u)$ is the isosteric heat of sorption, R is the universal gas constant, p_v is the equilibrium vapor pressure, T is the temperature, and the derivative is taken at constant moisture content u. The integration of Equation (4.26) between two sorption isotherms leads to the isosteric heat of adsorption, which can be expressed as follows:

$$q_{st}(u) = \frac{R}{M_v}\frac{T_1 T_2}{T_2 - T_1}\ln\left(\frac{p_v(T_2,u)}{p_v(T_1,u)}\right) \tag{4.27}$$

where q_{st} is the isosteric heat of sorption on a molar basis, R is the universal gas constant, M_v is the molar mass of water vapor, T_1 and T_2 are two different temperatures, and $P_v(T,u)$ is the equilibrium vapor pressure corresponding to moisture content u at temperature T. Determining q_{st} involves utilizing two sorption isotherms established at different temperatures, T_1 and T_2. For hemp concrete, isotherms at 10 °C and 23 °C were employed. By the incorporation of the q_{st} temperature effects on the determination of the sorption isotherm at a specific temperature

is evaluated. The Clausius-Clapeyron relationship between (T_1, p_{v1}) and (T_2, p_{v2}) at equilibrium with constant water content "u" is used for this assessment. Using the equation (4.28), an assumption of the sorption isotherm at temperature T_2 based on a sorption isotherm measured at temperature T_1. The results of sorption isotherms for the mycelium bio-composites are presented in chapter 3.

$$\varphi(T_2,u) = \varphi(T_1,u)\frac{p_{sat}(T_2)}{p_{sat}(T_1)}\exp\left(\frac{q_{st}(u)}{R}\left(\frac{T_2 - T_1}{T_1 T_2}\right)\right) \tag{4.28}$$

This equation allows extrapolation of sorption isotherms from one temperature to another. Poyet's model utilizes sorption isosteres to assess the isosteric heat. This involves selecting four points from four distinct sorption isotherms at constant moisture content, from which vapor pressure is determined and plotted against the inverse of temperature in Figure 4.2.

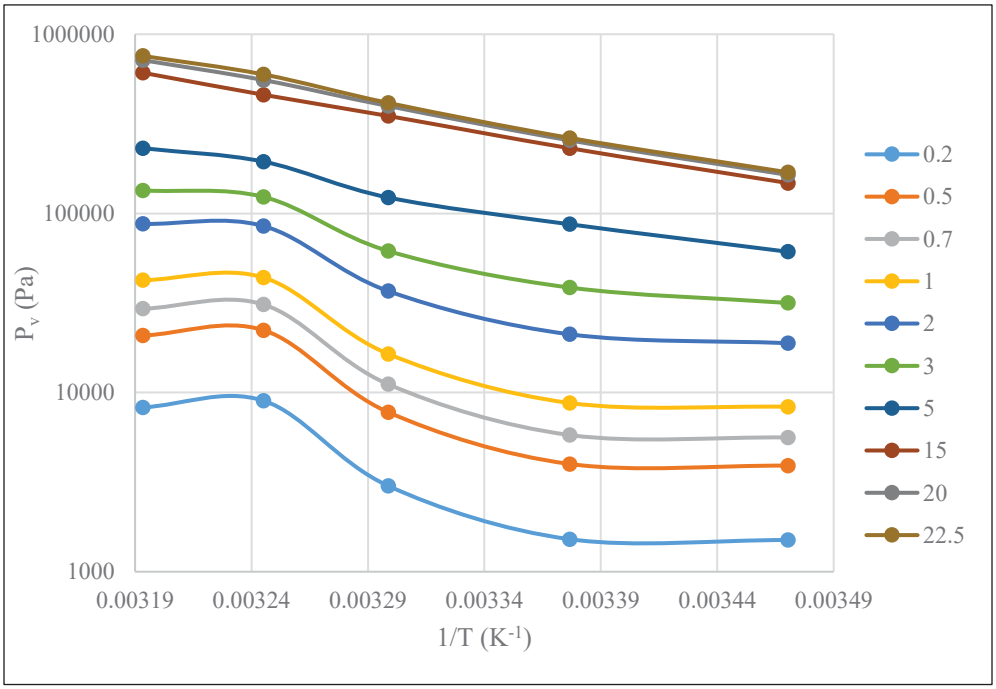

Figure 4.2 The evolution of isosteric heat as a function of temperature

In this figure, by graphing each isostere against water content, the isosteric heat of sorption can be discerned from the slope of the graph. This evolution of isosteric heat, linked with water content, is subsequently integrated into equation (4.28) to derive the sorption isotherms at a given temperature. The slope of the isosteres allows for the determination of the net sorption heat relative to water content, denoted as $Q_{st}(u)$.

$$Q_{st}(u) = L_v + \frac{a}{(b+u)^c} \tag{4.29}$$

where L_v is the latent heat of vaporization, and a, b, and c are empirical fitting parameters used to capture the variation of isosteric heat with moisture content u. Equation (4.29) is extracted from the model of Powers and Brownyard (Poyet & Charles, 2009). The isosteric heat of sorption is plotted against moisture content in Figure 4.3. for two distinct temperature sets to derive the constants of this equation.

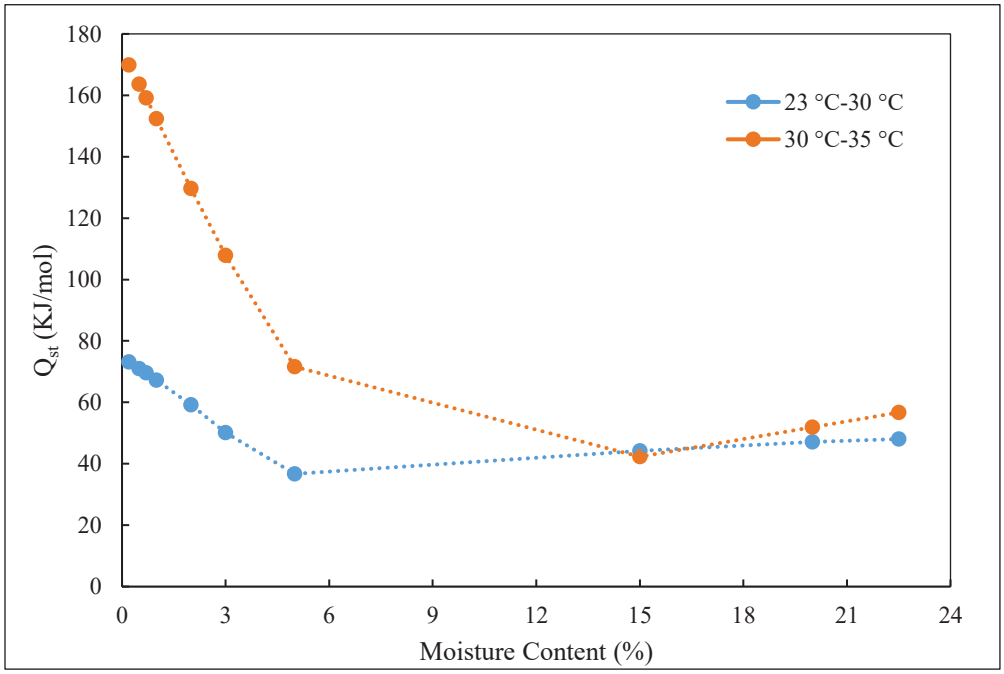

Figure 4.3 Variation of isosteric heat of sorption with moisture content at different temperatures

Figure 4.3 provides the moisture-dependent isosteric heat $Q_{st}(u)$ used to calibrate Equation (4.29) by nonlinear least-squares fitting, yielding the constants of the model. The calibrated $Q_{st}(u)$ is then combined with the Clausius–Clapeyron relation (Equations. 4.26–4.28) to compute $\varphi(T,u)$ at target temperatures and generate temperature-corrected sorption isotherms for the non-isothermal simulations. The resulting parameters are reported in Table 4.4 and are subsequently compared with experimental sorption data in the non-isothermal results. Q_{st}

4.3.3 Heat and mass convection coefficients

The thermal convection coefficient as a function of air velocity can be estimated using the following equation (Zirkelbach et al., 2007).

$$h_c = 4.5 + 0.33v \tag{4.30}$$

The air speeds on both sides of the wall were very low; therefore, following Zirkelbach et al. (2007), a convective heat transfer coefficient of 4.5 $W \cdot m^{-2} \cdot K^{-1}$ was adopted. Since the experimental setup did not receive direct solar radiation, the radiative heat transfer coefficient was estimated by linearization of the Stefan–Boltzmann law at ~20–25 °C (emissivity ≈ 0.9), which yields a typical value of about 6 $W \cdot m^{-2} \cdot K^{-1}$. To better reflect the boundary conditions of the test facility, this radiative contribution was partitioned into 3.5 $W \cdot m^{-2} \cdot K^{-1}$ for the side facing the laboratory and 2.5 $W \cdot m^{-2} \cdot K^{-1}$ for the side facing the climate chamber. For comparison, the internal combined surface heat transfer coefficient is taken as 8 $W \cdot m^{-2} \cdot K^{-1}$, a standard value reported by Künzel (1994) for modeling indoor surface exchanges.

The mass convection coefficient deduced from the equation (4.30 as a function of the Lewis number and h_c is equal to 0.004 $m \cdot s^{-1}$. This value is validated by employing the relationship $h_M = 7 \times 10^{-9}\ h_c$ from the works of Kunzel, a correlation that has been discussed also by Hasanuzzaman et al. (2012).

4.4 Results

This section presents the outcomes of the numerical simulations under both isothermal and non-isothermal conditions, highlighting how the developed model reproduces the sorption dynamics of mycelium-based composites.

4.4.1 Isothermal simulation

The isothermal simulation investigates the moisture sorption behavior under constant temperature conditions, employing both non-hysteresis and hysteresis approaches for model validation. The first mode, termed non-hysteresis simulation, computes moisture content by averaging the values between adsorption and desorption obtained from sorption results in DVS tests and then fitting GAB equations on the average dataset. The implemented calculation in COMSOL starts with relative humidity of the environment as the input. In both models, vapor pressure within the material domain is calculated using the PDE equation of mass transfer, which is solved by manually implementing the corresponding function in COMSOL. Figure 4.4 shows the flow diagram of the mean average sorption model.

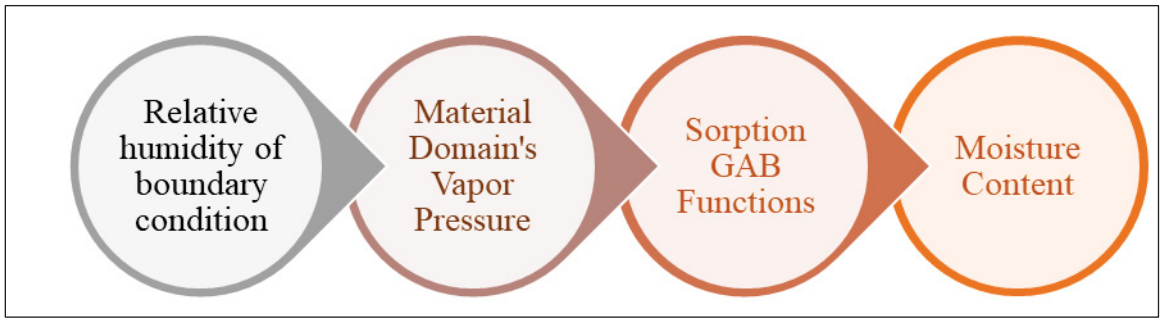

Figure 4.4 Mean sorption model flow diagram

The sorption function is computed by utilizing the GAB equation derived from the curve-fitted charts presented in Figure 3.9. This function is then used to calculate the final moisture content by multiplying it with the free moisture content. In the second mode, an intermediary step is introduced, involving the definition of basic functions L and H (equations (4.12) and (4.13). Subsequently, moisture content for adsorption and desorption is determined separately using

equations (4.17) and (4.18), respectively. Figure 4.5 shows the calculation flow of the moisture content as the output implemented in the numerical simulation.

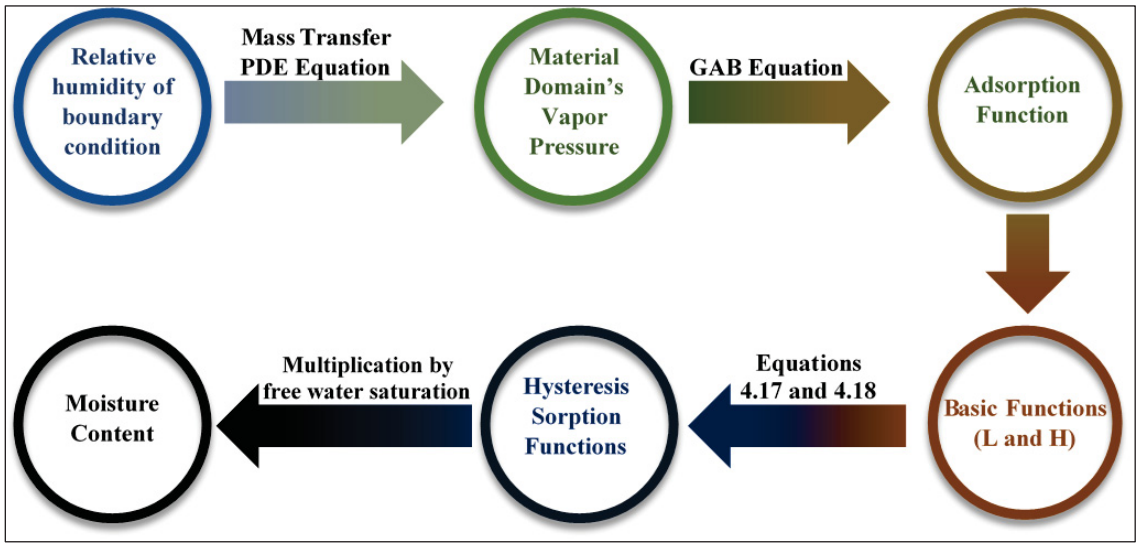

Figure 4.5 Hysteresis model flow diagram

The validation of isothermal simulation is done by MBV (Annex II) test as a non-intrinsic property of the material. By imposing cyclic boundary conditions (Table 4.1) in the numerical simulation, the accuracy of the numerical results compared to the experimental data are assessed, illustrated in Figure 4.6. Both hysteresis and non-hysteresis methods show close proximity with the experimental data.

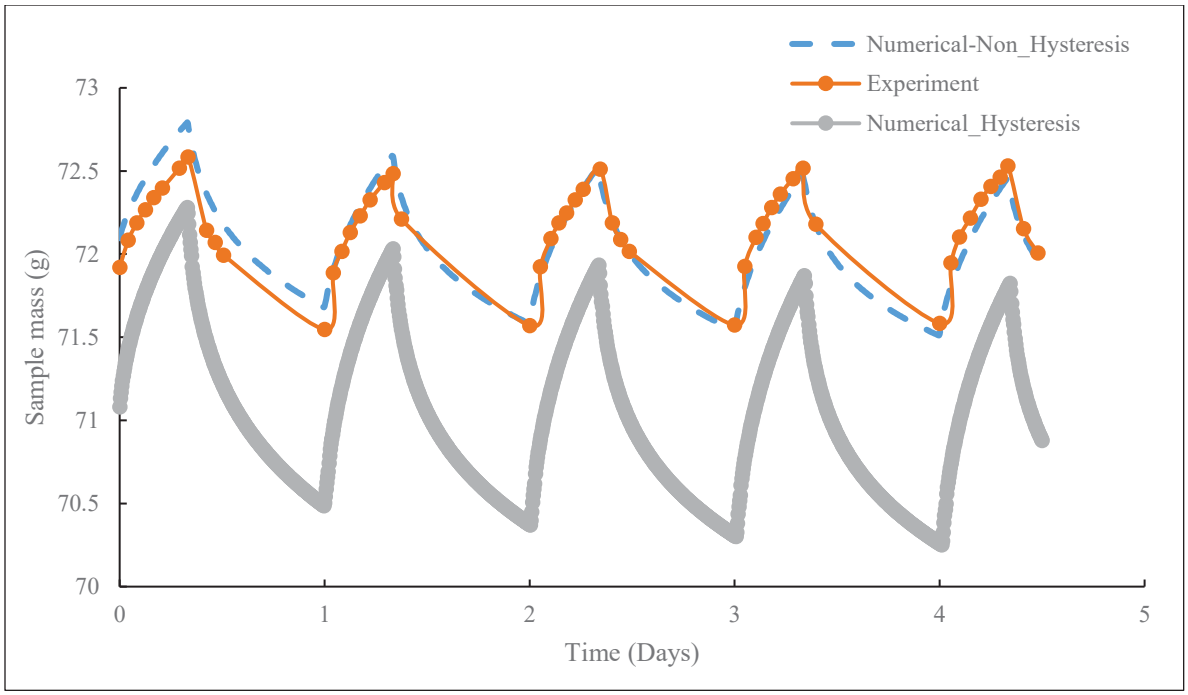

Figure 4.6 Validation of isothermal simulation with experimental results

As illustrated in Figure 4.6, the hysteresis method exhibits a higher error rate when contrasted with the non-hysteresis model. Nonetheless, as indicated in Table 4.3, despite the variance in initial values, the amplitude of moisture content fluctuation demonstrates relatively less error when compared to the experimental data. In the comparison between the implemented numerical processes, the hysteresis model is employed and computed indirectly following the scheme outlined in Figure 4.5, potentially introducing sources of error. Moreover, since validation is conducted via the MBV test (Appendix II), which encompasses a relative humidity range of 33 % to 75 %, corresponding to a linear area on the sorption curve, direct utilization of the hysteresis method utilizing the mean sorption curve would be highly accurate within this specified range.

Table 4.3 Accuracy of the isothermal simulation

Mode	**R-Squared**	**MAPE (%)**	**Amplitude MAPE%**
Non- Hysteresis	0.85	0.96	-0.03
Hysteresis	0.89	7.94	4.13

According to these results, the isothermal simulations demonstrate strong agreement with experimental results, confirming that both non-hysteresis and hysteresis schemes reliably capture the sorption dynamics, with the non-hysteresis method offering higher accuracy due to reduced error propagation.

4.4.2 Non-isothermal simulation

The non-isothermal simulation extends the model by incorporating temperature-dependent sorption isotherms, allowing validation across a wider range of hygrothermal conditions. The validation methodology for the non-isothermal simulation involves comparing the sorption isotherms obtained from DVS tests with the numerical sorption results generated at temperatures different from the reference temperature of the input GAB equation of the simulated material. Figure 4.7 illustrates the comparison of sorption charts with non-isothermal numerical simulation results.

The figure illustrates the comparison between experimental sorption isotherms and non-isothermal numerical simulation results at four temperatures (15 °C, 30 °C, 35 °C, and 40 °C). The agreement between experimental and simulated data is generally good, particularly at lower humidity levels where both trends overlap closely. At higher relative humidities, deviations become more pronounced, especially at 35 °C and 40 °C, where the simulations tend to underestimate moisture uptake compared to the experimental results. These discrepancies highlight the sensitivity of the model to temperature-dependent sorption formulations and boundary assumptions. Nevertheless, the overall correspondence across all temperature ranges supports the model's capability to capture the hygrothermal response of mycelium-based composites under non-isothermal conditions.

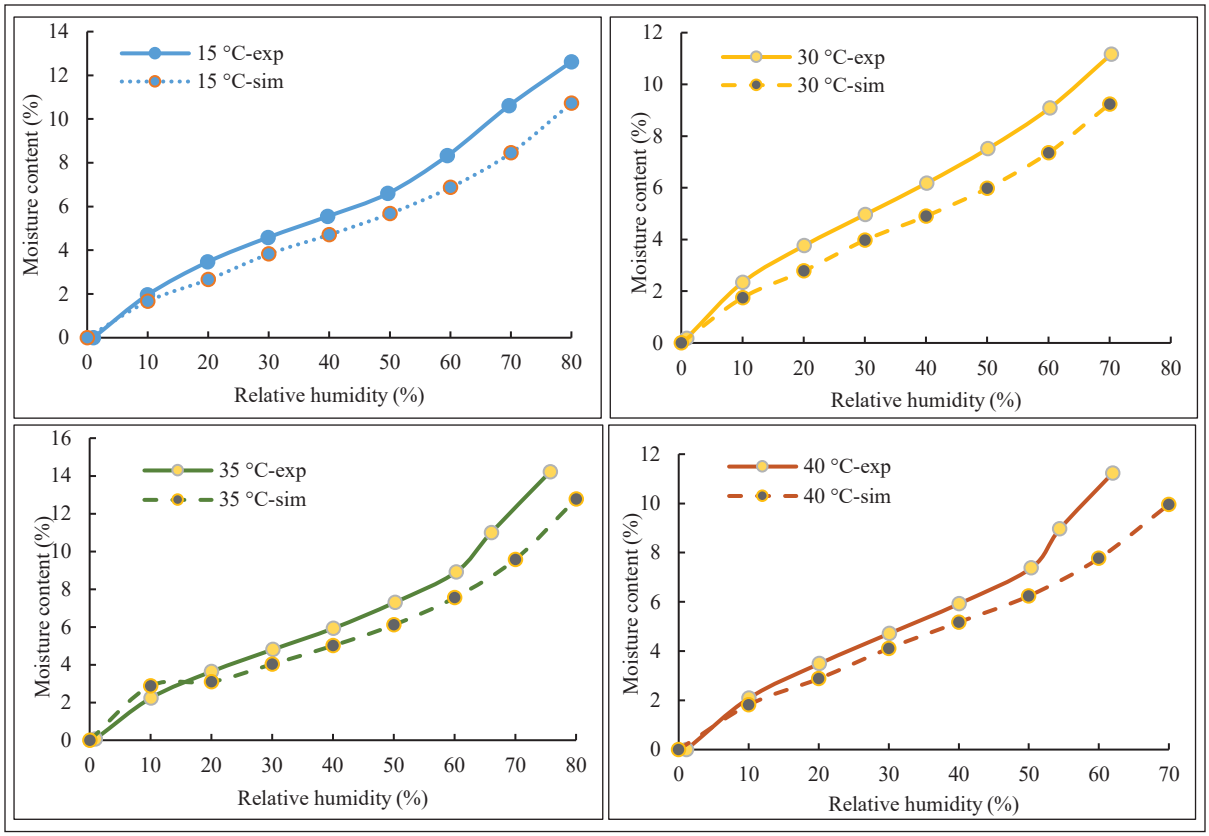

Figure 4.7 Comparison of experimental sorption isotherms (exp) with non-isothermal numerical simulation (sim) results

Experimental and numerical results are compared by curve fitting and calculating the GAB parameters, with corresponding statistical parameters calculated accordingly. The simulation incorporates the hysteresis method to accurately model the effect of sorption on desorption.

Table 4.4 Table 4.4 illustrates the GAB parameters alongside the corresponding statistical errors indicated by the R-Squared and SSE parameters. The Mean Average Percentage Error (MAPE) across all relative humidity steps is calculated accordingly. The highest calculated error, occurring at 30 °C, is 19.268 %.

Table 4.4 Fitted GAB parameters: experimental (Exp) vs. simulation (Sim) under non-isothermal conditions

Type	Temperature (°C)	w	c	k	R-Squared	SSE (*10⁻⁶)	MAPE %
Exp	15	0.05423	5.935	0.7697	0.9972	3.656	17.401
Sim	15	0.04247	8.275	0.7996	0.9997	3.227	
Exp	30	0.05494	6.638	0.8127	0.9979	6.667*10	19.268
Sim	30	0.04291	6.327	0.8305	0.9996	2.261	
Exp	35	0.04490	8.133	0.9243	0.9983	2.626*10	18.157
Sim	35	0.03468	19.33	0.9189	0.9972	3.312*10	
Exp	40	0.08159	3.444	0.6822	0.9824	227.7	17.121
Sim	40	0.04275	6.482	0.8686	0.9993	3.57	

The results demonstrate strong agreement between experimental and simulated data, with R^2 values consistently above 0.98, indicating a robust fit across all conditions. The sum of squared errors (SSE) remains relatively low for most cases, further confirming the model's accuracy, although higher deviations are observed at 40 °C due to increased sensitivity of sorption behavior to temperature effects. The Mean Absolute Percentage Error (MAPE) values range between 17.1 % and 19.3 %, reflecting the challenges of accurately reproducing sorption characteristics at elevated temperatures.

Together, these findings confirm the robustness of the modeling framework and establish a solid foundation for the comparative analysis presented in the conclusion.

4.5 Conclusion

Simulations were conducted in both isothermal and non-isothermal modes. In isothermal conditions, the accuracy and disparity between hysteresis and non-hysteresis modes were examined, resulting in maximum mean absolute percentage errors (MAPE) of 0.96 % and 7.94 %, respectively. The average errors in fluctuation amplitude were within the range of absolute values up to 0.03 % in the non-hysteresis mode and 4.13 % in the hysteresis mode. This discrepancy primarily stems from the indirect nature of hysteresis calculation and the specific range of relative humidity utilized, which adopts a linear approach in sorption isotherms leading to higher accuracy in non-hysteresis mode.

Conversely, in the non-isothermal mode, incorporating hysteresis into the numerical simulation, which is validated in the full range of relative humidity, results in improved accuracy according to the reviewed literature. MAPE varied across different temperatures in the non-isothermal simulation, ranging between 17.12 % at 40 °C to 19.27 % at 30 °C. It's worth noting that due to the differing nature of the simulations in the aforementioned modes, distinct validation methods were employed, leading to varying average errors.

Overall, the findings confirm that the model reproduces experimental observations well under isothermal conditions, while non-isothermal scenarios highlight its sensitivity to boundary conditions and the need for refined sorption curve formulations. Despite these limitations, the model reliably captures fundamental hygrothermal behavior of MBCs, particularly their moisture-buffering and thermal regulation capacity. These insights provide a foundation for improved parameterization, extended validation, and integration with experimental hygrothermal characterization, ultimately enhancing predictive reliability for the use of MBCs as sustainable building insulation.

CONCLUSION

Reducing emissions from the construction sector and addressing the embodied carbon of building materials, which account for 40 % of total emissions, is crucial for achieving net-zero goals under the Paris Agreement. Sustainable building materials play a pivotal role in tackling embodied carbon. Besides carbon emissions, other environmental and non-environmental impacts call for a circular economy approach in material development, both within and beyond the building value chain. Last but not least, efficiency comparable to traditional materials like concrete (for load-bearing), brick (for facades), and Styrofoam (for insulation, non-load bearing) is essential for these sustainable alternatives.

This thesis has primarily centered on advancing mycelium-based materials as the insulation blocks for buildings. To this end, through a tailored fabrication process, employing a trial-and-error methodology, extensive experimental analyses were conducted to comprehensively characterize hygric, thermal, and mechanical properties of these materials. In the final stage, a numerical model was developed to simulate both isothermal and non-isothermal conditions, encapsulating the culmination of the research endeavor.

The literature review in chapter1 consolidates a decade of research on mycelium bio-composites (MBCs), emphasizing how fabrication methods—including mold-based, 3D printing, and hybrid techniques—critically influence mechanical consistency, scalability, and microstructure. The review concludes that performance is tightly linked to fungal strain, substrate type, and densification, with densified MBCs exhibiting superior insulation and moisture resistance. While environmental assessments confirm low or negative embodied carbon in optimized cases, long-term durability under humidity remains a limitation, though hybridization and post-treatments offer potential solutions. Fire performance is generally favorable due to high char yield and low smoke emissions. To advance MBC adoption in sustainable construction, future work should prioritize standardized fabrication protocols, development of bio-hybrid and robotic systems, extended durability testing under varied climatic conditions, microstructural modeling for thermal-moisture coupling, and region-

specific life cycle and end-of-life analyses. Together, these directions can support the integration of MBCs into high-performance, low-carbon building systems.

In the second chapter, detailed fabrication practice is described. The combination of seventeen different mixtures and their behavior in terms of water absorption, evaporation, and shrinkage, with each material suitable for different applications. The compatibility of different fungi types with straw and hemp is explored. Straw is proven to be ideal for applications requiring a moisture buffer, particularly in layers close to interior spaces to regulate indoor humidity. On the other hand, hemp demonstrates greater effectiveness in providing moisture insulation closer to the exterior, exhibiting reduced water absorption, particularly when a compact mycelium layer is deliberately created on its surface. Furthermore, the interaction of mycelium with mold materials is assessed. PVC supported beneficial fungi growth near the mold, while cast iron inhibited mycelium interaction, leading to damage and compromising the material's integrity.

The study investigates the hygroscopic behavior of mycelium-based composites, considering sorption isotherms, vapor permeability, liquid water transport, and moisture buffering across various sample combinations. Similarities are observed in sorption isotherms between hemp and *Ganoderma*-based samples, with hemp-*Ganoderma* blends and samples containing additives showing superior performance, particularly at high humidity levels. Vapor permeability testing revealed higher permeability for the straw and *Ganoderma* composition, consistent with its more open and porous microstructure. In contrast, the GHOP formulation exhibited consistently reduced vapor permeability, capillary absorption, and thermal variation due to its denser hyphal network. The lower porosity in such dense structures reduced condensation in the capillary region, thereby lowering resistance to vapor flow through the material.

The thermal conductivities varied between 0.056 $W \cdot m^{-2} \cdot K^{-1}$ at 24 °C in the dry state (VHOS) and 0.083 $W \cdot m^{-2} \cdot K^{-1}$ under conditions of 80 % relative humidity and 30 °C (GSWS). The study revealed that moisture content, regarded as the primary influencing factor, had a more

substantial impact compared to relative humidity and temperature, which were considered as secondary factors. Microstructural analysis showed that *Ganoderma lucidum* formed dense, interconnected hyphal networks, while *Trametes versicolor* produced more porous structures. Moisture uptake was primarily influenced by substrate and additives, while fungal species and treatments had more modest effects. Importantly, the results revealed that effective insulation depended not merely on high porosity, but on closed pores within cohesive hyphal matrices that limited moisture ingress and thermal drift. The exponential model further confirmed that porous, disconnected structures were more sensitive to vapor pressure changes. Overall, the study demonstrated that hygrothermal performance in MBCs is governed by microstructural geometry and connectivity, which can be tuned through fungal and processing choices to develop energy-efficient, bio-based insulation materials.

Finally, development of the numerical model in both isothermal and non-isothermal simulations was conducted. In comparison between hysteresis and non-hysteresis modes in isothermal mode revealed maximum mean absolute percentage errors (MAPE) of 0.96 % and 7.94 % respectively. Fluctuation amplitude errors ranged within 0.03 % in non-hysteresis mode and 4.13 % in hysteresis mode, primarily due to the indirect nature of hysteresis calculation and the specific range of relative humidity utilized. Conversely, in non-isothermal mode incorporating hysteresis improved accuracy across the full range of relative humidity, with MAPE varying between 17.12 % at 40 °C and 19.27 % at 30 °C. Different validation methods were applied for each mode, but both offer robust predictions for mycelium-based composites' functionality in diverse building envelope settings and climates. In particular, the Moisture Buffer Value (MBV) test results, presented in Annex II, provided the experimental basis for validating the numerical simulations.

Contributions and Originality:

The originality of this work lies in combining fabrication, experimental analysis, and numerical modeling into a unified framework. The main contributions are:

- **Fabrication methodology**: Systematic optimization of substrates, fungal species, additives, and mold materials provided reproducible protocols and tailored composites for specific applications.
- **Experimental hygrothermal dataset**: Generation of rare and detailed measurements—particularly sorption isotherms, vapor permeability, thermal conductivity–moisture correlations, and MBV (Moisture Buffer Value, presented in Annex II)—addressed a major gap in the literature.
- **Numerical innovation**: Introduction of a coupled heat–moisture model integrating sorption hysteresis, experimentally calibrated and validated, represents a novel approach for bio-based insulation.
- **Holistic evaluation**: By linking microstructural features to hygrothermal performance and embedding them in a predictive model, the thesis created a bridge between fundamental material science and applied building engineering.

RECOMMENDATIONS

The increasing demand for low-carbon, bio-based building materials has positioned mycelium-based composites (MBCs) as a promising solution for sustainable architecture. However, transitioning from laboratory-scale demonstrations to large-scale adoption requires a focused set of technical, infrastructural, and design-oriented advancements. The following recommendations aim to address key limitations, unlock scalability, and enhance the viability of MBCs in modern building practices—particularly within the emerging landscape of prefabricated housing in Canada.

1. Durability and Long-Term Testing

Despite their environmental advantages, the durability of MBCs under realistic service conditions remains insufficiently characterized. It is critical to conduct long-term experimental campaigns examining wetting–drying cycles**,** freeze–thaw resistance**,** biological degradation, and UV exposure to determine their performance envelope across diverse climatic zones. These tests should mirror the environmental stressors present in real-world applications, especially in regions like Canada where seasonal moisture and freeze-thaw cycles are particularly aggressive. Establishing confidence in service life is essential for achieving product certification and widespread architectural acceptance.

2. Moisture Protection and Functional Coatings

Given the hydrophilic nature of bio-composites, future work must develop bio-based hydrophobic coatings**,** engineered surface treatments, or integrated lamination techniques that protect against moisture while retaining biodegradability. Promising avenues include the use of waxes, oils, or bio-derived resins to form breathable yet water-resistant membranes. Densification strategies, especially those involving hot pressing or controlled mycelial compaction, should also be explored for their dual benefits in improving mechanical strength

and reducing moisture absorption. These improvements are particularly critical for semi-exposed or load-bearing elements.

3. Monolithic Wall Systems and Integration in Prefabricated Panels

To enable mainstream construction applications, MBCs must be integrated into structural assemblies that meet conventional building performance standards. A compelling opportunity lies in embedding MBCs into monolithic wall systems, such as those used in Hempcrete and other dense bio-based walls. This approach could be extended into SIP-like prefabricated panels, where the mycelium composite acts as a core insulating and hygroscopic buffer layer enclosed by structural facings.

This concept aligns well with the rapidly growing prefabricated housing market in Canada, which emphasizes modularity, speed of assembly, and environmental performance. Embedding MBCs into panelized systems enables both high performance and low-carbon credentials, particularly when paired with digital fabrication and off-site production techniques. As more Canadian builders and policymakers shift toward next-generation prefab homes, such integration would position MBCs as a critical enabling technology in decarbonized construction.

4. Scaling Up and Industrial Prototyping

Scaling MBC production beyond artisanal and lab-scale methods will require pilot-scale manufacturing, automated molding, and modular growth infrastructure. Collaborative efforts between academia, startups, and prefab housing manufacturers could test industrial incubation processes, robotic inoculation, and programmable mold designs. Real-world prototypes deployed in demonstration projects can provide crucial performance feedback and help refine supply chains, production times, and quality control protocols.

5. Development of Hybrid Bio-Composites

To expand the scope of MBCs for structural or semi-structural applications, research into hybrid material systems should be accelerated. This includes reinforcing mycelium matrices with natural fibers, cellulose nanofibrils, bacterial cellulose, or biodegradable mesh layers. Such reinforcements can mitigate brittleness, improve flexural and tensile strength, and enhance thermal and hygric stability. These strategies are particularly important for composite panels used in flooring, roofing, or wall sheathing applications, where greater resilience is required.

6. Advanced Modeling and Whole-Building Integration

Finally, the development of coupled heat-moisture transfer models must evolve to incorporate anisotropic behavior, microbial degradation dynamics, and multilayer configurations. Integrating these models with building energy simulation tools (e.g., EnergyPlus, WUFI, or TRNSYS) will support predictive analysis of MBC assemblies in real architectural contexts. Parametric modeling of wall assemblies containing MBCs will allow architects and engineers to optimize envelope design for thermal buffering, passive humidity control, and low embodied carbon.

With targeted research and focused engineering development, MBCs have the potential to move beyond niche applications into core elements of climate-conscious architecture. Their integration into monolithic wall systems and prefabricated panels—especially within Canada's evolving modular housing market—represents a timely and scalable pathway for transforming construction toward circular and regenerative material practices. These recommendations collectively outline a roadmap for realizing that potential.

ANNEX I

THE EVOLUTION OF CROP-BASED MATERIALS IN THE BUILT ENVIRONMENT: A REVIEW OF THE APPLICATIONS, PERFORMANCE, AND CHALLENGES

Sina Motamedi [1], Daniel R. Rousse [1,*] and Geoffrey Promis [2]

[1]Research Group in Energy Technologies and Energy Efficiency (t3e), École de Technologie Supérieure (ÉTS), Université du Québec, Montréal, QC H3C 1K3, Canada; seyedsina.motamedi.1@ens.etsmtl.ca
[2]Innovative Technologies Laboratory (LTI), University of Picardie Jules Verne, CEDEX 1, 80025 Amiens, France; geoffrey.promis@u-picardie.fr
*Correspondence: daniel.rousse@etsmtl.ca; Tel.: +1-(514)-396-8462

Paper published in *Journal of Energies*, April 2023

Abstract: The use of bio-based building materials as an alternative to replacing concrete or insulation materials is called to become a growing trend in the construction industry. On Science direct, publications concerning "bio-based materials" have increased from 4 in 2002 to 1073 twenty years later, demonstrating a growing interest in these materials However, among bio-based materials, crop or plant-based materials are not as popular. Due to their relative novelty, little is known about their potential applications, physical characteristics, and environmental impacts. The aim of this review is to qualitatively investigate the technical and environmental viability of crop-based materials in modern building applications. The specific objectives of the study consider greenhouse gas (GHG) emissions using life cycle assessment (LCA) approaches, contribution to the circular economy, and physical and hygrothermal characteristics. Another objective is to examine the progress of crop-based materials' R&D, current bottlenecks, and a future roadmap for their evolution in state-of-the-art renewable buildings. The paper is broad enough to capture a large readership rather than experts in the domain. The review reveals that crop-based materials have the potential to replace traditional, highly emissive building materials. They offer low environmental impacts, in all stages of their life cycle.

Keywords: crop-based materials; building applications; life cycle assessment (LCA); biogenic carbon; thermo-hygro-mechanical characteristics; R&D challenges; viability

ANNEX II

COMPARATIVE ANALYSIS OF MYCELIUM MBV AND CONVENTIONAL MATERIALS

1. Moisture Buffer Value (MBV)

In the building context, relative humidity is one of the most important factors to consider when assessing hygrothermal comfort. High indoor humidity influences air quality and can lead to the degradation of the building structure, significantly reducing the durability of construction materials (Toftum et al., 1998). Several authors (Rahim et al., 2015; Rode et al., 2007; Shea et al., 2012) have demonstrated that hygroscopic materials help mitigate indoor relative humidity variations, thereby enhancing occupants' comfort and facilitating energy consumption reduction.

The Nordtest project (Rode et al., 2007) proposed an experimental protocol to assess the hygric inertia of hygroscopic materials through the definition of Moisture Buffer Value (MBV). This experimental procedure has since been formalized under ISO 24353 for moisture buffering characterization. A similar method was suggested in the Japanese industrial standard (Association, 2002). The two methods differ in the cycle periods, imposed humidity levels, and sample thickness (Roels & Janssen, 2006). It is argued that the MBV is a comprehensive parameter but not an intrinsic property of the material, as it considers mass transfer resistances (mass convection).

2. Practical MBV, Ideal MBV, and Penetration Depth

The hygric buffer capacity is experimentally measured following the NORDTEST protocol (Rode et al., 2007). Samples undergo a relative humidity (RH) variation: 8 hours at 75 %, followed by 16 hours at 33 %. The same 24-hour cycle is repeated for 5 cycles until equilibrium is reached. The test temperature is maintained at a constant 23 °C. The moisture buffer value (MBV) is calculated using the following equation:

$$MBV = \frac{\Delta m}{S(RH_{max} - RH_{min})} \quad \text{(AII.1)}$$

The NORDTEST project defines the theoretical hygric buffer value and develops a simulation tool to determine the ideal MBV, utilizing the hygric properties of the material. The ideal MBV is given by the following equation:

$$MBV_{ideal} = 0.00568.P_{sat}.b_m.\sqrt{t_p} \quad \text{(AII.2)}$$

The hygric effusivity, b_m, is expressed by:

$$b_m = \sqrt{\frac{\delta_p.\rho_0.\frac{\partial u}{\partial \phi}}{P_{sat}}} \quad \text{(AII.3)}$$

The ideal MBV is based on the assumption that the studied materials are considered homogeneous and have a thickness that exceeds the penetration depth (semi-infinite medium). It is important to introduce the concept of Penetration Depth (d_p). It provides a theoretical approximation of the sample thickness required to measure the MBV. The penetration depth is defined as the distance between the exposed surface and the point where the amplitude of variation in water vapor concentration does not exceed 1% of that at the surface. It is given by the following expression:

$$d_p = 4.61\sqrt{\frac{D_w.t_p}{\pi}} \quad \text{(AII.4)}$$

This formula is derived from the model of a homogeneous semi-infinite wall subjected to a sinusoidal variation of relative humidity on its surface (Arfvidsson, 1999). The MBV is not an

intrinsic property of the material since the mass convection coefficient at the boundary plays a significant role.

3. Experimental protocol

The MBV of hemp and Ganoderma composite is experimentally measured according to the NORDTEST protocol (Rode et al., 2007). The experimental setup (climatic chamber) used allows control of temperature and relative humidity in the range of 8-65 °C with a precision of ±0.3°C and 10-98 % relative humidity with a precision of ±2 %. As shown in Figure AII-1 the temperature is kept constant at 23°C. Relative humidity steps (75 % for 8 hours, followed by 33 % for 16 hours) are set manually in the climatic chamber.

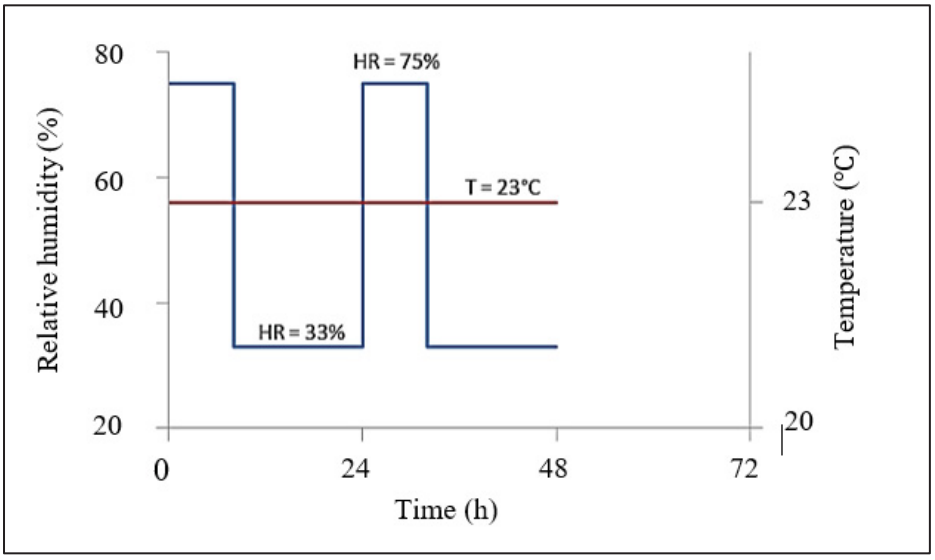

Figure AII-1 Imposed temperature and relative humidity in MBV of GHOP composite test

Based on the theoretical values of penetration depths found previously, sample thicknesses should be at least 3 cm. In this study 39 mm samples were used. The moisture-exposed surface exceeds 100 cm^2, a value that adheres to the recommendations of the NORDTEST protocol. The samples were pre-dried in an oven at 70 °C until mass stabilization. The bottom and peripheral faces of the samples were sealed using aluminum tape before being placed inside the climatic chamber. Weighing of the samples was conducted outside the climatic chamber

using a balance with an accuracy of 0.01 g. Samples were weighed at least eight times during the absorption period and three times during the desorption period.

4. Results and discussion

Figure AII-2 presents the variation of relative humidity in the climatic chamber and the mass evolution of the samples with thicknesses of 39 mm. In the first cycle, more water is desorbed than adsorbed, likely attributed to starting the test at 50 percent humidity, rather than initiating from a completely dry state. After the first cycle, four remaining cycles tend to maintain a constant MBV value and samples experience rapid stabilization.

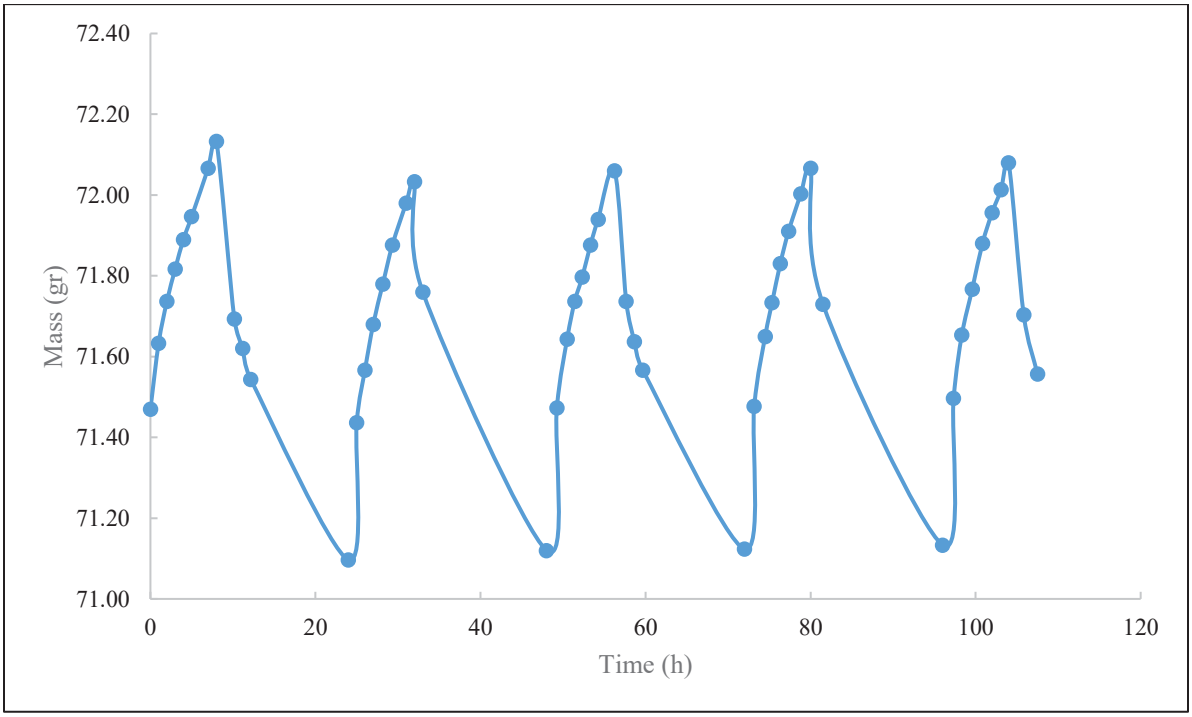

Figure AII-2 Sample's mass Evolution in MBV of hemp and Ganoderma composite test

Additionally, in Figure AII-3, MBV is calculated and illustrated in the consecutive cycles of wetting and drying until the stabilization of the mass. Rapid stabilization observed in Figure AII-2 and Figure AII-3 can be attributed not only to its high porosity but also to the presence of larger pore sizes. This distribution of pore sizes largely arises from the emission of gas by

the fungi during the fabrication process. As the fungi grow on the substrate, the emitted gas contributes to the formation of larger pores, facilitating faster stabilization and enhancing the material's verall moisture capacity. Thus, stability conditions are met, when the mean MBV values' variations remain less than 5% in the last three cycles.

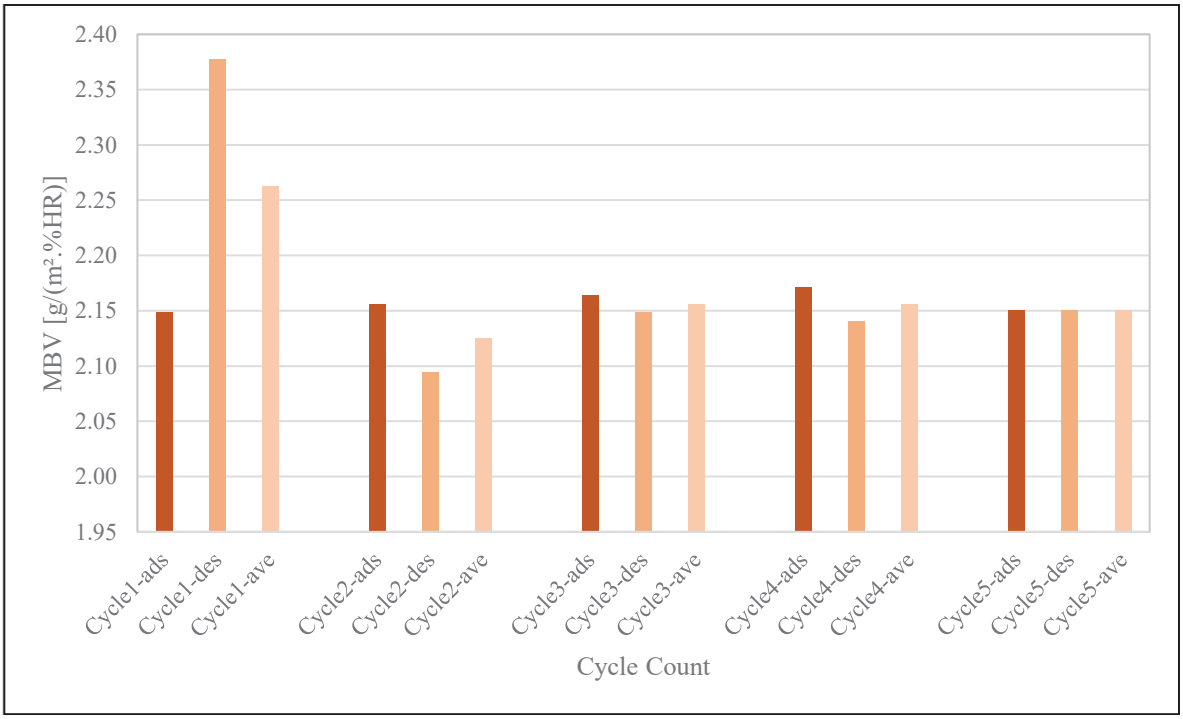

Figure AII-3 Calculated MBV of GHOP composite in Consecutive Cycles

5. Comparison

According to the MBV test results, GHOP composite exhibits an "Excellent" level of moisture buffering capability compared to other traditional building materials (Figure AII-4). The correlation between open porosity and density, depicted in chapter 3, illustrates that the majority of pores within the material are open. This distinguishes the GHOP composite from other insulation materials, such as EPS, which, despite its high porosity, exhibits a low moisture buffer value.

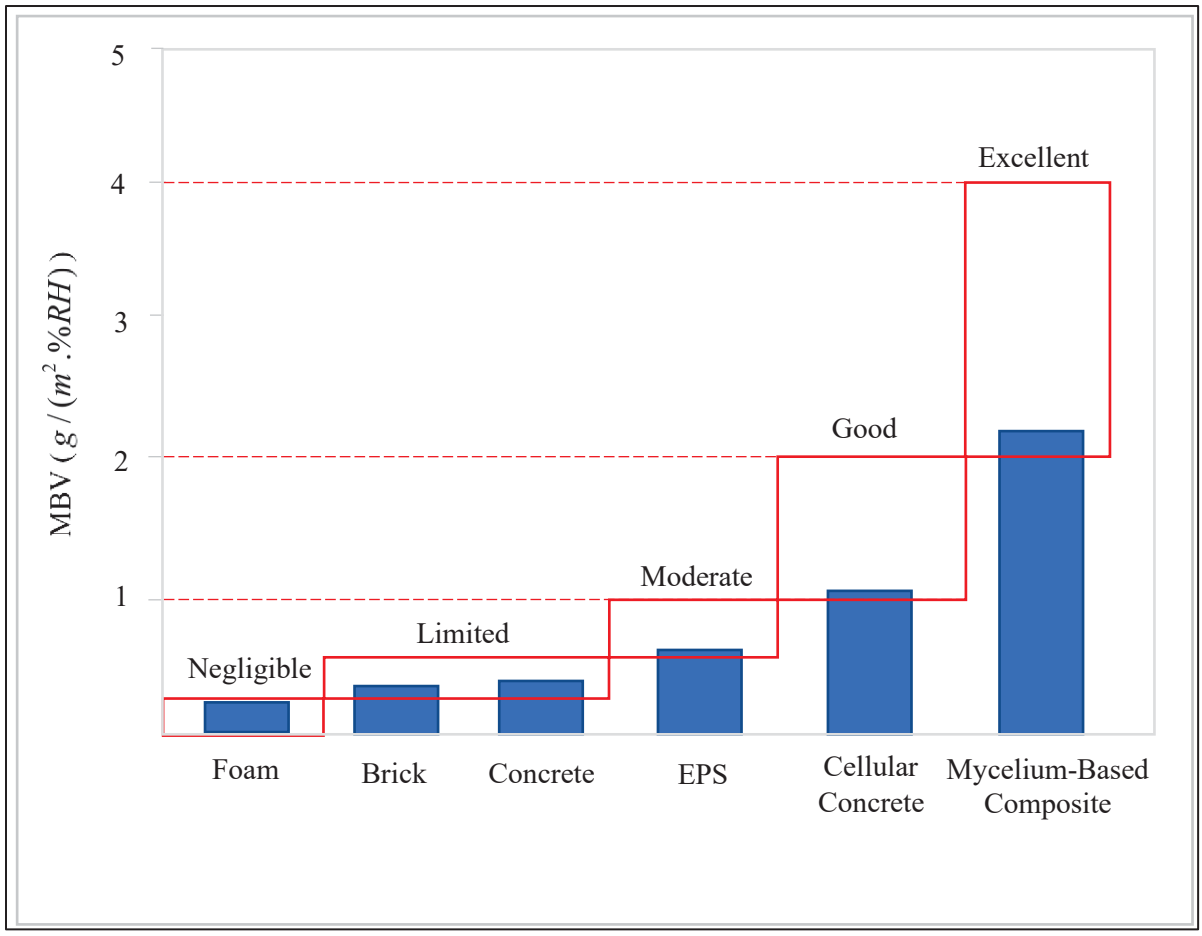

Figure AII-4 Comparison of Mycelium MBV with other traditional building materials
Comparison results adapted from Maaroufi et al. (2021, p. 7) and Rode et al. (2007, p. 41)

LIST OF BIBLIOGRAPHICAL REFERENCES

Abadie, M., Deblois, J.-P., & Mendes, N. (2005). A comparison exercise for calculating heat and moisture transfers using TRNSYS and PowerDomus. *IEA Annex*, *41*.

Abahri, K., Belarbi, R., & Trabelsi, A. (2011). Contribution to analytical and numerical study of combined heat and moisture transfers in porous building materials. *Building and environment*, *46*(7), 1354-1360.

Adaskaveg, J. E., & Gilbertson, R. L. (1986). In vitro decay studies of selective delignification and simultaneous decay by the white rot fungi Ganoderma lucidum and G. tsugae. *Canadian Journal of Botany*, *64*(8), 1611-1619.

Aiduang, W., Kumla, J., Srinuanpan, S., Thamjaree, W., Lumyong, S., & Suwannarach, N. (2022). Mechanical, physical, and chemical properties of mycelium-based composites produced from various lignocellulosic residues and fungal species. *Journal of Fungi*, *8*(11), 1125.

Akromah, S., Chandarana, N., Rowlandson, J. L., & Eichhorn, S. J. (2024). Potential environmental impact of mycelium composites on African communities. *Scientific Reports*, *14*(1), 11867.

Alaneme, K. K., Anaele, J. U., Oke, T. M., Kareem, S. A., Adediran, M., Ajibuwa, O. A., & Anabaranze, Y. O. (2023). Mycelium based composites: A review of their bio-fabrication procedures, material properties and potential for green building and construction applications. *Alexandria Engineering Journal*, *83*, 234-250.

Alaux, N., Vašatko, H., Maierhofer, D., Saade, M. R. M., Stavric, M., & Passer, A. (2023). Environmental potential of fungal insulation: a prospective life cycle assessment of mycelium-based composites. *The International Journal of Life Cycle Assessment*, 1-18.

Alaux, N., Vašatko, H., Maierhofer, D., Saade, M. R. M., Stavric, M., & Passer, A. (2024). Environmental potential of fungal insulation: A prospective life cycle assessment of mycelium-based composites. *The International Journal of Life Cycle Assessment*, *29*(2), 255-272.

Alemu, D., Tafesse, M., & Mondal, A. K. (2022). Mycelium-based composite: The future sustainable biomaterial. *International journal of biomaterials*, *2022*.

Appels, F. V., Camere, S., Montalti, M., Karana, E., Jansen, K. M., Dijksterhuis, J., Krijgsheld, P., & Wösten, H. A. (2019). Fabrication factors influencing mechanical, moisture-and water-related properties of mycelium-based composites. *Materials & Design*, *161*, 64-71.

Arfvidsson, J. (1999). A new algorithm to calculate the isothermal moisture penetration for periodically varying relative humidity at the boundary. *Nordic Journal of Building Physics*, *2*(11).

Association, J. S. (2002). Test method of adsorption/desorption efficiency for building materials to regulate an indoor humidity. *Japanese Industrial Standard (JIS) A 1470-2*.

Attias, N., Danai, O., Abitbol, T., Tarazi, E., Ezov, N., Pereman, I., & Grobman, Y. J. (2020). Mycelium bio-composites in industrial design and architecture: Comparative review and experimental analysis. *Journal of Cleaner Production*, *246*, 119037.

Attias, N., Danai, O., Tarazi, E., Pereman, I., & Grobman, Y. J. (2019). Implementing bio-design tools to develop mycelium-based products. *The Design Journal*, *22*(sup1), 1647-1657.

Babenko, M., Kononets, Y., Bartos, P., Pont, U., Spalek, F., Zoubek, T., & Kriz, P. (2024). Perspectives of Insulating Biodegradable Composites Derived from Agricultural Lignocellulosic Biomass and Fungal Mycelium: A Comprehensive Study of Thermal Conductivity and Density Characteristics. *Biomimetics*, *9*(11), 707.

Barta, D.-G., Simion, I., Tiuc, A.-E., & Vasile, O. (2024). Mycelium-based composites as a sustainable solution for waste management and circular economy. *Materials*, *17*(2), 404.

Beccali, M., Cellura, M., Fontana, M., Longo, S., & Mistretta, M. (2013). Energy retrofit of a single-family house: Life cycle net energy saving and environmental benefits. *Renewable and Sustainable Energy Reviews*, *27*, 283-293.

Belleudy, C., Woloszyn, M., Chhay, M., & Cosnier, M. (2016). A 2D model for coupled heat, air, and moisture transfer through porous media in contact with air channels. *International Journal of Heat and Mass Transfer*, *95*, 453-465.

Bhardwaj, A., Vasselli, J., Lucht, M., Pei, Z., Shaw, B., Grasley, Z., Wei, X., & Zou, N. (2020). 3D printing of biomass-fungi composite material: a preliminary study. *Manufacturing Letters*, *24*, 96-99.

Bitting, S., Derme, T., Lee, J., Van Mele, T., Dillenburger, B., & Block, P. (2022). Challenges and opportunities in scaling up architectural applications of mycelium-based materials with digital fabrication. *Biomimetics*, *7*(2), 44.

Brunauer, S., Deming, L. S., Deming, W. E., & Teller, E. (1940). On a theory of the van der Waals adsorption of gases. *Journal of the American Chemical society*, *62*(7), 1723-1732.

Cai, J., Han, J., Ge, F., Lin, Y., Pan, J., & Ren, A. (2023). Development of impact-resistant mycelium-based composites (MBCs) with agricultural waste straws. *Construction and Building Materials*, *389*, 131730.

Camilleri, E., Narayan, S., Lingam, D., & Blundell, R. (2025). Mycelium-based composites: An updated comprehensive overview. *Biotechnology Advances*, *79*, 108517.

Canada Energy Regulator. (2023). Canada's Energy Future 2023: Energy Supply and Demand Projections to 2050. *Canada Energy Regulator: Calgary, AB, Canada*. https://www.cer-rec.gc.ca/en/data-analysis/canada-energy-future/2023/

Carvalheiro, F., Silva-Fernandes, T., Duarte, L. C., & Gírio, F. M. (2009). Wheat straw autohydrolysis: process optimization and products characterization. *Applied biochemistry and biotechnology*, *153*, 84-93.

Cerimi, K., Akkaya, K. C., Pohl, C., Schmidt, B., & Neubauer, P. (2019). Fungi as source for new bio-based materials: a patent review. *Fungal biology and biotechnology*, *6*(1), 1-10.

Chen, H., Klemm, S., Dönitz, A. G., Ou, Y., Schmidt, B., Fleck, C., Simon, U., & Völlmecke, C. (2024). Tailoring the Mechanical Properties of Fungal Mycelium Mats with Material Extrusion Additive Manufacturing of PHBH and PLA Biopolymers. *ACS omega*, *9*(50), 49609-49617.

Chulikavit, N., Wang, C., Huynh, T., Yuen, A. C. Y., Khatibi, A., & Kandare, E. (2023). Fireproofing flammable composites using mycelium: Investigating the effect of deacetylation on the thermal stability and fire reaction properties of mycelium. *Polymer Degradation and Stability*, *215*, 110419.

Chutimanukul, P., Sukdee, S., Prajuabjinda, O., Thepsilvisut, O., Panthong, S., Athinuwat, D., Chuaboon, W., Poomipan, P., & Vachirayagorn, V. (2023). The Effects of Soybean Meal on Growth, Bioactive Compounds, and Antioxidant Activity of Hericium erinaceus. *Horticulturae*, *9*(6), 693.

Cuéllar-Franca, R. M., & Azapagic, A. (2012). Environmental impacts of the UK residential sector: Life cycle assessment of houses. *Building and Environment*, *54*, 86-99.

Diakité, M.-S., Lenormand, H., Lequart, V., Arufe, S., Martin, P., & Leblanc, N. (2021). Cell wall composition of hemp shiv determined by physical and chemical approaches. *Molecules*, *26*(21), 6334.

Dutil, Y., Rousse, D., & Quesada, G. (2011). Sustainable buildings: An ever evolving target. *Sustainability*, *3*(2), 443-464.

Elsacker, E., Søndergaard, A., Van Wylick, A., Peeters, E., & De Laet, L. (2021). Growing living and multifunctional mycelium composites for large-scale formwork applications using robotic abrasive wire-cutting. *Construction and Building Materials*, *283*, 122732.

Elsacker, E., Vandelook, S., Brancart, J., Peeters, E., & De Laet, L. (2019). Mechanical, physical and chemical characterisation of mycelium-based composites with different types of lignocellulosic substrates. *PLoS One*, *14*(7), e0213954.

Elsacker, E., Vandelook, S., Damsin, B., Van Wylick, A., Peeters, E., & De Laet, L. (2021). Mechanical characteristics of bacterial cellulose-reinforced mycelium composite materials. *Fungal biology and biotechnology*, *8*, 1-14.

Es-sakali, N., Charai, M., Kaitouni, S. I., Ait Laasri, I., Mghazli, M. O., Cherkaoui, M., Pfafferott, J., & Ukjoo, S. (2023). Energy efficiency and hygrothermal performance of hemp clay walls for Moroccan residential buildings: An integrated lab-scale, in-situ and simulation-based assessment. *Applied Energy*, *352*, 121967.

Es-sakali, N., Pfafferott, J., Mghazli, M. O., & Cherkaoui, M. (2025). Towards climate-responsive net zero energy rural schools: A multi-objective passive design optimization with bio-based insulations, shading, and roof vegetation. *Sustainable Cities and Society*, *120*, 106142.

Escobar, N., & Laibach, N. (2021). Sustainability check for bio-based technologies: a review of process-based and life cycle approaches. *Renewable and Sustainable Energy Reviews*, *135*, 110213.

Farrahnoor, A., Sazali, N. A. A., Yusoff, H., & Zhou, B. T. (2024). Effect of beeswax and coconut oil as natural coating agents on morphological, degradation behaviour, and water barrier properties of mycelium-based composite in modified controlled environment. *Progress in Organic Coatings*, *196*, 108763.

Farrera-Vázquez, N., Aviles-Trujilo, L., Moreira-Acosta, J., García-Ramos, O., Velazquez-Gurrola, A., Aguilar-Castillejos, A., Vargas-Estrada, L., & Sebastian, P. (2022). Development of an insulating material based on Trametes elegans mycelium and the study of its hygrothermal properties. *Green Materials*, *11*(1), 28-36.

Gaff, M., Hosseini, S. B., Paulasová, D., Kamboj, G., Rezaei, F., & Paul, D. (2024). Functionality of production processes in mycelium-based composites. *Composite Structures*, 118309.

Gan, J. K., Soh, E., Saeidi, N., Javadian, A., Hebel, D. E., & Le Ferrand, H. (2022). Temporal characterization of biocycles of mycelium-bound composites made from bamboo and Pleurotus ostreatus for indoor usage. *Scientific Reports*, *12*(1), 19362.

Gauvin, F., Tsao, V., Vette, J., & Brouwers, H. J. H. (2022). Physical properties and hygrothermal behavior of mycelium-based composites as foam-like wall insulation material. *Construction Technologies and Architecture*, *1*, 643-651.

Gauvin, F., & Vette, I. J. (2020). *Characterization of mycelium-based composites as foam-like wall insulation material* [Master's thesis, Eindhoven University of Technology]. Eindhoven, The Netherlands.

Gezer, E. D., & Kuştaş, S. (2024). Acoustic and thermal properties of mycelium-based insulation materials produced from desilicated wheat straw–Part B. *BioResources*, *19*(1), 1348.

Girometta, C., Picco, A. M., Baiguera, R. M., Dondi, D., Babbini, S., Cartabia, M., Pellegrini, M., & Savino, E. (2019). Physico-mechanical and thermodynamic properties of mycelium-based biocomposites: a review. *Sustainability*, *11*(1), 281.

Gorse, C., Thomas, F., Glew, D., & Shenton, D. M. (2016). Achieving sustainability in new build and retrofit: building performance and life cycle analysis. In *Building Sustainable Futures* (pp. 183-207). Springer.

Hamilton, I., Rapf, O., Kockat, D. J., Zuhaib, D. S., Abergel, T., Oppermann, M., Otto, M., Loran, S., Fagotto, I., & Steurer, N. (2020). Global status report for buildings and construction. *United Nations Environmental Programme: Nairobi, Kenya*.

Haneef, M., Ceseracciu, L., Canale, C., Bayer, I. S., Heredia-Guerrero, J. A., & Athanassiou, A. (2017). Advanced materials from fungal mycelium: fabrication and tuning of physical properties. *Scientific Reports*, *7*(1), 41292.

Hasanuzzaman, M., Rahman, M., Öztop, H. F., Rahim, N., & Saidur, R. (2012). Effects of Lewis number on heat and mass transfer in a triangular cavity. *International Communications in heat and mass transfer*, *39*(8), 1213-1219.

Holt, G. A., Mcintyre, G., Flagg, D., Bayer, E., Wanjura, J., & Pelletier, M. (2012). Fungal mycelium and cotton plant materials in the manufacture of biodegradable molded packaging material: Evaluation study of select blends of cotton byproducts. *Journal of Biobased Materials and Bioenergy*, *6*(4), 431-439.

Irbe, I., Kirpluks, M., Kampuss, M., Andze, L., Milbreta, U., & Filipova, I. (2024). Assessing the Conformity of Mycelium Biocomposites for Ecological Insulation Solutions. *Materials*, *17*(24), 6111.

Islam, M., Tudryn, G., Bucinell, R., Schadler, L., & Picu, R. (2018). Stochastic continuum model for mycelium-based bio-foam. *Materials & Design*, *160*, 549-556.

Islam, M. R., Tudryn, G., Bucinell, R., Schadler, L., & Picu, R. (2018). Mechanical behavior of mycelium-based particulate composites. *Journal of Materials Science*, *53*(24), 16371-16382.

Ito, K. (2012). Numerical prediction model for fungal growth coupled with hygrothermal transfer in building materials. *Indoor and Built Environment*, *21*(6), 845-856.

Janetti, M. B., Ochs, F., & Colombo, L. P. (2016). Hygrothermal modeling: a numerical and experimental study on drying. The 2016 COMSOL Conference in Munich,

Jansson, G., Schade, J., & Olofsson, T. (2013). Requirements management for the design of energy efficient buildings. *Journal of Information Technology in Construction (ITcon)*, *18*, 321-337.

Jiang, J., Zhou, P., Yi, Y., Chen, D., Hu, G., Liu, X., & Tang, L. (2025). Dual-crosslinked network structured polybenzoxazine/PBO nanofiber aerogel with thermal insulation, flame retardancy, and super-hydrophobicity. *Polymer Degradation and Stability*, 111216.

Jiang, L., Walczyk, D., McIntyre, G., Bucinell, R., & Tudryn, G. (2017). Manufacturing of biocomposite sandwich structures using mycelium-bound cores and preforms. *Journal of Manufacturing Processes*, *28*, 50-59.

Jiang, L., Walczyk, D., Mooney, L., & Putney, S. (2013). Manufacturing of mycelium-based biocomposites. Proceedings of the international SAMPE technical conference,

Jin, Q., Zhang, Z., & Chen, J. (2024). A study on the thermal performance of Pleurotus Ostreatus/Straw mycelium composites and its application in building envelopes. *Journal of Building Engineering*, *92*, 109646.

Jones, D., & Brischke, C. (2017). *Performance of bio-based building materials*. Woodhead Publishing.

Jones, M. (2019). *Waste-derived Mycelium materials for non-structural and semi-structural applications* [Ph.D. thesis, Melbourne, VIC, Australia.

Jones, M., Bhat, T., Kandare, E., Thomas, A., Joseph, P., Dekiwadia, C., Yuen, R., John, S., Ma, J., & Wang, C.-H. (2018). Thermal degradation and fire properties of fungal mycelium and mycelium-biomass composite materials. *Scientific Reports*, *8*(1), 17583.

Jones, M., Huynh, T., Dekiwadia, C., Daver, F., & John, S. (2017). Mycelium composites: a review of engineering characteristics and growth kinetics. *Journal of Bionanoscience*, *11*(4), 241-257.

Joseph, P., & Tretsiakova-McNally, S. (2010). Sustainable non-metallic building materials. *Sustainability*, *2*(2), 400-427.

Karana, E., Blauwhoff, D., Hultink, E.-J., & Camere, S. (2018). When the material grows: A case study on designing (with) mycelium-based materials. *International Journal of Design*, *12*(2), 119-136. https://research.tudelft.nl/en/publications/when-the-material-grows-a-case-study-on-designing-with-mycelium-b

Khasreen, M. M., Banfill, P. F., & Menzies, G. F. (2009). Life-cycle assessment and the environmental impact of buildings: a review. *Sustainability*, *1*(3), 674-701.

Knarud, J. I., & Geving, S. (2015). Implementation and benchmarking of a 3D hygrothermal model in the COMSOL Multiphysics software. *Energy Procedia*, *78*, 3440-3445.

Koh, C. H., Gauvin, F., Schollbach, K., & Brouwers, H. (2022). Investigation of material characteristics and hygrothermal performances of different bio-based insulation composites. *Construction and Building Materials*, *346*, 128440.

Koh, C. H., Gauvin, F., Schollbach, K., & Brouwers, J. Investigation of Material Characteristics and Hygrothermal Performances of Different Bio-Based Insulation Composites. *Available at SSRN 4128574*.

Künzel, H. M. (1994). *Verfahren zur ein-und zweidimensionalen Berechnung des gekoppelten Wärme-und Feuchtetransports in Bauteilen mit einfachen Kennwerten* Universität Stuttgart Stuttgart].

Künzel, H. M. (1995). Simultaneous heat and moisture transport in building components. *One-and two-dimensional calculation using simple parameters. IRB-Verlag Stuttgart*, *65*.

Kuribayashi, T., Lankinen, P., Hietala, S., & Mikkonen, K. S. (2022). Dense and continuous networks of aerial hyphae improve flexibility and shape retention of mycelium composite in the wet state. *Composites Part A: Applied Science and Manufacturing*, *152*, 106688.

Kuştaş, S., & Gezer, E. D. (2024). Physical and Mechanical Properties of Mycelium-based Insulation Materials Produced from Desilicated Wheat Straws-Part A. *BioResources*, *19*(1).

Kwiatkowski, J., Woloszyn, M., & Roux, J.-J. (2009). Modelling of hysteresis influence on mass transfer in building materials. *Building and Environment*, *44*(3), 633-642.

Lawrence, M. (2015). Reducing the environmental impact of construction by using renewable materials. *Journal of renewable materials*, *3*(3), 163-174.

Lingam, D., Narayan, S., Mamun, K., & Charan, D. (2023). Engineered mycelium-based composite materials: Comprehensive study of various properties and applications. *Construction and Building Materials*, *391*, 131841.

Livne, A., Wösten, H. A., Pearlmutter, D., & Gal, E. (2022a). Fungal mycelium bio-composite acts as a CO2-sink building material with low embodied energy. *ACS Sustainable Chemistry & Engineering*, *10*(37), 12099-12106.

Livne, A., Wösten, H. A., Pearlmutter, D., & Gal, E. (2022b). Fungal Mycelium Bio-Composite Acts as a CO2-Sink Building Material with Low Embodied Energy. *ACS Sustainable Chemistry & Engineering*.

Luo, D., Yang, J., & Peek, N. (2025). 3D-Printed Mycelium Biocomposites: Method for 3D Printing and Growing Fungi-Based Composites. *3D Printing and Additive Manufacturing*.

Maaroufi, M., Belarbi, R., Abahri, K., & Benmahiddine, F. (2021). Full characterization of hygrothermal, mechanical and morphological properties of a recycled expanded polystyrene-based mortar. *Construction and Building Materials*, *301*, 124310.

Madusanka, C., Udayanga, D., Nilmini, R., Rajapaksha, S., Hewawasam, C., Manamgoda, D., & Vasco-Correa, J. (2024). A review of recent advances in fungal mycelium based composites. *Discover Materials*, *4*(1), 13.

Maliki, M., Laredj, N., Bendani, K., & Missoum, H. (2017). Two-dimensional transient modeling of energy and mass transfer in porous building components using COMSOL Multiphysics. *Journal of Applied Fluid Mechanics*, *10*(1), 319-328.

Meyer, V., Schmidt, B., Pohl, C., Cerimi, K., Schubert, B., Weber, B., Neubauer, P., Junne, S., Zakeri, Z., & Rapp, R. (2020). *Mind the Fungi*. Universitätsverlag der Technischen Universität Berlin.

Milly, P. C. D. (1982). Moisture and heat transport in hysteretic, inhomogeneous porous media: A matric head-based formulation and a numerical model. *Water Resources Research*, *18*(3), 489-498.

Mohseni, A., Vieira, F. R., Pecchia, J. A., & Gürsoy, B. (2023). Three-dimensional printing of living mycelium-based composites: Material compositions, workflows, and ways to mitigate contamination. *Biomimetics*, *8*(2), 257.

Motamedi, S., Rousse, D. R., & Promis, G. (2023). The evolution of crop-based materials in the built environment: A review of the applications, performance, and challenges. *Energies*, *16*(14), 5252.

Motamedi, S., Rousse, D. R., & Promis, G. (2025). Microstructure-Driven Hygrothermal Behavior of Mycelium-Based Composites for Bio-Based Insulation. *Energies*, *18*(11), 2864.

Moussa, T., Maalouf, C., Ingrao, C., Scrucca, F., Costantine, G., & Asdrubali, F. (2018). Bio-based and recycled-waste materials in buildings: A study of energy performance of hemp-lime concrete and recycled-polyethylene terephthalate façades for office facilities in France and Italy. *Science and Technology for the Built Environment*, *24*(5), 492-501.

Nguyen, D. M., Grillet, A.-C., Diep, T. M. H., Thuc, C. N. H., & Woloszyn, M. (2017). Hygrothermal properties of bio-insulation building materials based on bamboo fibers and bio-glues. *Construction and Building Materials*, *155*, 852-866.

Nikitsin, V. I., & Backiel-Brzozowska, B. (2012). Methods of determination of liquid transfer coefficient in building materials. *International journal of heat and mass transfer*, *55*(15-16), 4318-4322.

Nussbaumer, M., Van Opdenbosch, D., Engelhardt, M., Briesen, H., Benz, J. P., & Karl, T. (2023). Material characterization of pressed and unpressed wood–mycelium composites derived from two Trametes species. *Environmental Technology & Innovation*, *30*, 103063.

Pan, J., Jain, R., Paul, S., Vu, T., Saifullah, A., & Sha, M. (2015). An internet of things framework for smart energy in buildings: designs, prototype, and experiments. *IEEE Internet of Things Journal*, *2*(6), 527-537.

Peng, L., Yi, J., Yang, X., Xie, J., & Chen, C. (2023). Development and characterization of mycelium bio-composites by utilization of different agricultural residual byproducts. *Journal of Bioresources and Bioproducts*, *8*(1), 78-89.

Philip, J., & De Vries, D. d. (1957). Moisture movement in porous materials under temperature gradients. *Eos, Transactions American Geophysical Union*, *38*(2), 222-232.

Pittau, F., Carcassi, O., Servalli, M., Pellegrini, S., & Claude, S. (2022, 23–25 September 2020). Hygrothermal characterization of bio-based thermal insulation made of fibres from invasive alien lake plants bounded with mycelium. IOP Conference Series: Earth and Environmental Science, Beijing, China.

Poyet, S., & Charles, S. (2009). Temperature dependence of the sorption isotherms of cement-based materials: Heat of sorption and Clausius–Clapeyron formula. *Cement and Concrete Research*, *39*(11), 1060-1067.

Promis, G., Douzane, O., Le, A. T., & Langlet, T. (2018). Moisture hysteresis influence on mass transfer through bio-based building materials in dynamic state. *Energy and Buildings*, *166*, 450-459.

Rahim, M., Douzane, O., Le, A. T., Promis, G., Laidoudi, B., Crigny, A., Dupre, B., & Langlet, T. (2015). Characterization of flax lime and hemp lime concretes: Hygric properties and moisture buffer capacity. *Energy and Buildings*, *88*, 91-99.

Rahim, M., Douzane, O., Le, A. T., Promis, G., & Langlet, T. (2016). Characterization and comparison of hygric properties of rape straw concrete and hemp concrete. *Construction and Building Materials*, *102*, 679-687.

Rahman, A. M., Bhardwaj, A., Pei, Z., Ufodike, C., & Castell-Perez, E. (2022). The 3D printing of biomass–fungi composites: effects of waiting time after mixture preparation on mechanical properties, rheological properties, minimum extrusion pressure, and print quality of the prepared mixture. *Journal of Composites Science*, *6*(8), 237.

Rode, C., Peuhkuri, R., Time, B., Svennberg, K., Ojanen, T., & Mukhopadhyaya, P. (2007). *Moisture buffer value of building materials*. ASTM International.

Roels, S., & Janssen, H. (2006). A comparison of the Nordtest and Japanese test methods for the moisture buffering performance of building materials. *Journal of Building Physics*, *30*(2), 137-161.

Sağlam, S. S., & Özgünler, S. A. (2024). Production of mycelium-based composite materials and evaluation of thermal insulation performance. *Journal of Green Building*, *19*(2), 193-222.

Scheffler, G. A. (2008). Validation of hygrothermal material modelling under consideration of the hysteresis of moisture storage.

Schultz, N., Fazli, A., Piros, S., Barranco-Origel, Y., DeLa Cruz, P., & Schneider, D. Y. (2024). Characterization of Mycelium Biocomposites under Simulated Weathering Conditions. *ACS Applied Bio Materials*, *7*(12), 8408-8422.

Scott, J., Kaiser, R., Ozkan, D., Hoenerloh, A., Agraviador, A., Elsacker, E., & Bridgens, B. (2022). Knitted cultivation: Textiling a multi-kingdom bio architecture. In *Structures and Architecture A Viable Urban Perspective?* (pp. 3-10). CRC Press.

Shea, A., Lawrence, M., & Walker, P. (2012). Hygrothermal performance of an experimental hemp–lime building. *Construction and Building Materials*, *36*, 270-275.

Shin, H.-J., Ro, H.-S., Kawauchi, M., & Honda, Y. (2025). Review on mushroom mycelium-based products and their production process: from upstream to downstream. *Bioresources and Bioprocessing*, *12*(1), 1-21.

Sisti, L., Gioia, C., Totaro, G., Verstichel, S., Cartabia, M., Camere, S., & Celli, A. (2021). Valorization of wheat bran agro-industrial byproduct as an upgrading filler for mycelium-based composite materials. *Industrial Crops and Products*, *170*, 113742.

Soh, E., Chew, Z. Y., Saeidi, N., Javadian, A., Hebel, D., & Le Ferrand, H. (2020). Development of an extrudable paste to build mycelium-bound composites. *Materials & Design*, *195*, 109058.

Soh, E., Teoh, J. H., Leong, B., Xing, T., & Le Ferrand, H. (2023). 3D printing of mycelium engineered living materials using a waste-based ink and non-sterile conditions. *Materials & Design*, *236*, 112481.

Song, H., Hon, K. C., Gauvin, F., Pantaleo, S., Berger, F., Chen, W., & Brouwers, H. (2025). Durability assessment of alkyl ketene dimer hydrophobic treatment of bio-based thermal insulation materials. *Resources, Conservation and Recycling*, *212*, 107983.

Stelzer, L., Hoberg, F., Bach, V., Schmidt, B., Pfeiffer, S., Meyer, V., & Finkbeiner, M. (2021). Life cycle assessment of fungal-based composite bricks. *Sustainability*, *13*(21), 11573.

Sun, W., Tajvidi, M., Hunt, C. G., McIntyre, G., & Gardner, D. J. (2019). Fully bio-based hybrid composites made of wood, fungal mycelium and cellulose nanofibrils. *Scientific Reports*, *9*(1), 1-12.

Sydor, M., Cofta, G., Doczekalska, B., & Bonenberg, A. (2022). Fungi in mycelium-based composites: usage and recommendations. *Materials*, *15*(18), 6283.

Takano, A., Hughes, M., & Winter, S. (2014). A multidisciplinary approach to sustainable building material selection: A case study in a Finnish context. *Building and Environment*, *82*, 526-535.

Tariku, F., Kumaran, K., & Fazio, P. (2010). Transient model for coupled heat, air and moisture transfer through multilayered porous media. *International journal of heat and mass transfer*, *53*(15-16), 3035-3044.

Teoh, J. H., Soh, E., & Le Ferrand, H. (2024). Manipulating fungal growth in engineered living materials through precise deposition of nutrients. *International Journal of Bioprinting*, *10*(5), 3939. https://doi.org/10.36922/ijb.3939

Toftum, J., Jørgensen, A. S., & Fanger, P. O. (1998). Upper limits of air humidity for preventing warm respiratory discomfort. *Energy and Buildings*, *28*(1), 15-23.

Van Wylick, A., Elsacker, E., Yap, L. L., Peeters, E., & De Laet, L. (2022). Mycelium composites and their biodegradability: An exploration on the disintegration of mycelium-based materials in soil. *Construction Technologies and Architecture*, *1*, 652-659.

Vandelook, S., Elsacker, E., Van Wylick, A., De Laet, L., & Peeters, E. (2021). Current state and future prospects of pure mycelium materials. *Fungal biology and biotechnology*, *8*(1), 20.

Verhelst, J., Vandersanden, S., Nouwen, O., & Rineau, F. (2024). Fungal Strain Influences Thermal Conductivity, Hydrophobicity, Color Homogeneity, and Mold Contamination of Mycelial Composites. *Materials*, *17*(24), 6050.

Volk, R., Schröter, M., Saeidi, N., Steffl, S., Javadian, A., Hebel, D. E., & Schultmann, F. (2024). Life cycle assessment of mycelium-based composite materials. *Resources, Conservation and Recycling*, *205*, 107579.

Wang, H., Tao, J., Wu, Z., Weiland, K., Wang, Z., Masania, K., & Wang, B. (2024). Fabrication of living entangled network composites enabled by mycelium. *Advanced Science*, *11*(24), 2309370.

Wattanavichean, N., Phanthuwongpakdee, J., Koedrith, P., Laoratanakul, P., Thaithatgoon, B., Somrithipol, S., Kwantong, P., Nuankaew, S., Pinruan, U., & Chuaseeharonnachai, C. (2025). Mycelium-Based Breakthroughs: Exploring Commercialization, Research, and Next-Gen Possibilities. *Circular Economy and Sustainability*, 1-43. https://doi.org/10.1007/s43615-025-00539-x

Wildman, J., Shea, A., Walker, P., & Henk, D. (2024). Extrinsic and intrinsic determinants of thermal conductivity in mycelium composites. *Building Services Engineering Research & Technology*, 01436244241306631.

Yang, L., Park, D., & Qin, Z. (2021). Material function of mycelium-based bio-composite: A review. *Frontiers in Materials*, *8*, 737377.

Zhang, M., Zhang, Z., Zhang, R., Peng, Y., Wang, M., & Cao, J. (2023). Lightweight, thermal insulation, hydrophobic mycelium composites with hierarchical porous structure: Design, manufacture and applications. *Composites Part B: Engineering*, *266*, 111003.

Zhang, X., Künzel, H. M., Zillig, W., Mitterer, C., & Zhang, X. (2016). A Fickian model for temperature-dependent sorption hysteresis in hygrothermal modeling of wood materials. *International Journal of Heat and Mass Transfer*, *100*, 58-64.

Zhang, Z. (2014). *Modelling of sorption hysteresis and its effect on moisture transport within cementitious materials* Paris Est].

Zhou, Y., Trabelsi, A., Xiang, L., & El Mankibi, M. (2025). Investigation of hygrothermal behavior of a novel bio-based panel: Experiment and numerical simulation. *Clean Energy Science and Technology*, *3*(1), 249.

Zirkelbach, D., Schmidt, T., Kehrer, M., & Künzel, H. (2007). Wufi® pro–manual. *Fraunhofer Institute*.